



LYONSE&N & ELYT Global

LyonSE&N & ELYT Global workshop 2021

Lyon Saint Etienne & Nippon Scientific Network

Engineering sciences Lyon Tohoku

JSPS Core to core 1st symposium

Construction of an international research exchange center for ammonia combustion and materials toward the realization of a low-carbon society

Workshop Proceedings

Online, June 21st-25th 2021



LyonSE&N & ELYT workshop 2021 / JSPS Core to core 1st symposium

Organizing committee

Mickaël LALLART (INSA Lyon)

Tetsuya UCHIMOTO (Tohoku University)

Jean-Yves CAVAILLE (INSA Lyon-Tohoku University)

Makoto OHTA (Tohoku University)

Gaël SEBALD (INSA Lyon-CNRS-Tohoku University)

Yutaka SATO (Tohoku University)

Nicolas MARY (INSA Lyon)

Julien FONTAINE (CNRS-ECL)

<https://www.elyt-lab.com/en/content/elyt-workshop-2021>

Table of Contents

Table of Contents	5
Forewords.....	9
Useful information	11
Presentations (Zoom Meeting)	11
Time and Date	11
Join Zoom Meeting.....	11
Presentation	11
Q & A	11
Gathering (Gather Town)	12
Use of the platform	12
Map.....	12
Program	15
Overview.....	15
Day 1.....	16
Day 2.....	17
Day 3.....	18
Day 4.....	19
Day 5.....	20
Extended abstracts	21
Invited talks	21
Biomechanical energy harvesting for leadless pacemaker application	23
Presentation of the corrosion loop CORRETEX	25
Oral presentations.....	27
Tribology for health devices: 15 years of collaboration between Tohoku University (Ohta lab) and ECL (LTDS).....	29
Reduced oxygen availability triggers aerotaxis and aerokinesis of Dictyostelium.....	31
Virtual Angiography System as a Platform for Blood Flow estimation	33
MagnetoRheological Materials for energy conversion	34
Nozzle design for polymer coating by cold spray process.....	37
Magnetic characterization of Metglas under tensile stress for energy harvesting applications ..	39
Elastocaloric cooling using natural rubber: material properties, heat transfer and heat losses effects on proof of concept performances	41
Progressive improvement in deposition efficiency for cold sprayed fluoropolymer coatings	43
EMAR monitoring system of a carbon steel thinning in a corrosive environment	45

Table of Contents

Heat engine based on MultiPhysic Memory Alloys and pyroelectric conversion for thermal energy harvesting 47

Towards the *in situ* mechanical characterization of cerebral aneurysms: first steps of experimental and numerical designs. 49

Structured hexahedral meshing of a physiological model of vessel n-furcation for computational fluid dynamics..... 53

Endothelial cells distribution after the flow exposure experiment 55

In situ characterization and modeling of the deformation and fracture of an aluminum foam .. 57

Beating Thermal Coarsening in Nanoporous Materials via High-Entropy Design..... 59

Tensile properties and microstructure of cellulose nanofiber reinforced silkworm silk fibers 61

CarboEDiffSim : Simulation off Carbon electro-diffusion in iron with phase change 63

Research of 5d-4f fast emission in trivalent lanthanides-doped fluoro-oxide glasses as neutron scintillator materials..... 65

Characterization of gas-atomized powders and electron beam melted Co-Cr-Mo-C alloys..... 67

Role of Charge Carrier Transport in the mechanisms of Polyurethane Actuation..... 69

Influence of mechanical surface treatment on passive and oxide behavior of 304L Stainless Steel 71

Modeling ferroelectric phase transitions for energy harvesting..... 73

Magnetization mechanisms NDT..... 75

Shape optimization with respect to mechanical stability criteria 77

Simulations and Experiments Exploring the Role of OH-Termination in the Lubricity and Stability of H-free DLC 79

Langevin Navier-Stokes simulation of the protoplasmic streaming 81

Local stabilization dynamics of ammonia/methane non-premixed flames..... 85

Modal approach for extracting flow structure related to the subsonic jet noise generation 87

JSPS Core to core 1st symposium: Construction of an international research exchange center for ammonia combustion and materials toward the realization of a low-carbon society 89

Lab poster list 91

Participant list..... 93

A 93

B 93

C 93

D 93

F 93

G 93

H 93

I 94

Table of Contents

J..... 94
K..... 94
L..... 94
M..... 94
N..... 94
O..... 94
P..... 94
R..... 95
S..... 95
T..... 95
U..... 95
W..... 95
X..... 95
Y..... 95
Z..... 95

Forewords

Dear Colleagues, Dear Friends,

Since the last LyonSE&N/ELyT workshop that was successfully held on February 17th-19th, 2020 in Vogüé, Ardèche, France, international collaborations and exchanges have experienced hard time. However, the ELyT (*Engineering Sciences Lyon-Tohoku*) network has shown its resilience thanks to its long history and strength. The activity in the framework of the network has never been so lively, involving 77 people and 21 laboratories for 2020. Such a dynamism yielded outstanding scientific production (+58% compared to 2019), 5 new projects (for a total of 26 actions), 5 new Double Degree Ph.D. students, and, last but not least, significant exchanges despite the restrictions that arose on the major part of 2020, partly thanks to the STARMAJ initiative allowing the scientific visit of Japanese Masters students in Lyon/St-Etienne site as well as JSPS support for French scientist visit in Sendai. Such achievements were also strongly supported by the actions through the LyonSE&N (*Lyon St-Etienne & Nippon*) initiative that structures the collaborative actions between Japan and the Lyon-St-Etienne site, in the field of Energy, Health, Urbanism and, as a transverse domain, Data Science and Artificial Intelligence.

The benefit of the network and collaborations for the collaborative progress in engineering science serving the societal stakes also contributed to several major outcomes in terms of support. Hence, in addition to common project fundings, this permitted the renewal of both ELyTMaX as an International Research Laboratory (IRL) and ELyT Global as an International Research Network (IRN), as well as the obtention of a JSPS Core-to-Core program on the “Construction of an International research exchange center for ammonia combustion and materials toward the realization of a low-carbon society”. These new structures allow us to open new routes for the collaborations, while keeping the founding strength that is making them so successful.

We are grateful to our institutions, at multilevel scales, for their continuous trust. Such support is definitely linked to the scientific researchers that strongly contribute to the network through their outstanding common scientific contributions. We therefore deeply thank them as well, and are proud to have some of them performing talks during the workshop. We express our sincere gratitude to the workshop presenters, in the form of oral and invited presentations or lab. Tours, as well as to the participants that make this workshop a success.

Despite the particular conditions that require the organization of the workshop as a virtual event, we were amazed by the responsiveness of the network and the number of contributions we received, and we sincerely hope you will enjoy this event as much as we did organizing it.

Hoping that we will be able to meet face-to-face soon, we sincerely and deeply thank you for your participation to this workshop and more generally for your precious contributions to the network activities.

The LyonSE&N-ELyT workshop 2021 Organizing Committee

Useful information

Presentations (Zoom Meeting)

Talks will be given by **Zoom**. **Link and passwords** are sent **upon registration**.

Time and Date

Date:

- Monday, June 21st
- Tuesday, June 22nd
- Wednesday, June 23rd
- Thursday, June 24th
- Friday, June 25th

Time: 15:30 - 18:00 (JST) / 8:30 - 11:00 (CEST)

* Same through the workshop period.

* Attendees will be able to join 30 minutes before start time on June 21st.

* Attendees will be able to join 10 minutes before start time on June 22nd, 23rd, 24th and 25th.

Join Zoom Meeting

Please enter your name in English. (First Name / Last Name)

When you change your name after joining Zoom Meeting,

1. Click "Participants" at the bottom
2. Place the cursor over your name  More  Rename

Presentation

For Presenter:

1. Unmute your microphone and start your video.
2. To start your presentation, click "Share Screen" and select your slide-show or PPT.

For Audience:

****IMPORTANT**** In order to provide a nicer and more friendly experience, we opted out for **Zoom Meeting**, so that everyone can see each other. We ask you to **turn off your microphone and camera** during presentation, except for questions you want to ask directly.

Q & A

For Questioner:

Do not hesitate to ask question either:

- By **typing your question in the chat**. The chairperson will pick chat questions at the end of presentation.
- By **raising hand** at the end of the presentation:
 1. Click "**Participants**" at the bottom.
 2. Click "**Raise Hand**".
 3. A **chair appoints you**, and then, **you unmute your microphone and start your video** by yourself and make a question.
 4. After your questions, click "**Lower Hand**" and **mute your microphone and stop your video** by yourself.

Information

Gathering (Gather Town)

In addition to presentations on Zoom and to feel as close as possible to a real conference, an **exchange space** has been set up using the **Gather Town** platform. Gather Town allows you to walk around and interact with people or objects. The gather town **link and password** are sent **upon registration**.

Use of the platform

At first connection, a quick tutorial will allow you getting familiar with the platform. We remind some useful commands however:

- Move using the **arrow keys** of your computer (the platform is not operating on phone and tablet).
- Type **"x"** key on your keyboard to interact with an object (e.g., poster), and again **"x"** key to close the object.
- When you entre a **"private space"** (usually around tables for example), people outside the same space cannot interact with people inside.
- There are two **"spotlights"**  (one in the garden and one in the lounge). When walking on it, everybody in the room will hear and see you.

The platform will be kept **open during the whole conference duration**, please feel free to use it. There are also some **dedicated times slots** for gathering (see program).

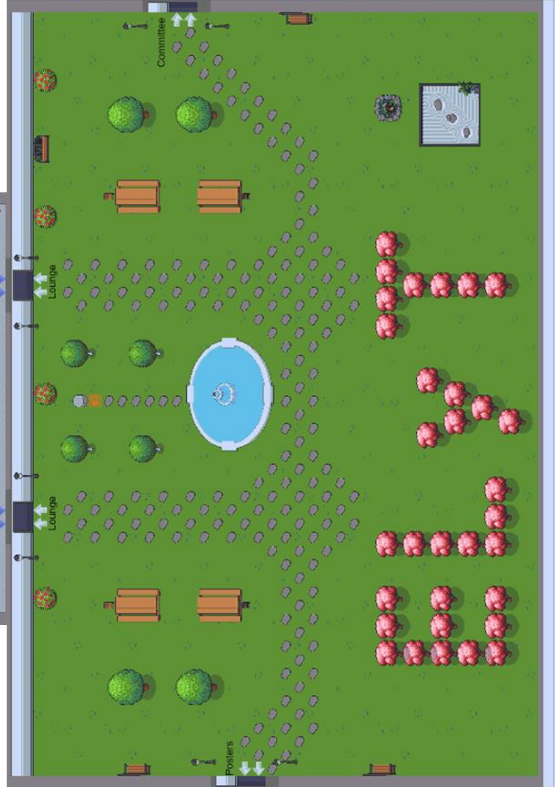
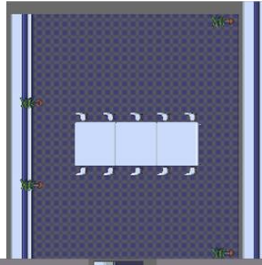
Map

The space map is given hereinafter.

Lounge
Enjoy some fruitful discussion around a cup of tea or coffee!



Committee room
Please do not use

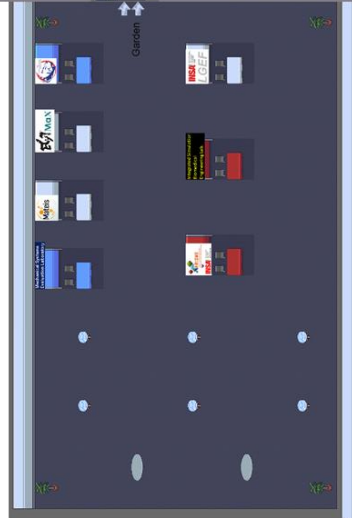


Garden

Enjoy some fresh air with colleagues. Have a look to nice cherry blossoms at the south of the garden!

Poster room

Look at the description of lab activities and find new collaboration opportunities!



Program
Overview

Start	End FR	Day 1 (June 21st)	Day 2 (June 22nd)	Day 3 (June 23rd)	Day 4 (June 24th)	Day 5 (June 25th)	Start	End JP
08:30	08:35	Chair: T. Shoji / J.-Y. Cavallé	Chair: M. Ohta / D. Fabrigère	Chair: H. Miki / M. Lallart	Chair: T. Uchimoto / G. Sebald	Chair: K. Ogawa / N. Mary	15:30	15:35
08:35	08:40	Opening - A.-C. Hladky (CNRS) - M. Kotani (Tohoku) - M. Lallart / J. Fontaine, T. Uchimoto / Y. Sato (ELT Global) - M.-C. Baletto (INSA Lyon) - K. Maruta (IFS TU) - C. Corre (ECL)					Invited H. Kobayashi Role of ammonia combustion and Japan's perspectives	Invited Elie Lefeuve, Marion Woytasik, Xavier Leroux, Fabien Perrain Biomechanical energy harvesting for leadless pacemaker application
08:40	08:45	JSPS Core to core program symposium - Construction of an international research exchange center for ammonia combustion and materials toward the realization of a low-carbon society	Introduction of Core to Core program* K. Maruta and T. Tokumasu	G. Plet, J. Raviol, H. Magoaric, C. Pailler-Mattei Towards the in situ characterization of cerebral aneurysms: first steps of experimental and numerical designs	K. Kita, T. Mabuchi, P. Chantrenne, T. Tokumasu CarboDiffSim: Simulation of Carbon electro-diffusion in iron with phase change	G. Beaulin, Y. Guyot, C. Dujardin, A. Yoshikawa, K. Kamada, S. Kuroawa, N. Sarikura, M. Enpuku, M. Yuki, M. Cadatal-Rabhan, T. Murata, K. Kawano, K. Yamano, T. Shimizu, M. Guzik Research of Sr-doped fluorite emission in trivalent lanthanides-doped fluoro-oxide glasses as neutron scintillator materials	15:45	15:50
08:45	08:50						Invited M. Ohta, V. Fridrici Tribology for health devices: 15 years of collaboration between Tohoku University (Ohta lab) and ECL (LIDS)	Characterization of gas-atomized powders and electron beam melted Co-Cr-Mo-C alloys
08:50	08:55	Coffee break & Gathering	Panel discussion Moderator: N. Mary Materials System for Ammonia Combustion	M. Decroocq, E. Maury, G. Lavoué, C. Frindel, M. Ohta Structured hexahedral meshing of a physiological model of vessel bifurcation for computational fluid dynamics	G. Coathy, G. Digue, K. Yuse, L. Seveyrat, V. Perrin, F. Dalmas, S. Livi, H. Takana, J. Courbon, J.-Y. Cavalle Role of Charge Carrier Transport in the Mechanisms of Polyurethane Actuation	S. Colson, M. Kuhni, A. Hayakawa, H. Kobayashi, C. Galizzi, D. Escudé Local stabilization dynamics of ammonia/methane non-premixed flames	15:55	16:00
08:55	09:00						Y. Kohata, H. Anzai, M. Decroocq, S. Rit, C. Frindel, M. Ohta Virtual Angiography System as a Platform for Blood Flow estimation	Influence of mechanical surface treatment on passive and oxide behavior of 304L Stainless Steel
09:00	09:05	Coffee break & Gathering	Chair: F. Gilot / A. Kamiya	Chair: L. Joly-Pottuz / Y. Sato	Chair: V. Fridrici / A. Chiba	Chair: S. Obayashi	16:05	16:10
09:05	09:10						Y. Kaneko, W. L. Sulen, C. A. Bernard, H. Salto, Y. Ichikawa, K. Ogawa Progressive improvement in deposition efficiency for cold sprayed fluoropolymer coatings	Group Photo Coffee break & Gathering
09:10	09:15	Coffee break & Gathering	G. Digue, H. Miyauchi, S. Takeda, T. Uchimoto, N. Mary, T. Takagi EMAR monitoring system of a carbon steel thinning in a corrosive environment	T. Wada, S. H. Joo, H. Kato Beating Thermal Coarsening in Nanoporous Materials via High-Entropy Design	S. Zhang, S. Takeda, T. Uchimoto, G. Sebald, B. Ducharme Magnetization mechanisms NDT	S. Morita, A. Yakeno, C. Boge, S. Obayashi Modal approach for extracting flow structure related to the subsonic jet noise generation	16:15	16:20
09:15	09:20						M. Lallart, H. Miki, L. Yan, G. Sebald, G. Digue, M. Ohtsuka, M. Kohl Heat engine based on Multi-Physics Memory Alloys and pyroelectric conversion for thermal energy harvesting	F. Gillot, P. Mohanasundaram, S. Besset, K. Shimoyama Shape optimization with respect to mechanical stability criteria
09:20	09:25	Coffee break & Gathering	Chair: M. Lallart / H. Kurita	Chair: T. Wada / S. H. Joo / H. Kato	Chair: S. Zhang / S. Takeda / T. Uchimoto / G. Sebald / B. Ducharme	Chair: S. Morita / A. Yakeno / C. Boge / S. Obayashi	16:25	16:30
09:25	09:30						Y. Liu, B. Ducharme, K. Makihara, G. Sebald, M. Lallart Magnetic characterization of Metglas under tensile stress for energy harvesting applications	M. Kubo, Y. Wang, M.-I. De Barros Bouchet, J.-M. Martin Simulations and Experiments Exploring the Role of OH-Termination in the Lubricity and Stability of H-free DLC
09:30	09:35	Coffee break & Gathering	Chair: M. Lallart / H. Kurita	Chair: T. Wada / S. H. Joo / H. Kato	Chair: S. Zhang / S. Takeda / T. Uchimoto / G. Sebald / B. Ducharme	Chair: S. Morita / A. Yakeno / C. Boge / S. Obayashi	16:35	16:40
09:35	09:40						G. Sebald, G. Lombardi, J. Bay, A. Kamiya, X. Sze Wey, G. Coathy, H. Haisoume, L. Leboun Elastocatic cooling using natural rubber: material properties, heat transfer and heat losses effects on proof of concept performances	Vincent Fridrici Presentation of LIDS
09:40	09:45	Coffee break & Gathering	Chair: M. Lallart / H. Kurita	Chair: T. Wada / S. H. Joo / H. Kato	Chair: S. Zhang / S. Takeda / T. Uchimoto / G. Sebald / B. Ducharme	Chair: S. Morita / A. Yakeno / C. Boge / S. Obayashi	16:45	16:50
09:45	09:50						16:45	16:50
09:50	09:55	Coffee break & Gathering	Chair: M. Lallart / H. Kurita	Chair: T. Wada / S. H. Joo / H. Kato	Chair: S. Zhang / S. Takeda / T. Uchimoto / G. Sebald / B. Ducharme	Chair: S. Morita / A. Yakeno / C. Boge / S. Obayashi	16:50	16:55
09:55	10:00						16:50	16:55
10:00	10:05	Coffee break & Gathering	Chair: M. Lallart / H. Kurita	Chair: T. Wada / S. H. Joo / H. Kato	Chair: S. Zhang / S. Takeda / T. Uchimoto / G. Sebald / B. Ducharme	Chair: S. Morita / A. Yakeno / C. Boge / S. Obayashi	16:55	17:00
10:05	10:10						16:55	17:00
10:10	10:15	Coffee break & Gathering	Chair: M. Lallart / H. Kurita	Chair: T. Wada / S. H. Joo / H. Kato	Chair: S. Zhang / S. Takeda / T. Uchimoto / G. Sebald / B. Ducharme	Chair: S. Morita / A. Yakeno / C. Boge / S. Obayashi	17:00	17:05
10:15	10:20						17:00	17:05
10:20	10:25	Coffee break & Gathering	Chair: M. Lallart / H. Kurita	Chair: T. Wada / S. H. Joo / H. Kato	Chair: S. Zhang / S. Takeda / T. Uchimoto / G. Sebald / B. Ducharme	Chair: S. Morita / A. Yakeno / C. Boge / S. Obayashi	17:05	17:10
10:25	10:30						17:05	17:10
10:30	10:35	Coffee break & Gathering	Chair: M. Lallart / H. Kurita	Chair: T. Wada / S. H. Joo / H. Kato	Chair: S. Zhang / S. Takeda / T. Uchimoto / G. Sebald / B. Ducharme	Chair: S. Morita / A. Yakeno / C. Boge / S. Obayashi	17:10	17:15
10:35	10:40						17:10	17:15
10:40	10:45	Coffee break & Gathering	Chair: M. Lallart / H. Kurita	Chair: T. Wada / S. H. Joo / H. Kato	Chair: S. Zhang / S. Takeda / T. Uchimoto / G. Sebald / B. Ducharme	Chair: S. Morita / A. Yakeno / C. Boge / S. Obayashi	17:15	17:20
10:45	10:50						17:15	17:20
10:50	10:55	Coffee break & Gathering	Chair: M. Lallart / H. Kurita	Chair: T. Wada / S. H. Joo / H. Kato	Chair: S. Zhang / S. Takeda / T. Uchimoto / G. Sebald / B. Ducharme	Chair: S. Morita / A. Yakeno / C. Boge / S. Obayashi	17:20	17:25
10:55	11:00						17:20	17:25

Day 1

Start FR	End FR	Day 1 (June 21st)	Start JP	End JP
		<i>Chair: T. Shoji / J.-Y. Cavallé</i>		
08:30	08:35	Opening - A.-C. Hladky (CNRS) - M. Kotani (Tohoku) - M. Lallart/J. Fontaine, T. Uchimoto/Y. Sato (ELyT Global) - M.-C. Baietto (INSA Lyon) - K. Maruta (IFS TU) - C. Corre (ECL)	15:30	15:35
08:35	08:40		15:35	15:40
08:40	08:45		15:40	15:45
08:45	08:50		15:45	15:50
08:50	08:55		15:50	15:55
08:55	09:00		15:55	16:00
09:00	09:05	M. Ohta, V. Fridrici	16:00	16:05
09:05	09:10	<i>Tribology for health devices: 15 years of collaboration between Tohoku University (Ohta lab) and ECL (LTDS)</i>	16:05	16:10
09:10	09:15		16:10	16:15
09:15	09:20	S. Hirose, J.-P. Rieu, C. Anjard, O. Cochet-Escartin, K. Funamoto	16:15	16:20
09:20	09:25	<i>Reduced oxygen availability triggers aerotaxis and aerokinesis of Dictyostelium</i>	16:20	16:25
09:25	09:30		16:25	16:30
09:30	09:35	Y. Kohata, H. Anzai, M. Decroocq, S. Rit, C. Frindel, M. Ohta	16:30	16:35
09:35	09:40	<i>Virtual Angiography System as a Platform for Blood Flow estimation</i>	16:35	16:40
09:40	09:45		16:40	16:45
09:45	09:50		16:45	16:50
09:50	09:55	<i>Coffee break & Gathering</i>	16:50	16:55
09:55	10:00		16:55	17:00
		<i>Chair: M. Lallart / H. Kurita</i>		
10:00	10:05	G. Diguët, G. Sebald, M. Nakano, M. Lallart, J.-Y. Cavallé <i>MagnetoRheological Materials for energy conversion</i>	17:00	17:05
10:05	10:10		17:05	17:10
10:10	10:15		17:10	17:15
10:15	10:20	C. A. Bernard, H. Takana, O. Lame, K. Ogawa, J.-Y. Cavallé <i>Nozzle design for polymer coating by cold spray process</i>	17:15	17:20
10:20	10:25		17:20	17:25
10:25	10:30		17:25	17:30
10:30	10:35	Y. Liu, B. Ducharne, K. Makihara, G. Sebald, M. Lallart <i>Magnetic characterization of Metglas under tensile stress for energy harvesting applications</i>	17:30	17:35
10:35	10:40		17:35	17:40
10:40	10:45		17:40	17:45
10:45	10:50	G. Sebald, G. Lombardi, L. Maury, J. Jay, A. Komiya, X. Sze Way, G. Coativy, H. Haissounne, L. Lebrun <i>Elastocaloric cooling using natural rubber: material properties, heat transfer and heat losses effects on proof of concept performances</i>	17:45	17:50
10:50	10:55		17:50	17:55
10:55	11:00		17:55	18:00

Start FR	End FR	Day 2 (June 22nd)		Start JP	End JP	
		<i>Chair: M. Ohta / D. Fabrègue</i>				
08:30	08:35	<i>JSPS Core to core program symposium - Construction of an international research exchange center for ammonia combustion and materials toward the realization of a low-carbon society</i>	Introduction of "Core to Core program" K. Maruta and T. Tokumasu	15:30	15:35	
08:35	08:40			15:35	15:40	
08:40	08:45			15:40	15:45	
08:45	08:50			15:45	15:50	
08:50	08:55			Invited H. Kobayashi	15:50	15:55
08:55	09:00			<i>Role of ammonia combustion and Japan's perspectives</i>	15:55	16:00
09:00	09:05				16:00	16:05
09:05	09:10				16:05	16:10
09:10	09:15				16:10	16:15
09:15	09:20				16:15	16:20
09:20	09:25				16:20	16:25
09:25	09:30				16:25	16:30
09:30	09:35			Panel discussion Moderator: N. Mary	16:30	16:35
09:35	09:40			<i>Materials System for Ammonia Combustion</i>	16:35	16:40
09:40	09:45				16:40	16:45
09:45	09:50				16:45	16:50
09:50	09:55			16:50	16:55	
09:55	10:00	<i>Coffee break & Gathering</i>		16:55	17:00	
10:00	10:05	<i>Chair: F. Gillot / A. Komiya</i>		17:00	17:05	
10:05	10:10	<i>Y. Kaneko, W. L. Sulen, C. A. Bernard, H. Saito, Y. Ichikawa, K. Ogawa Progressive improvement in deposition efficiency for cold sprayed fluoropolymer coatings</i>		17:05	17:10	
10:10	10:15			17:10	17:15	
10:15	10:20			17:15	17:20	
10:20	10:25	<i>G. Diguët, H. Miyauchi, S. Takeda, T. Uchimoto, N. Mary, T. Takagi EMAR monitoring system of a carbon steel thinning in a corrosive environment</i>		17:20	17:25	
10:25	10:30			17:25	17:30	
10:30	10:35			17:30	17:35	
10:35	10:40	<i>M. Lallart, H. Miki, L. Yan, G. Sebald, G. Diguët, M. Ohtsuka, M. Kohl Heat engine based on MultiPhysic Memory Alloys and pyroelectric conversion for thermal energy harvesting</i>		17:35	17:40	
10:40	10:45			17:40	17:45	
10:45	10:50			17:45	17:50	
10:50	10:55	<i>Vincent Fridrici Presentation of LTDS</i>		17:50	17:55	
10:55	11:00			17:55	18:00	

Start FR	End FR	Day 3 (June 23rd)	Start JP	End JP
		<i>Chair: H. Miki / M. Lallart</i>		
08:30	08:35	Invited Elie Lefeuvre, Marion Woytasik, Xavier Leroux, Fabien Parrain <i>Biomechanical energy harvesting for leadless pacemaker application</i>	15:30	15:35
08:35	08:40		15:35	15:40
08:40	08:45		15:40	15:45
08:45	08:50		15:45	15:50
08:50	08:55		15:50	15:55
08:55	09:00		15:55	16:00
09:00	09:05	G. Plet, J. Raviol, H. Magoariec, C. Pailler-Mattei <i>Towards the in situ characterization of cerebral aneurysms: first steps of experimental and numerical designs</i>	16:00	16:05
09:05	09:10		16:05	16:10
09:10	09:15		16:10	16:15
09:15	09:20	M. Decroocq, E. Maury, G. Lavoué, C. Frindel, M. Ohta <i>Structured hexahedral meshing of a physiological model of vessel n-furcation for computational fluid dynamics</i>	16:15	16:20
09:20	09:25		16:20	16:25
09:25	09:30		16:25	16:30
09:30	09:35	Z. Wang, H. Anzai, Y. Kojima, N. K. Putra, J.-P. Rieu, N. Ohtsu, H. Taniho, M. Ohta <i>Endothelial cells distribution after the flow exposure experiment</i>	16:30	16:35
09:35	09:40		16:35	16:40
09:40	09:45		16:40	16:45
09:45	09:50	<i>Coffee break & Gathering</i>	16:45	16:50
09:50	09:55		16:50	16:55
09:55	10:00		16:55	17:00
		<i>Chair: L. Joly-Pottuz / Y. Sato</i>		
10:00	10:05	S. Dancette, Y. Amani, J. Luksch, A. Jung and E. Maire <i>In situ characterization and modeling of the deformation and fracture of an aluminum foam</i>	17:00	17:05
10:05	10:10		17:05	17:10
10:10	10:15		17:10	17:15
10:15	10:20	T. Wada, S.-H. Joo, H. Kato <i>Beating Thermal Coarsening in Nanoporous Materials via High-Entropy Design</i>	17:15	17:20
10:20	10:25		17:20	17:25
10:25	10:30		17:25	17:30
10:30	10:35	H. Kurita, T. Kanno, Z. Wang, F. Narita <i>Tensile properties and microstructure of cellulose nanofiber reinforced silkworm silk fibers</i>	17:30	17:35
10:35	10:40		17:35	17:40
10:40	10:45		17:40	17:45
10:45	10:50	Toshiyuki Takagi <i>Introduction of Tohoku Forum for Creativity Activities</i>	17:45	17:50
10:50	10:55		17:50	17:55
10:55	11:00		17:55	18:00

Start FR	End FR	Day 4 (June 24th)	Start JP	End JP
		<i>Chair: T. Uchimoto / G. Sebald</i>		
08:30	08:35	K. Kita, T. Mabuchi, P. Chantrenne, T. Tokumasu	15:30	15:35
08:35	08:40	<i>CarboEDiffSim: Simulation off Carbon electro-diffusion in iron with phase change</i>	15:35	15:40
08:40	08:45		15:40	15:45
08:45	08:50	G. Boulon, Y. Guyot, C. Dujardin, A. Yoshikawa, K. Kamada, S. Kurosawa, N. Sarukura, M. Empizo, M. Yuki, M. Cadatal-Raduban, T. Murata, K. Kawano, K. Yamanoi, T. Shimizu, M. Guzik <i>Research of 5d-4f fast emission in trivalent lanthanides-doped fluoro-oxide glasses as neutron scintillator materials</i>	15:45	15:50
08:50	08:55		15:50	15:55
08:55	09:00		15:55	16:00
09:00	09:05	S. Aota, A. Chiba, K. Yamanaka, E. Maire, J. Adrien, D. Fabrègue <i>Characterization of gas-atomized powders and electron beam melted Co-Cr-Mo-C alloys</i>	16:00	16:05
09:05	09:10		16:05	16:10
09:10	09:15		16:10	16:15
09:15	09:20	G. Coativy, G. Diguët, K. Yuse, L. Seveyrat, V. Perrin, F. Dalmas, S. Livi, H. Takana, J. Courbon, J.-Y. Cavaille <i>Role of Charge Carrier Transport in the mechanisms of Polyurethane Actuation</i>	16:15	16:20
09:20	09:25		16:20	16:25
09:25	09:30		16:25	16:30
09:30	09:35	H. Abe, B. Ter-Ovanesian, K. Jaffré, N. Mary, Y. Watanabe, B. Normand <i>Influence of mechanical surface treatment on passive and oxide behavior of 304L Stainless Steel</i>	16:30	16:35
09:35	09:40		16:35	16:40
09:40	09:45		16:40	16:45
09:45	09:50	Group Photo	16:45	16:50
09:50	09:55	<i>Coffee break & Gathering</i>	16:50	16:55
09:55	10:00		16:55	17:00
		<i>Chair: V. Fridrici / A. Chiba</i>		
10:00	10:05	G. Taxil, M. Lallart, G. Sebald, E. Lefeuvre, B. Ducharne, A. Bartasyste, M. Ouhabaz, H. Kuwano, T. T. Nguyen <i>Modeling ferroelectric phase transitions for energy harvesting</i>	17:00	17:05
10:05	10:10		17:05	17:10
10:10	10:15		17:10	17:15
10:15	10:20	S. Zhang, S. Takeda, T. Uchimoto, G. Sebald, B. Ducharne <i>Magnetization mechanisms NDT</i>	17:15	17:20
10:20	10:25		17:20	17:25
10:25	10:30		17:25	17:30
10:30	10:35	F. Gillot, P. Mohanasundaram, S. Besset, K. Shimoyama <i>Shape optimization with respect to mechanical stability criteria</i>	17:30	17:35
10:35	10:40		17:35	17:40
10:40	10:45		17:40	17:45
10:45	10:50	M. Kubo, Y. Wang, M.-I. De Barros Bouchet, J.-M. Martin <i>Simulations and Experiments Exploring the Role of OH-Termination in the Lubricity and Stability of H-free DLC</i>	17:45	17:50
10:50	10:55		17:50	17:55
10:55	11:00		17:55	18:00

Start FR	End FR	Day 5 (June 25th)	Start JP	End JP
		<i>Chair: K. Ogawa / N. Mary</i>		
08:30	08:35	Invited J. Kittel and F. Ropital <i>Presentation of the corrosion loop CORRETEX</i>	15:30	15:35
08:35	08:40		15:35	15:40
08:40	08:45		15:40	15:45
08:45	08:50		15:45	15:50
08:50	08:55		15:50	15:55
08:55	09:00		15:55	16:00
09:00	09:05	H. Koibuchi, S. Noro, S. Hongo, S. Nagahiro, H. Ikai, M. Nakayama, T. Uchimoto, J.-P. Rieu <i>Langevin Navier-Stokes simulation of the protoplasmic streaming</i>	16:00	16:05
09:05	09:10		16:05	16:10
09:10	09:15		16:10	16:15
09:15	09:20	S. Colson, M. Kuhni, A. Hayakawa, H. Kobayashi, C. Galizzi, D. Escudie <i>Local stabilization dynamics of ammonia/methane non-premixed flames</i>	16:15	16:20
09:20	09:25		16:20	16:25
09:25	09:30		16:25	16:30
09:30	09:35	S. Morita, A. Yakeno, C. Bogey, S. Obayashi <i>Modal approach for extracting flow structure related to the subsonic jet noise generation</i>	16:30	16:35
09:35	09:40		16:35	16:40
09:40	09:45		16:40	16:45
09:45	09:50	Closing	16:45	16:50
09:50	09:55		16:50	16:55
09:55	10:00		16:55	17:00
10:00	10:05	Gathering time	17:00	17:05
10:05	10:10		17:05	17:10
10:10	10:15		17:10	17:15
10:15	10:20		17:15	17:20
10:20	10:25		17:20	17:25
10:25	10:30		17:25	17:30
10:30	10:35		17:30	17:35
10:35	10:40		17:35	17:40
10:40	10:45		17:40	17:45
10:45	10:50		17:45	17:50
10:50	10:55		17:50	17:55
10:55	11:00	17:55	18:00	

Extended abstracts

Extended abstracts

Invited talks

Biomechanical energy harvesting for leadless pacemaker application

ELyT Global Theme (to precise) Scientific topic (to precise)

	Prof. Elie Lefeuve		Prof. Marion Woytasik
	Xavier Leroux		Prof. Fabien Parrain

Centre for Nanoscience and Nanotechnology, University of Paris-Saclay - CNRS, Palaiseau, France

Abstract

Active implantable medical devices (AIMD) play an important role in monitoring, diagnosing and treating patients. In-body medical device development has been facing an increasingly stronger demand with increases at a pace of 6% yearly. The current technical challenge in this field is creating smart, small and long-term use implants that improve the patients' health and life quality. In this context, while implanted power sources have been almost exclusively based on traditional batteries, mechanical energy-harvesting devices exhibit clear advantages and could be used in many AIMD in the near future. Using the example of the pacemaker, this talk presents technologies and strategies to efficiently convert mechanical energy into electricity, highlighting the main challenges that need to be addressed in the particular context of the human body (low vibration frequency, extreme miniaturization, high reliability) as well as the technological and methodological evolutions required to move towards industrialization of implanted biomechanical energy harvesters.

Presentation of the corrosion loop CORRTEX

Jean Kittel¹	<u>Francois Ropital^{1,2}</u>
--------------------------------	--

¹ IFP Energies nouvelles, Rond-point de l'échangeur de Solaize, BP 3, 69360 Solaize, France

² Univ. Lyon, INSA-LYON, MATEIS UMR CNRS 5510, 69621 Villeurbanne cedex, France

The high-pressure high-temperature corrosion loop developed by the CORRTEX consortium on Axel'One PPI site will be presented. Under well controlled conditions, the purpose of the corrosion loop is to deal with problems of corrosion under high pressure (as in CO₂ and with traces of H₂S), which are encountered in many energy-related environments. : capture, transport, storage and recovery of CO₂, geothermal energy, etc. In these environments, increases in gas pressures and temperatures constitute major challenges for the resistance of metallic materials, which can be subjected to corrosion (general or local loss of thickness) on the one hand and to environmental-assisted cracking (hydrogen embrittlement and / or stress corrosion) on the other hand. The members of the CORRTEX consortium are Axel'One, CNRS, IFP Energies nouvelles, Institut de la Corrosion, INSA-Lyon, MECM, Ecole des Mines de St Etienne and Lyon 1 University.

Extended abstracts

Oral presentations

Tribology for health devices: 15 years of collaboration between
Tohoku University (Ohta lab) and ECL (LTDS)

ELyT Global
Engineering for Health
Surfaces & Interfaces / Materials & Structure design



Affiliations

a: Institute of Fluid Science, Tohoku University, Sendai, Miyagi, Japan

b: ELYTMAX UMI 3757, CNRS – Université de Lyon – Tohoku University, International Joint Unit, Tohoku University, Sendai, Miyagi, Japan

c: Laboratoire de Tribologie et Dynamique des Systèmes, UMR CNRS 5513, Ecole Centrale de Lyon, Université de Lyon, Ecully, France

Abstract

In June 2006, Makoto OHTA, at that time Associate Professor at Tohoku University (Institute of Fluid Science), spent one month at Ecole Centrale de Lyon, as an invited professor. It was the first step of a long scientific collaboration between him and Vincent FRIDRICI (LTDS, Ecole Centrale de Lyon) on the topic of tribology for health devices, followed by the stay of Vincent FRIDRICI at TU in February-March 2008.

15 years later, after many stays of French researchers in Sendai and Japanese researchers in Ecully, we propose to present the main results obtained during the different projects on tribology for health devices, that were held within ELYT lab and ELYT Global.

Tribological behavior of PVA hydrogel (BioCath project)

Various medical devices are directly in contact with soft living tissues in medical fields. There are sometimes frictional problems; e.g. stents are moved from the targeted site during early implantation. This phenomenon indicates that the friction study of materials for medical application under the in vivo conditions is important for the development and design of medical devices. In order to investigate the friction behavior of different materials, an in vitro biomodel, which has realistic mechanical properties of soft tissue, is also useful. In this project, we employed poly (vinyl alcohol) hydrogel (PVA-H) as a biomodels of soft tissue. The evaluation of friction behavior of hydrogels (with different water contents,

different solvents and characteristics of the PVA powders) in contact with different materials (metallic alloys, polymers) in different conditions (sliding speed, normal load) and in controlled environment (presence of water at the interface, or PBS with addition of different chemicals, like albumin or gamma globulin) was carried out. Together with measurements of the dispersive and polar components of surface free energy (Owens-Wendt method) and mechanical properties of the gels, it helps up understand the lubrication phenomena of this contact based on the analysis of the typical Stribeck curves in presence of a soft material. This curve shows hydrodynamic lubrication and elastic friction which is a feature of contact with soft matter.

Contributions to this project were coming from Keisuke MAMADA (master TU 2008/2010 + awarda), Hiroyuki KOSUKEGAWA (PhD thesis TU 2008/2011 + post-doc at ECL 2011/2013 with grants from French embassy in Japan and labex Manutech-SISE), Boyko STOIMENOV (post-doc CNRS 2009/2010) and two groups of undergraduate students during their Study Projects at ECL, one of them getting the Best Project award.

AblaCath project

Radiofrequency catheter ablation has revolutionized treatment for tachyarrhythmia and has become first-line therapy for some tachycardias. The objective of this project is to understand and model the tribological phenomena that occur at the interface between the tip of the ablation catheter with electrode vibration and the heart tissue (friction, damage, temperature rise). It helps us to optimize the tip of the catheter (geometry, material, roughness) and the working conditions (frequency and displacement amplitude of the vibration) to be sure to destroy only the tissue at the origin of tachycardia without damaging the healthy tissue in the vicinity. This project relies on the master thesis (2011/2013) and PhD thesis (2013/2016) of Kaihong YU.

BoneDrill project

The objective of this project is to develop bones biomodels with drilling characteristics similar to the ones of natural bones. These biomodels could be used for the training of doctors or development / evaluation of medical devices. Important characteristics are mechanical properties (hardness, elasticity modulus) and friction between the biomodel and a drill, in order to give to the doctors the same feeling as with natural bones for the drilling of the bones.

Different composite materials, based on PMMA, have been developed and characterized (in mechanical tests and drilling tests), in order to understand the effects of different types of additives on hardness, elastic modulus, thrust force, maximum friction torque, drilling speed... This project focuses on the relationships between these parameters and the materials' microstructure, by taking into account temperature, lubrication and chips shape during drilling. Validation of the newly developed composites is performed by drilling tests realized by surgeons to rank developed composites, already existing bone biomodels and natural bones, in terms of feeling during drilling.

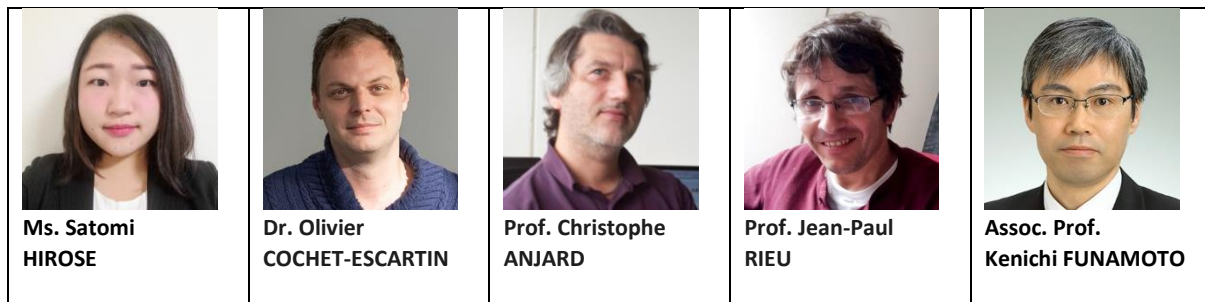
This project corresponds mainly to the research works of Yuta MURAMOTO, student of Graduate School of Biomedical Engineering, Tohoku University, during his TU master between 2014 and 2017 (including a full year at ECL – LTDS in 2014/2015) and his Double Degree PhD between TU and Ecole Centrale de Lyon, with many stays in France and in Japan between 2017 and 2020. PhD defense on March 13th, 2020, he was able to go back to Japan just before the lockdown. Yuta gets the President award from TU for best PhD thesis.

Reduced oxygen availability triggers aerotaxis and aerokinesis of Dictyostelium

ELyT Global

Theme: Engineering for Health

Scientific topic: Microsystems for cell Engineering



Affiliation

Hirose S., and Funamoto K. (Institute of Fluid Science, Tohoku University, Sendai, Japan)

Cochet-Escartin O., Anjard C., and Rieu J.P. (Institute of Light and Matter, University Claude Bernard Lyon1 and CNRS, Villeurbanne, France)

Abstract

It has been clarified for the last three decades that cells are able to sense and adapt to various oxygen (O_2) conditions, as just highlighted by the Nobel Prize in Physiology or Medicine 2019. In a hypoxic condition (low O_2), a hypoxia-inducible factor (HIF) complex associates with DNA to regulate expression of certain genes for adaptation, while it is degraded in presence of O_2 . It has also long been known that bacteria move seeking O_2 , which is a mechanism called aerotaxis, rather than regulating genes for adaptation [1]. Recently, it was demonstrated that epithelial cells also exhibit a directed migration toward O_2 using a very simple spot assay: after covering an epithelial cell monolayer by a coverglass non-permeable to O_2 , peripheral cells exhibited a strong outward directional migration to escape hypoxia from the center of the colony [2]. Following that assay, we showed at iLM that the social amoeba *Dictyostelium discoideum* (*Dd*) also displayed a spectacular phenotype when the cells consumed the surrounding O_2 (Fig. 1(a)): most cells moved quickly outward of the hypoxia area, forming a dense expanding ring moving at a constant speed. Hence, aerotaxis seems a conserved mechanism in various eukaryotic cells. However, the detection and sensing mechanisms (sensitivity to a threshold or to a gradient, response time, and cell adaptation) of O_2 -directed migration observed with *Dd* are still an enigma. To get insight into the sensing mechanisms, we developed a new experimental system using a microfluidic device with O_2 controllability (Fig. 1(b)). The device was 3x3 cm square mainly composed of polydimethylsiloxane. The O_2 concentration inside the device was controlled by gas exchange between the media channels for cell culture and the gas channels into which gas mixtures at certain O_2 concentrations are supplied. It is possible to apply a uniform O_2 concentration when the same gas mixture is

applied in each gas channel for probing aerokinesis (modification of cell motility by modifying the global O₂ concentration), or to apply a gradient in the maximum range (0.3%-21%) with two different mixtures in each gas channel for probing aerotaxis.

We found that *Dd* cells increase their migration under uniform hypoxia below 2% (Fig. 2(a)) and those in the hypoxic side migrate toward higher O₂ area under an O₂ concentration gradient (Fig. 2(b)). Thus, both aerokinesis and aerotaxis are induced in *Dd* under hypoxia [3]. The main future objectives of this project are to screen an available *Dd* mutant collection, especially the mutants associated with proteins involved in the HIF pathway, and to understand O₂-driven cell motility by simple spot assay and microsystems.

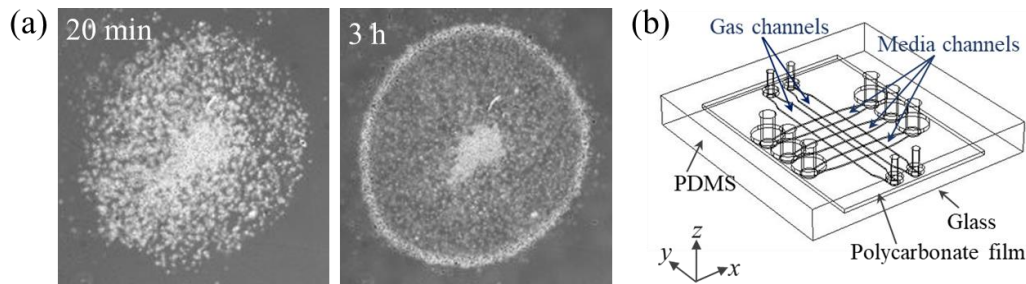


Figure 1. Experimental methods: (a) a spot of initially densely packed *Dd* cells (20 min) quickly moved outward with the formation of a ring of cells when covered by a coverglass (3 h). Each spot contained 2000 cells at the beginning of the assay. (b) a microfluidic device containing two gas channels above three media channels.

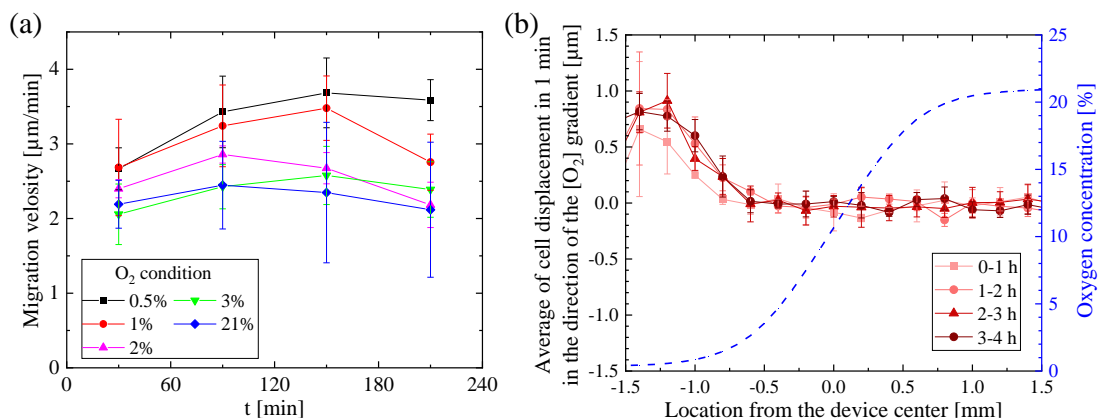


Figure 2. (a) The migration velocity of *Dd* cells under different isotropic O₂ conditions ($n = 4$). Each condition refers to the O₂ concentration flowed into the gas channels, and the cells were computationally assumed to be exposed to 0.3% higher O₂. (b) The average of displacement in 1 min of all tracked cells under an O₂ concentration gradient generated by supplying gas mixtures with different O₂ concentrations to the gas channels ($n = 3$). The blue dashed line referring to the right axis shows the calculated O₂ concentration in the media channel. The error bars show the standard deviation.

References:

[1] M. Alder, et al. Studies of bacterial aerotaxis in a microfluidic device. *Lab Chip*, 12(22) (2012) 4835–4847.
 [2] M. Deygas, et al. Redox regulation of EGFR steers migration of hypoxic mammary cells towards oxygen. *Nat. Comm.* 9 (2018) 4545.
 [3] O. Cochet-Escartin, et al. “Hypoxia triggers collective aerotactic migration in Dictyostelium discoideum”, *BioRxiv*: <https://doi.org/10.1101/2020.08.17.246082>, (2020)

Virtual Angiography System as a Platform for Blood Flow estimation

ELyT Global Medical Applications Simulation

	D.D. student Yutaro KOHATA *1,2		Assistant Prof. Hitomi ANZAI *1		Prof. Makoto OHTA *1
	D.D. student Meghane DECROOCQ *1,2,3,4		Associate Prof. Carole FRINDEL *1, 3		Dr. Simon RIT *3

1. Institute of Fluid Science, Tohoku University

2. Graduate School of Biomedical Engineering, Tohoku University

3. CREATIS, INSA Lyon

4. ELyTMaX UMI 3757, CNRS – Université de Lyon – Tohoku University International joint Unit, Tohoku University, 980-8577, Sendai, Japan

Abstract

1. Introduction

Angiography images help clinicians to assess patient blood flow. They are utilized either at diagnosis and also during interventional radiology (operations). A proper condition is chosen for each angiography operation, so that the angiography images can visualize flow using a radiopaque contrast agent in blood vessels. Conventionally, angiography images are mainly used for the qualitative assessment of blood flow: blockage of blood flow by medical device, a degree of stenosis from visual observation, and so on. Angiography images offer the possibility to quantitatively estimate blood flow by analyzing the movement of the contrast agent in angiography images.

Several studies have worked on blood flow estimation based on angiography images. Pereira *et al* validated the flow estimation by combining the blood flow rate and the agent-injection flow rate [1]. Ruijters *et al* demonstrated an estimation of flow velocity magnitudes and vectors, which is now part of real angiography systems [2]. Although in their studies, few

conditions of angiography images were examined such as the angle, the frame rate, the X-ray tube parameters, and other parameters during the operation.

Estimation algorithms must be validated with the various conditions of medical images to optimize the accuracy of blood flow estimation. Therefore, the purpose of our study is to establish Virtual Angiography System (VAS) that can generate various types of angiography images for the validation of blood flow estimation.

2. Method

VAS consists of five steps: 1) Preparing an original flow field, 2) Generating virtual angiography, 3) Estimating velocity based on virtual angiography, 4) Preparing a control velocity field as a 2D projection of the original flow field, and 5) Evaluating the estimation accuracy by comparing with the control.

3. Results

VAS can generate an original flow field, virtual angiography image, estimated velocity field, control velocity field, and error velocity field, which is shown in Fig. 1.

4. Discussion and Conclusion

We have developed Virtual Angiography System (VAS). This can generate virtual angiography images with different acquisition conditions and evaluate the accuracy of blood flow estimation on that images. Based on this system, the best estimation methods can be found for each angiography image, and subsequently, reliable and quantitative information of blood flow will be provided to clinicians.

References

- [1] V. Mendes Pereira et al., "Quantification of Internal Carotid Artery Flow with Digital Subtraction Angiography: Validation of an Optical Flow Approach with Doppler Ultrasound," *Am. J. Neuroradiol.*, vol. 35, no. 1, pp. 156–163, Jan. 2014, doi: 10.3174/ajnr.A3662.
- [2] D. Ruijters, "How to perform DSA-based Cerebral Aneurysm Flow measurements," *Eur. Soc. Radiol.*, p. 20, 2016, doi: 10.1594/ecr2016/c-1919.

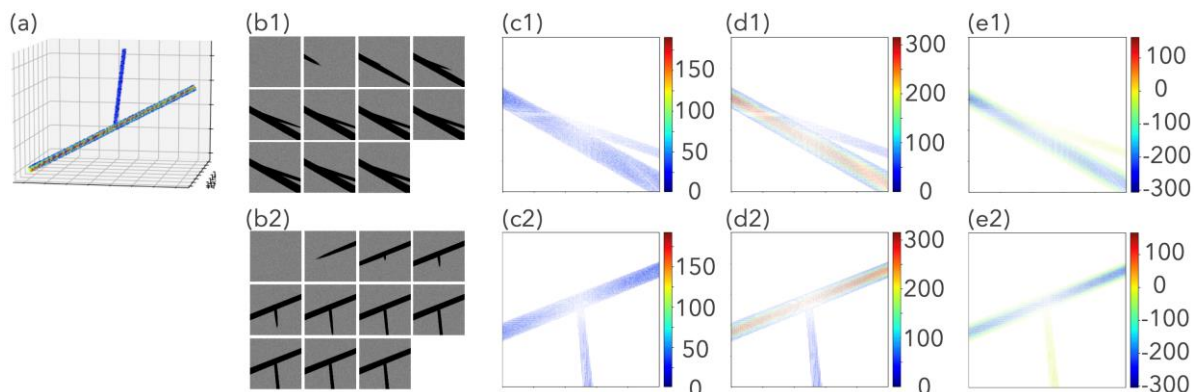


Figure 1. Results of VAS, where 1 and 2 denote two different configurations: front view and side view, and the unit of velocity fields is mm/sec. (a) an original flow field, (b) virtual angiography images, (c) estimated velocity fields (d) control velocity fields, and (e) error of velocity fields calculated by subtracting ‘(d) control’ from ‘(c) estimated’.

MagnetoRheological Materials for energy conversion

ELyT Global
Project: MAGneto-Rheological elastomers for Energy CONversion
(MARECO)

Theme: Materials and structure design



Gildas Diguët¹, Gaël Sebald¹, Masami Nakano^{1,2}, Mickael Lallart³, Jean-Yves Cavailé¹

¹ELyTMaX UMI 3757, CNRS-Université de Lyon-Tohoku University International Joint Unit, Tohoku University, Sendai, Japan

²New Industry Creation Hatchery Center, Tohoku University, Sendai, Japan

³Univ. Lyon, INSA-Lyon, LGEF EA682, F69621 Villeurbanne, France

Abstract

For many energy conversion applications, materials that combine multiple properties are needed. A candidate that fulfills such conditions are Magneto Rheological Elastomers: they are composite materials based on a non-magnetic matrix filled by magnetic particles. With this simple combination, they exhibit a very soft mechanical behavior with a large magnetic response [1-2]. This MRE, can present an anisotropy axis by applying a magnetic field during solidification of the matrix: magnetic particles tend to align themselves along the field direction. It is this anisotropic axis that leads to the conversion of energy from a shear strain into an electrical signal [3-6].

The so-called pseudo-Villari effect is the change of magnetic permeability of the material as it experiences a mechanical shear strain. This change of magnetic permeability of a material inside the magnetic circuit thus induces a change of magnetic flux flowing in this circuit. The change may then be converted into an electrical signal through a pick-up coil (Fig.1).

Using this device, the amplitude of the signal can be triggered by changing i) operating parameters of the device: amplitude and/or frequency of vibration, amplitude of magnetic bias (used to magnetized the particles) and ii) MRE intrinsic parameters: number of particles.

The principle of this device is then extended to the compression mode. The silicon matrix was replaced by a foam that is highly compressible. The resulting change of magnetic properties is therefore magnified as demonstrated in Fig.2 for different composites that have different filling factors.

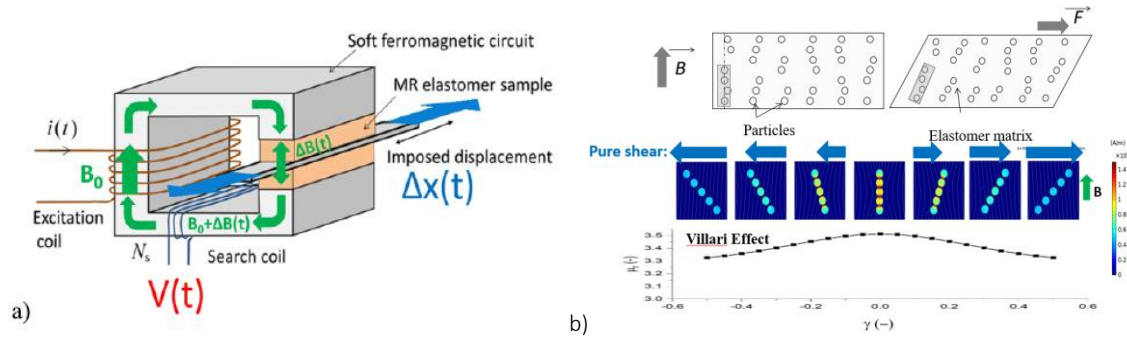


Fig.1. a) Mechanical shear to electric signal conversion device, and b) operating principle.

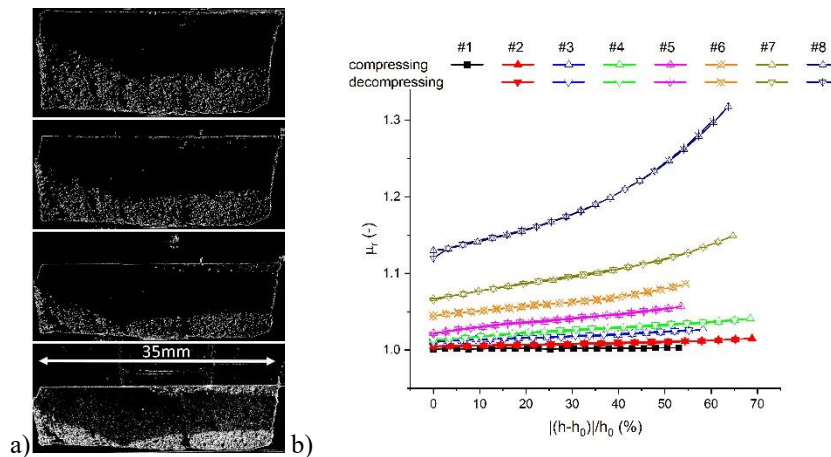


Fig.2. a) Image of the compressed Magnetic Foam, and b) the magnetic permeability versus compression for different filling factors.

The change of magnetic properties with the compression will be later tested in a similar device than the one shown in Fig.1, but modified here for energy conversion from mechanical compression into an electric signal.

- [1] Y. Li, Li J, W. Li and H. Du, A state-of-the-art review on magnetorheological elastomer devices. *Smart Mater. Struct.* (2014) 23 123001. <https://doi.org/10.1088/0964-1726/23/12/123001>
- [2] S. Samal, M. Škodová, L. Abate, I. Blanco. Magneto-Rheological Elastomer Composites. A Review. *Appl. Sci.* (2020) 10, 4899. <https://doi.org/10.3390/app10144899>
- [3] G. Sebald, M. Nakano, M. Lallart, T. Tian, G. Diguët and J.Y. Cavaille. Energy conversion in magneto-rheological elastomers. *Science and Technology of Advanced Materials* 18:1 (2017) 766-778, <https://doi.org/10.1080/14686996.2017.1377590>
- [4] M. Lallart, G. Sebald, G. Diguët, J.Y. Cavaille and M. Nakano. Anisotropic magnetorheological elastomers for mechanical to electrical energy conversion. *J. Appl. Phys.* 122 (2017) 103902. <https://doi.org/10.1063/1.4998999>
- [5] G. Diguët, G. Sebald, M. Nakano, M. Lallart and J.Y. Cavaille. Magnetic particle chains embedded in elastic polymer matrix under pure transverse shear and energy conversion. *Journal of Magnetism and Magnetic Materials* 481 (2019) 39–49. <https://doi.org/10.1016/j.jmmm.2019.02.078>
- [6] G. Diguët, G. Sebald, M. Nakano, M. Lallart and J.Y. Cavaille. Optimization of magneto-rheological elastomers for energy harvesting applications. *Smart Mater. Struct.* 29 (2020) 075017. <https://doi.org/10.1088/1361-665X/ab8837>
- [7] G. Diguët, G. Sebald, M. Nakano, M. Lallart and J.Y. Cavaille. Analysis of magneto rheological elastomers for energy harvesting systems. *International Journal of Applied Electromagnetics and Mechanics* 64 (2020) 439–446. <https://doi.org/10.3233/JAE-209350>

Nozzle design for polymer coating by cold spray process

ELyT Global Resilient polymeric cold spray coating Particle history

C. A. Bernard^{1,2,3}, H. Takana⁴, O. Lame⁵, K. Ogawa^{2,3}, J.-Y. Cavallé²



¹Frontier Research Institute for Interdisciplinary Sciences, Tohoku University, Sendai, Japan

²ELyTMax, UMI 3757, CNRS—Université de Lyon—Tohoku University International Joint Unit, Tohoku University, Sendai, Japan

³Fracture and Reliability Research Institute, Tohoku University, Sendai, Japan

⁴Institute of Fluid Science, Tohoku University, Sendai, Japan

⁵MATEIS, INSA LYON, Lyon, France

Abstract

Recently polymer coating by cold spray attracted more attention worldwide. The interest comes from the potential fabrication of new light-weighted structures which exhibit interesting properties for protection of metallic structures against wear, corrosion, hydrodynamic cavitation etc. However, to obtain a polymer coating by cold spray, relative high temperature of the polymer powder and low particle velocity during spraying is required. Such results can be obtained by the use of a relatively long nozzle, aiming to increasing the particle residence time inside the nozzle.

1. Introduction

During the past years, several research groups have tried to understand the formation of polymer coating by cold spray. Several of these works focus on polymer/polymer interactions [1, 2]. Particularly, they showed the existence of a deposition window for polymer/polymer adhesion evolving with the particle temperature and velocity. Thus, by increasing the particle temperature close to its melting temperature, adhesion can occur at low particle velocity due to the possibility of polymer chains to entangle with the substrate and neighboring particles. In the case of metal/polymer interaction, adhesion between the polymer particle and metallic substrate seems more complex due to the difference in the chemical-physical properties between both materials resulting in a low deposition efficiency [3-6]. A way to allow such interactions to occur is to (almost) melt the particles before their impact on the substrate, as (i) it decreases the stiffness of the polymer and improves its ability to deposit on the surface, and (ii) it decreases the elastic energy responsible for particle rebound. In this research, a new nozzle design on the particle history during cold spray process was investigated.

2. Nozzle design

A long nozzle presenting irregularities in its inner geometry has been studied to develop UHMWPE coating by cold spray. The nozzle consists in two 120 mm long nozzles attached together, leading to a 20% sharp reduction in the nozzle cross-section at the intersection between the two nozzles. As illustrated by Figure 1, at the intersection between the two nozzle sections, some particles exhibit higher temperature. These particles are going upstream due to their rebound at the intersection between the two nozzle sections. Therefore, their residence time increase leading to higher particle temperature but lower velocity (see Figure 2) due to the absence of supersonic flow in the trajectory of rebounded particles.

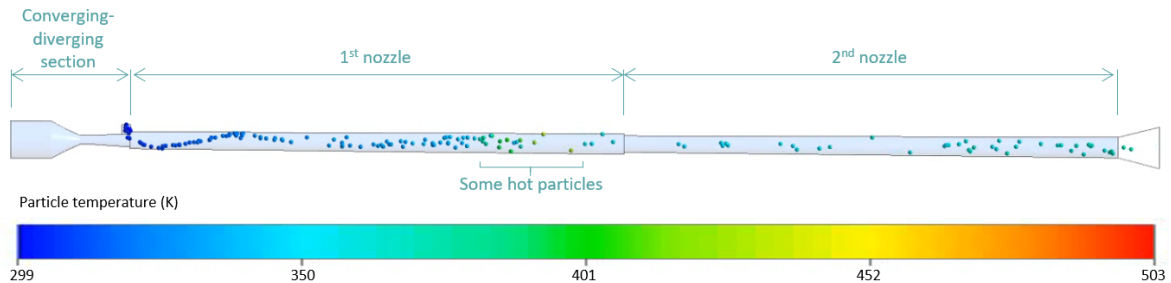


Figure 2: Particle trajectory inside the nozzle. At the intersection between the two nozzle sections, some particles are going upstream. All particles are 60 μm diameter.

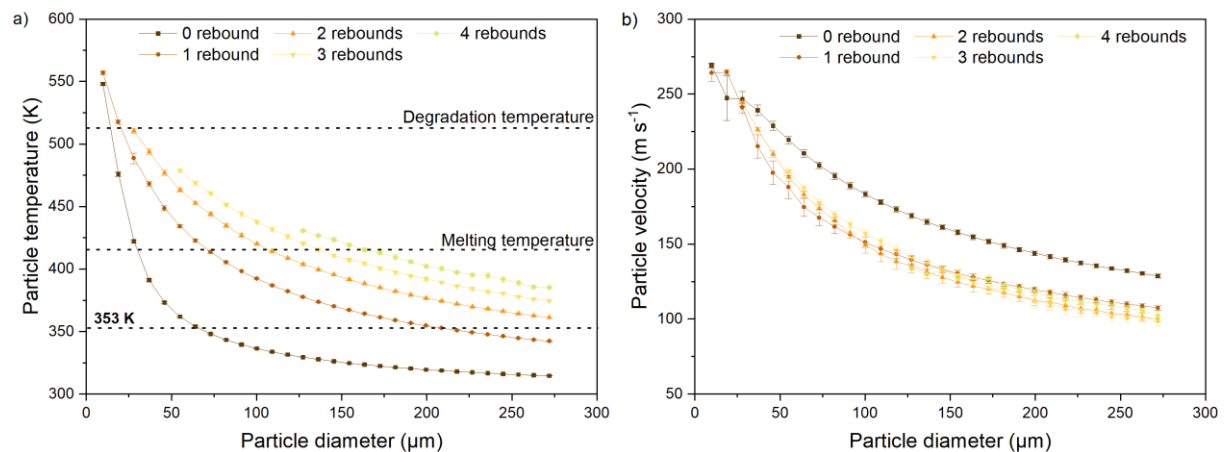


Figure 3: Evolution of the particle temperature and velocity in function of the particle diameter and number of rebound.

Acknowledgement

The authors would like to acknowledge the Institute of Fluid Science at Tohoku University, which supported this research through grants J20Ly03 and J21Ly08 under the label of the LyC Collaborative Research Project.

References

- [1] Khalkhali et al., Surface and Coatings Technology **351**, 99 (2018).
- [2] Khalkhali and Rosthein, Surface and Coatings Technology **383**, 125251 (2020).
- [3] Ravi et al., Journal of Thermal Spray Technology **25**, 160 (2016).
- [4] Ravi et al., Additive Manufacturing **21**, 191 (2018).
- [5] Ravi et al., Surface and Coatings Technology **373**, 17 (2019).
- [6] Sulen et al., Journal of Thermal Spray Technology **29**, 1643 (2020).

Magnetic characterization of Metglas under tensile stress for energy harvesting applications

ELyT Global

Theme: Energy

**Scientific topic: - Materials and structure design
- Simulation and modeling**



¹Univ. Lyon, INSA-Lyon, LGEF EA682, F-69621, France

²Space Structure Lab, Department of aerospace engineering, Tohoku University, Japan

³ELyTMax UMI 3757, CNRS – Université de Lyon – Tohoku University, International Joint Unit, Tohoku University, Sendai, Japan

[*mickael.lallart@insa-lyon.fr](mailto:mickael.lallart@insa-lyon.fr)

Abstract

1. Introduction

Energy harvesting, as an attractive solution to battery replacement for small devices such as sensors, triggered great interest since the usable electrical energy could be converted from ambient energy sources such as vibrations. In that framework, magnetostrictive alloys, one of the main categories of energy harvesting materials, have been used for energy conversion by exploiting Villari effect. Amorphous alloys, providing attractive characteristics such as flexibility, low hysteresis and high magnetostrictive properties, allows converting energy easily. In this study, Metglas 2605SA1 is chosen as the alloy for its high tensile strength. A new setup for magnetic characterization of alloy ribbon is developed. B-H curves measurement for Metglas 2605SA1 ribbon under different tensile stresses in the low frequency range are reported. The curve fitting of hysteresis loops and energy that can be harvested under application of tensile stress is computed theoretically.

2. Experimental

Supports of U-shaped ferrite is 3D printed with PLA. The pillars on both sides of the base allows act as a pulley for applying tensile stress by attaching masses through a cable. Specimen of Metglas 2605SA1 is cut according to the size of the ferrite and placed between them. A primary coil of 80 turns is wound separately and evenly on the two ferrites as shown in Fig.1. (a). A 5Ω resistance is connected to the primary coil, allowing to get the excitation field. A sensing coil (25 turns) is wounded on the specimen, allowing us to get the magnetic flux density. The result of the measurement is plotted in Fig.1. (b).

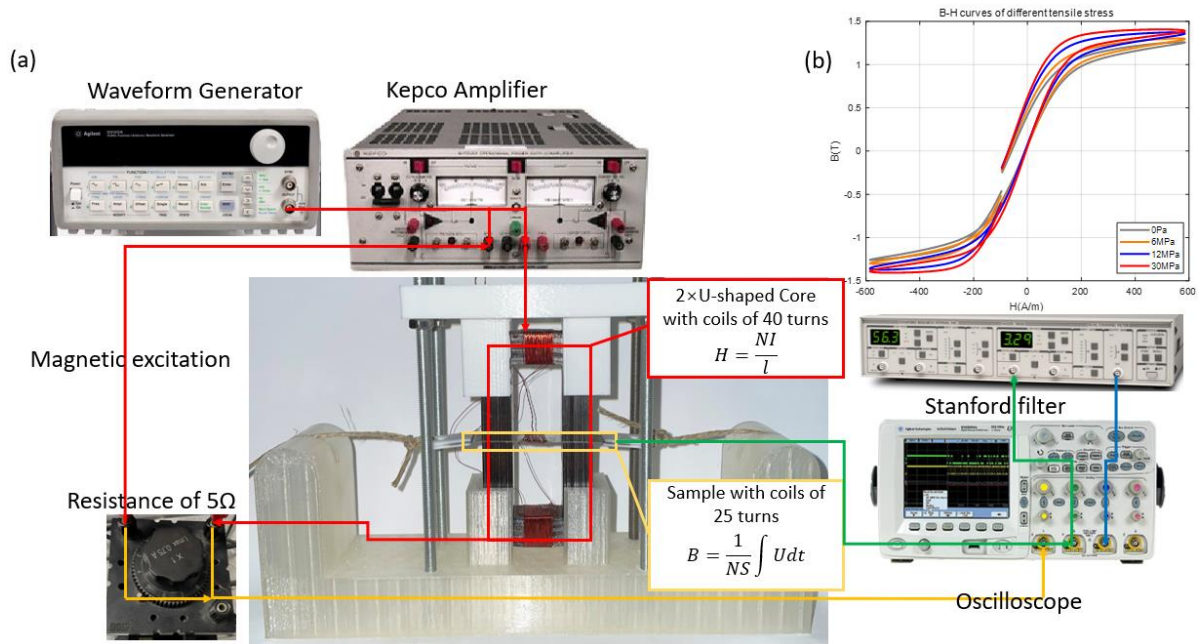


Figure 4 (a) Set up for the specimen characterization and (b) B-H curves of Metglas 2605SA1 under different tensile stress

3. Discussion

The curves fitting is done using hyperbolic tangent functions for B-H curves and are shown in Fig.2. (a). From these curves, the harvestable energy when the tensile stress changes can be derived. Fig.2. (b) shows the total energy available when applying a tensile stress varying from 0 MPa to 30MPa. In this case, the energy density for one positive cycle as shown in Fig.2. (b) is $276 \mu J/cm^3$.

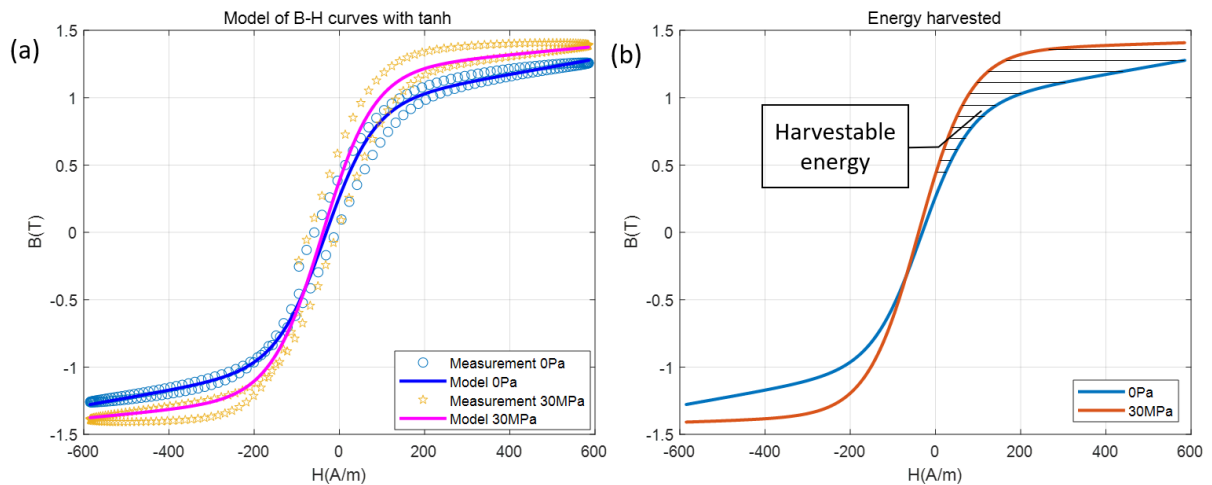


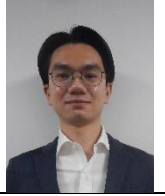
Figure 5 (a) Modeling of B-H curves with tanh function and (b) Energy that can be harvested when tensile stress changes

Acknowledgment

The authors are grateful to Tobias HEROLD, from HITACHI Metglas Europe GmbH, for kindly supplying Metglas 2605 SA1 specimen.

Elastocaloric cooling using natural rubber: material properties, heat transfer and heat losses effects on proof of concept performances

ELyT Global Theme Energy Scientific topic Materials and Simulation

				
Gaël SEBALD ^a	Atsuki KOMIYA ^{a,b}	Jacques JAY ^c	Gildas COATIVY ^d	Laurent LEBRUN ^d
				
Giulia LOMBARDI ^a	Hiba HAISSOUNE ^d	Xuen Sze WAY ^b	Lilian MAURY ^{a,b,c}	

^a ELYTMaX UMI 3757, CNRS – Université de Lyon – Tohoku University International joint Unit, Tohoku University, 980-8577, Sendai, Japan

^b Institute of Fluid Science, Tohoku University, 980-8577, Sendai, Japan

^c Univ. Lyon, CNRS, INSA-Lyon, CETHIL, UMR5008, F-69621, Villeurbanne, France

^d Univ. Lyon, INSA-Lyon, LGEF, EA682, F-69621, Villeurbanne, France

Caloric materials exhibit entropy variations when subjected to a physical quantity, such as electromagnetic field or mechanical stress. They are the main element of alternative refrigeration technique, in an attempt to go beyond the almost solely-used refrigerant gases. Among caloric materials, natural rubber appear to be a promising elastocaloric material offering several advantages, although barely investigated in the view of this application. Large adiabatic temperature variations ($\sim 3^\circ\text{C}$) are however observed when driven at elongation 4 to 6.

After decades of the search of the caloric material offering the highest entropy variation¹, the current scientific questioning go towards the heat transfer mechanisms involved in the application of the materials². When driven with cyclic source (i.e. periodic mechanical stress for an elastocaloric material), time variations of temperature are obtained, thus requiring a system able to convert it into spatial temperature gradient, or a heat transfer between a cold reservoir to a hot reservoir.

Within ELyT Global REFRESH project, supported partially by ANR ECPOR project (LGEF, CETHIL, MATEIS, LTEN, ELYTMaX) and by a JSPS Kakenhi Kiban C project (ELYTMaX, IFS), a focus is done on the development of experimental proof of concept of refrigeration device, assisted by *ad hoc* heat and mass transfer problems models.

Regenerative cooling devices are investigated. It consists of driving an elastocaloric material periodically while moving a fluid in contact at the same frequency. Doing so, under certain operating conditions, it is possible to obtain a net heat flux transported by the fluid along one direction.

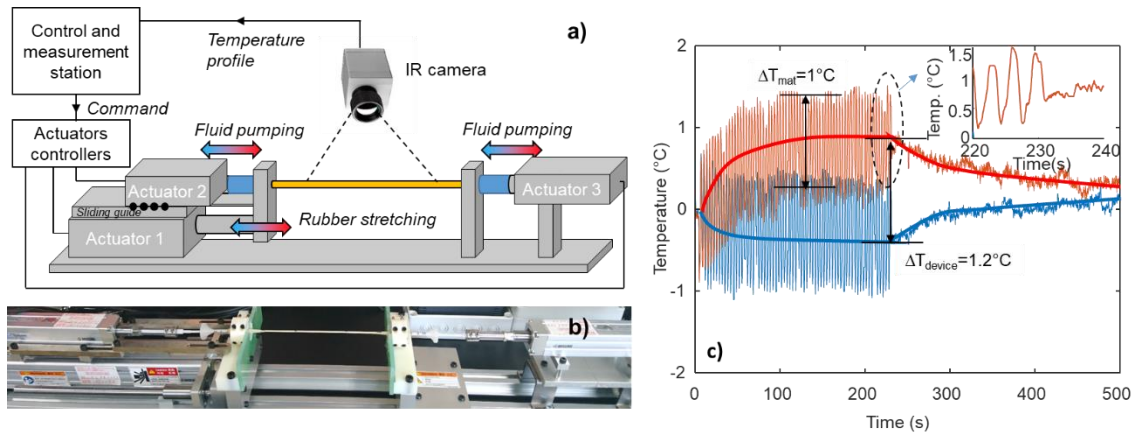


Figure 6: (a) Schematic of a regenerative cooling proof of concept using natural rubber and (b) Photograph of the experiment. (c) Resulting temperature profile with time. After Ref³

The exact mechanism of the heat flux generation remain unclear, the local temperature and heat flux measurement being impossible, and in the current state of the art, only numerical 1D to 3D models are proposed to assess the performance of one configuration, leaving open questions on the optimization routes and models accuracies.

To go beyond the current limitations, it is proposed here the development of analytical solutions of the heat transfer equations, with extensions to arbitrary signals and overall system heat losses and heat reservoir behaviors. It is shown especially some particular working points and details on the heat transfer mechanisms at the interface between fluid and elastocaloric material.

For the regenerative cooling system, it is also investigated experimentally the effect of heat losses on the proof of concept performances, as well as the operating conditions.

From a material point of view, after the determination of the best elongation to be applied, the question of the fatigue life of the material is raised and this latter point is being investigated on a tube geometry. Not only regenerative cooling is applicable to caloric materials, also so-called single stage systems may be investigated (e.g. on NiTi shape memory alloys⁴). It consists of moving mechanically the elastocaloric material when it is at its high temperature in contact to the hot reservoir, and to move it back in contact with the cold reservoir when it is at its lowest temperature.

Within this presentation, a general overview of the collaborative project between France and Japan will be given, with a focus on regenerative cooling systems, both from an experimental and a theoretical point of view.

References

- ¹ B. Nair, T. Usui, S. Crossley, S. Kurdi, G.G. Guzmán-Verri, X. Moya, S. Hirose, and N.D. Mathur, *Nature* **575**, 468 (2019).
- ² À. Torelló and E. Defay, *Int. J. Refrig.* **127**, 174 (2021).
- ³ G. Sebald, A. Komiya, J. Jay, G. Coativy, and L. Lebrun, *J. Appl. Phys.* **127**, 094903 (2020).
- ⁴ H. Ossmer, F. Wendler, M. Gueltig, F. Lambrecht, S. Miyazaki, and M. Kohl, *Smart Mater. Struct.* **25**, 085037 (2016).

Progressive improvement in deposition efficiency for cold sprayed fluoropolymer coatings

ELyT Global Fluoropolymer cold spray Polymer coating

Y. Kaneko¹, W. L. Sulen², C. A. Bernard^{3,4,5}, H. Saito⁵, Y. Ichikawa^{5,6}, K. Ogawa^{4,5}



¹Graduate School of Engineering, Tohoku University, Sendai, Japan

²Department of Occupational Safety and Health, Ministry of Human Resources, Putrajaya, Malaysia

³Frontier Research Institute for Interdisciplinary Sciences, Tohoku University, Sendai, Japan

⁴ELyTMax, UMI 3757, CNRS—Université de Lyon—Tohoku University International Joint Unit, Tohoku University, Sendai, Japan

⁵Fracture and Reliability Research Institute, Tohoku University, Sendai, Japan

⁶PRESTO, Japan Science and Technology Agency (JST), Saitama, Japan

Abstract

Polymer coatings by cold spray present interesting features, such as the possibility to protect metallic substrates or to add functionalities to a structure. However, it is usually characterized by a low deposition efficiency and a weak interface between the substrate and the coating. Many studies were dedicated to understanding the underlying cause of these problems to overcome it. In our previous study, it was found that fluoropolymer cold spray was able to deposit on metallic substrates by adding nano-sized ceramics and grooving the substrate by laser texturing before spraying. For further efficiency, we tried to deposit fluoropolymer on Cu and Ti bond coat and improvement of nano-ceramics mixing method. It leads to a progressive improvement of the deposition efficiency and the adhesion strength.

1. Introduction

Fluoropolymers have a large range of possible applications due to interesting properties. However, manufacturing fluoropolymer coatings on metallic or other substrates is difficult due to the inert property of the polymer and high temperature requirement. Among the existing methods to deposit fluoropolymer on metallic substrates, electro-spraying fluoropolymer onto laser textured substrate showed great promises but appears time consuming. Moreover, a multi-steps process also increases the production cost. Thus, we have developed a way to deposit fluoropolymer by cold spray, leading to a shorter processing time.

A previous study showed that grooving metallic substrates by laser texturing, and addition of fumed nano alumina (FNA), led to a successful deposition of Ultra-High Molecular Weight Polyethylene (UHMWPE) [1, 2], and have a specific effect on the deposition of Perfluoro alkoxy alkane (PFA) by cold spray [3]. It suggests that the deposition mechanism of polymer consists in (i) diving of the polymer particles into the groove and interlocking mechanically with the substrate (first layer), and (ii) deposition upon the deposited powder enhanced by the presence of the nano-sized ceramics (coating build-up) [3]. In this study, we tried to cold spray metallic bond coat prior to the polymer, and reconsidered the mixture PFA and FNA to achieve further efficiency.

2. Deposition efficiency of cold sprayed fluoropolymer on metallic bond coat

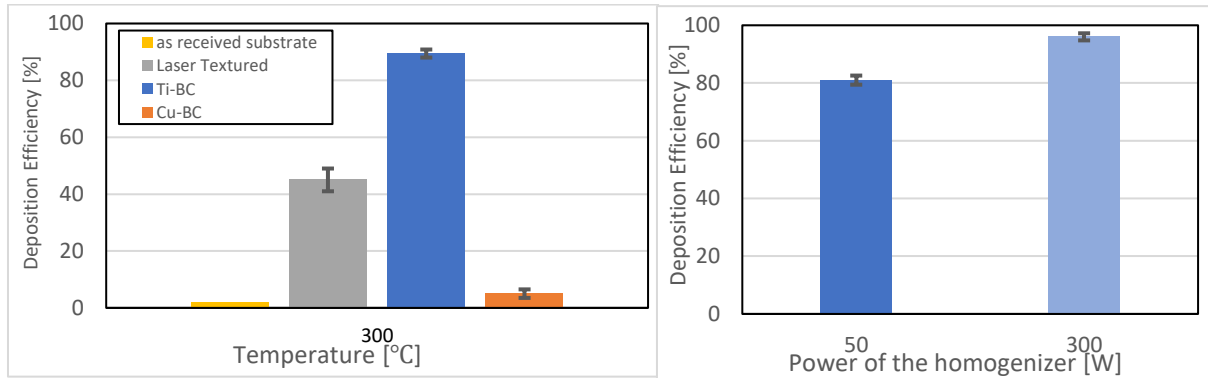


Figure 1: Deposition efficiency of PFA particles mixed with FNA sprayed at 300°C on as received substrate, laser textured substrate, and on Cu-BC and Ti-BC. Figure 2: The difference of deposition efficiency of PFA sprayed at 350°C, when changing the power of homogenizer, sprayed on Ti-BC.

Titanium or copper powder was cold sprayed on each steel substrate as a bond coat (Ti-BC and Cu-BC). On top of the metallic bond coat, PFA was sprayed at 300°C. 5wt% of FNA was mixed with the PFA by a homogenizer with ethanol suspension. Figure 1 shows an enormous deposition efficiency of cold sprayed PFA on bond coats, which are compared with the results in our previous study, that we sprayed on as received substrate and laser textured substrate. Figure 1 shows the deposition efficiency of PFA when sprayed at 300°C on different substrate surfaces. Especially, Ti-BC achieved an outstanding result where the deposition efficiency reached 81%, which is still hard to see even on metal-metal cold spray. These results were achieved by changing the homogenizer's output power from 50 W to 300 W, which allows enough mixing of the PFA and FNA. We further improve the deposition efficiency up to 96% by spraying at 350°C (Figure 2). Furthermore, adhesion strength was improved up to 3.2 MPa when PFA was sprayed at 400°C, while only 1.2 MPa was achieved on the laser textured substrate, or even unable to measure when sprayed on as received substrate.

References

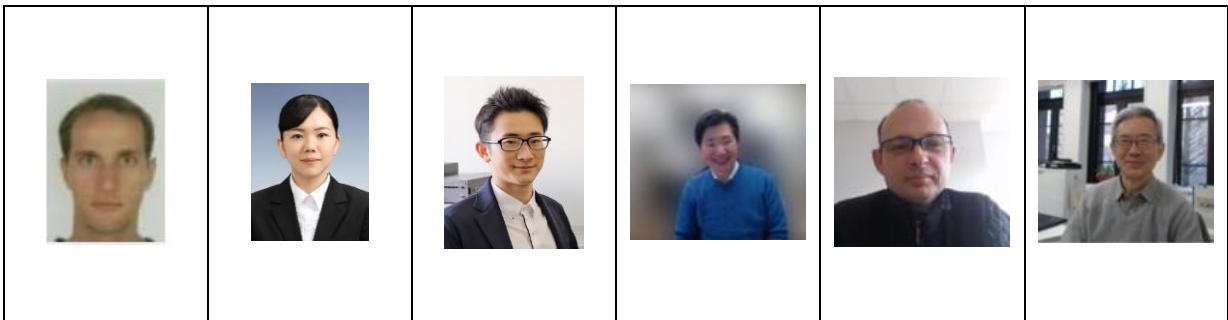
- [1] K. Ravi et al., J. Therm. Spray Technol. 24 (2015) 1015–1025.
- [2] K. Ravi et al., J. Therm. Spray Technol. 25 (2016) 160–169.
- [3] W.L. Sulen et al., Key Eng. Mater. 813 (2019) 141-146

EMAR monitoring system of a carbon steel thinning in a corrosive environment

ELyT Global

Project PYRAMID (Piping sYstem, Risk management on wAll thinning Monitoring and prediction)

Theme: Materials and structure design



Gildas Diguët¹, Hina Miyauchi¹, Sho Takeda¹, Tetsuya Uchimoto^{1,2}, Nicolas Mary², Toshiyuki Takagi^{2,3,4}

¹*Institute of Fluid Science, Tohoku University, Sendai, Japan*

²*ELyTMaX UMI 3757, CNRS – Université de Lyon – Tohoku University, International Joint Unit, Tohoku University, Sendai, Japan*

³*Tohoku Forum for Creativity, Organization for Research Promotion, Tohoku University, Sendai, Japan*

⁴*Center for Fundamental Research on Nuclear Decommissioning, Tohoku University, Sendai, Japan*

Abstract

The thinning of the pipes has different origins: mechanical erosion, chemical attack, [1-2]... To prevent the failure of pipes in industrial installation, it is necessary to monitor the present state of degradation of these pipes. To reduce the cost due to the removal and remounting of the pipes, such monitoring would be preferentially performed with a remote device. ElectroMagnetic Acoustic Transducer (EMAT) technique [3] is a good candidate for this objective: this Non-Destructive Technique (NDT) has the advantage of simplicity since it does not require any couplant medium, unlike the PieZoelectric Transducer (PZT).

To test this capacity of in-situ monitoring, a test Carbon Steel plate specimen was placed in an electrochemical cell to control the corrosion and monitor through the pick-up current the amount of material removed. The specimen is the working electrode, the counter electrode (graphite) and the reference electrode (Ag/AgCl/Saturated KCl). The solution for the corrosion was H₂SO₄ with a concentration of about 0.28 ml/L, and the pH was measured to be about 2.3 at 23.5°C.

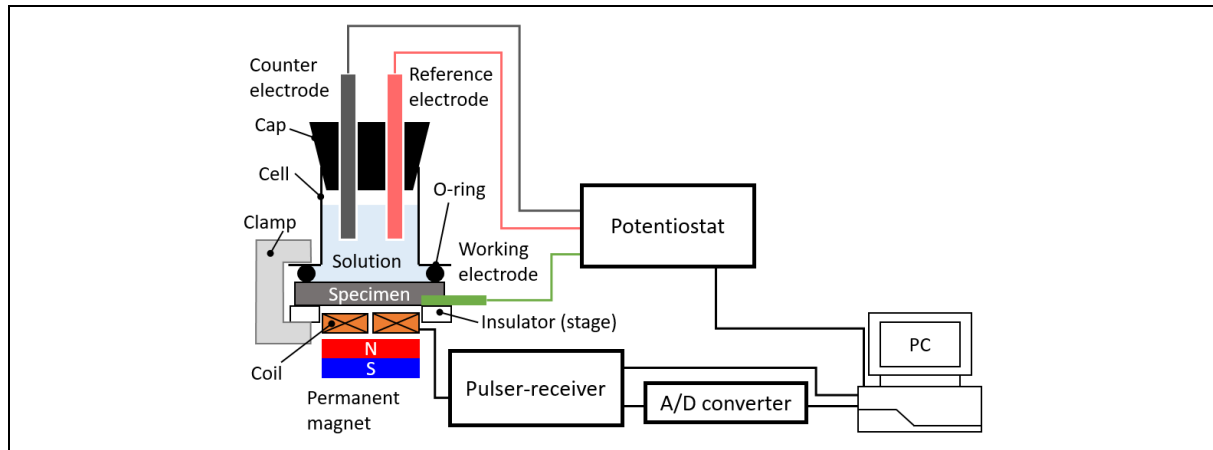


Fig. 1. Set-up for electrochemical and EMAR measurement on the same sample during the corrosion testing

Using the Resonant technique, the EMAR, the technique consists of sweeping the frequency and collecting the signal at each frequency. To separate the two parts of this experiment, the electrochemical cell corroding the specimen, is placed on the top surface, whereas the EMAR system: coil and magnets were placed below the specimen to monitor the specimen thickness as seen in Fig.1.

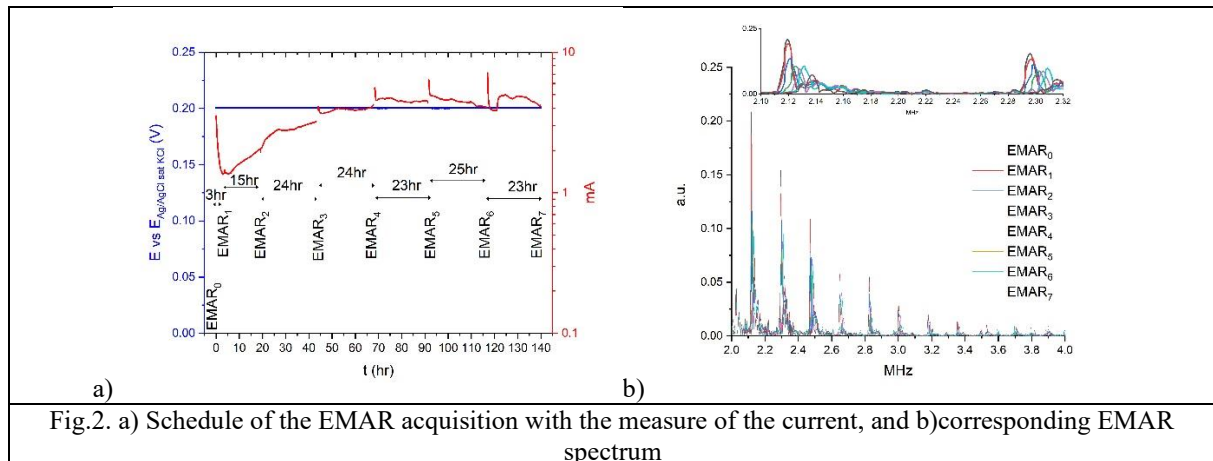


Fig.2. a) Schedule of the EMAR acquisition with the measure of the current, and b) corresponding EMAR spectrum

The experiment was performed for several days (Fig2a) to get significant specimen thinning. At different steps, EMAR signal was acquired for the monitoring as seen in Fig2b.

As time passed, the peaks of the EMAR spectrum were shifted to a higher frequency. According to the EMAR theory, the peaks are located at an integer multiple of resonant frequency $f_0 = C_T/2h$; where C_T is the sound velocity of the transverse mode and h is the thickness. The fact that f_0 is increasing is revealing a reduction of the specimen thickness.

[1] I. S. Cole, D. Marney. The science of pipe corrosion: A review of the literature on the corrosion of ferrous metals in soils. Corrosion Science 58 (2012) 1–11. <https://doi:10.1016/j.corsci.2011.12.001>

[2] Z. Panossian, N. L. de Almeida, R. M. Ferreira de Sousa, G. de Souza Pimenta, L. B. S. Marques. Corrosion of carbon steel pipes and tanks by concentrated sulfuric acid: A review. Corrosion Science 56 (2012) 5–16. <https://doi:10.1016/j.corsci.2012.01.025>

[3] M. Hirao, H. Ogi. EMATs for science and industry, non-contacting ultrasonic measurements. Springer Science & Business Media. 2003.

Heat engine based on MultiPhysic Memory Alloys and pyroelectric conversion for thermal energy harvesting

ELyT Global Theme: Energy Scientific topic: - Materials and structure design - Simulation and modeling



¹Univ. Lyon, INSA-Lyon, LGEF EA682, F-69621, France

²Institute of Fluid Science, Tohoku University, Sendai, Japan

³ELyTMaX UMI 3757, CNRS – Université de Lyon – Tohoku University, International Joint Unit, Tohoku University, Sendai, Japan

⁴Institute of Multidisciplinary Research for Advanced Materials, Tohoku University, 2-1-1, Katahira, Aoba-ku, Sendai 980–8577, Japan

⁵Institute of Microstructure Technology (IMT), Karlsruhe Institute of Technology (KIT), Hermann-von-Helmholtz-Platz 1 76344 Eggenstein-Leopoldshafen

[*mickael.lallart@insa-lyon.fr](mailto:mickael.lallart@insa-lyon.fr)

Abstract

With the development of ultralow-power wireless devices such as autonomous sensors, ensuring long-term stable power supply has become an issue. Conventional solutions using batteries show strong limits when dealing with remote and/or relatively harsh environments due to the self-discharge of such devices ([1]). To address these restrictions, energy harvesting, consisting of using energy directly available from the device's surroundings, has been investigated for many years now ([2]). Among available sources, thermal energy is of particular interest due to its wide availability and high energy levels. Conventional thermal energy harvesting solutions, based on thermoelectric modules, however feature severe shortcomings due to their high thermal conductivity that prevents energy from entering the material ([3]). To address this issue, disruptive approaches based on heat engines have been proposed ([4], [5]). This talk will present the design and analysis of a heat engine based on MultiPhysic Memory Alloys that links the structural, magnetic and thermal domains ([6]). While most of previously designed heat engines relies on an electromechanical transducer (e.g., magnetodynamic or piezoelectric) for converting the thermally generated vibrations into electricity, the present concept takes advantage of pyroelectric elements for directly converting the time-domain temperature variation (obtained from temperature gradients) into electricity, hence shortening the energy path for higher efficiency. The principles of the proposed heat engine, shown in Figure 7, are as follows:

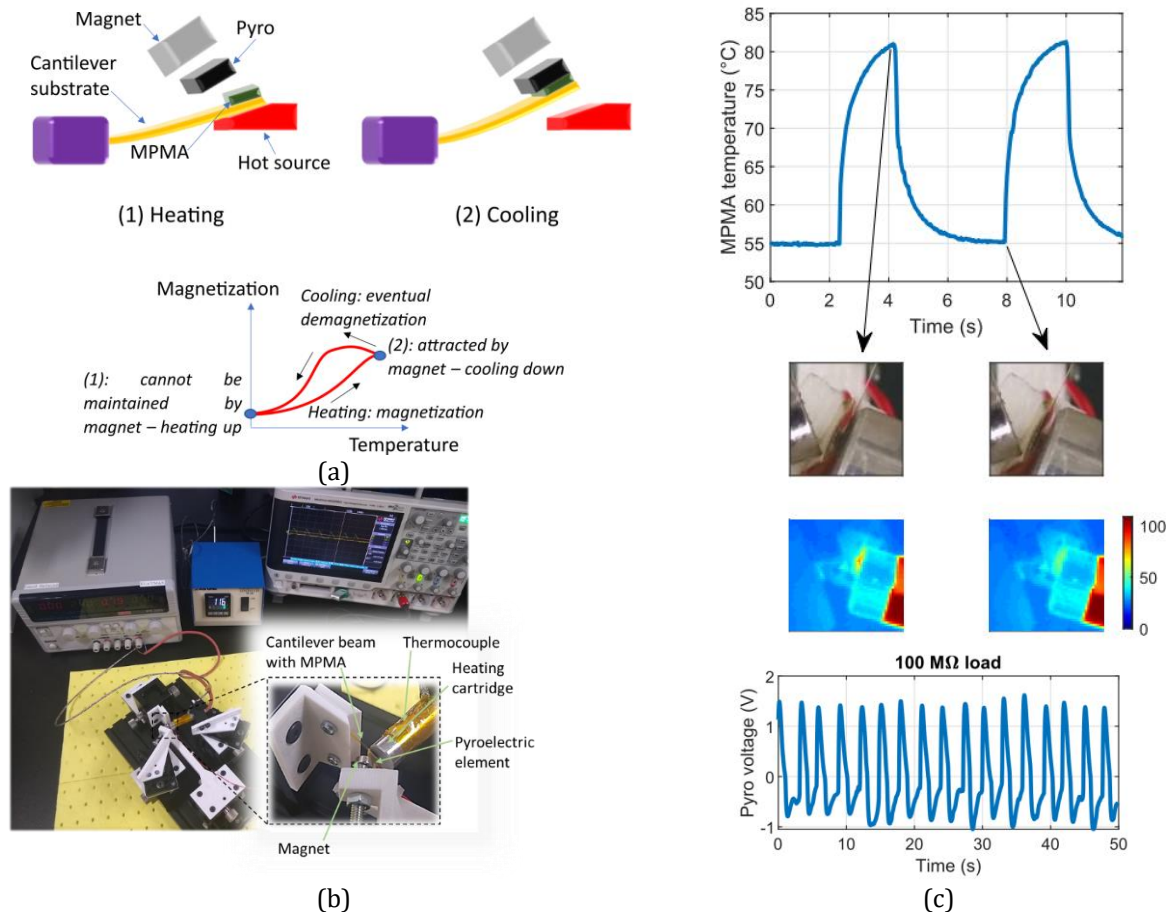


Figure 7. MPMA/pyroelectric heat engine: (a) schematics, (b) implementation and (c) experimental response

1. In contact with the hot source, the MPMA heats up, gaining magnetic properties
2. Once the magnetization is high enough to counteract the restoring force of the beam, the MPMA is attracted by the magnet and meets the pyroelectric element.
3. Once in contact, the stored heat in the MPMA is transferred to the pyroelectric element, which converts part of this thermal energy into electricity. Meanwhile, the MPMA cools down and progressively loses its magnetic properties.
4. When the MPMA magnetic susceptibility is no longer sufficient to maintain magnetic force able to counteract the restoring force of the beam (MPMA temperature sufficiently low), the cantilever beam pulls the material back to the hot side, thus restarting a new cycle.

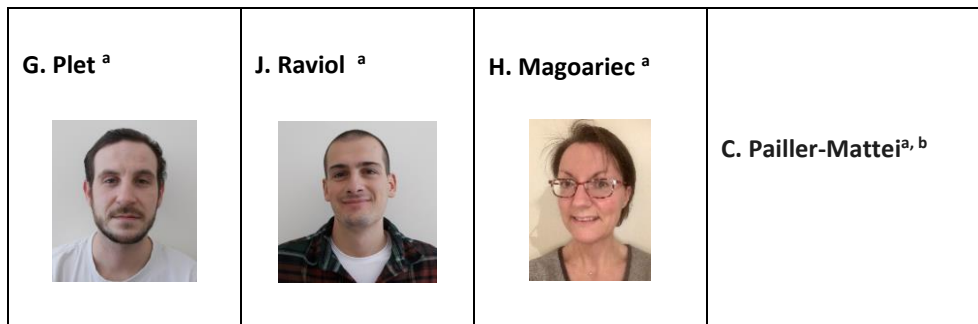
Compared to previous works, it is shown that such an approach permits gains up to one order of magnitude in terms of output or energy power densities ($1.17 \mu\text{W}\cdot\text{cm}^{-3}$ considering MPMA, beam and transducer volume).

The authors gratefully acknowledge the support of JSPS through invitational fellowship grant number L19530 and postdoctoral fellowship grant number PE19727, as well INSA-Lyon for its support through the CRCT program. This work has been partly performed in the framework of the TATAMI project funded under the Collaborative Research Project of Lyon Center, IFS, Tohoku University (project code J20Ly05) and supported by IFS Lyon Center and ELYT Global IRN (projects TATAMI and MISTRAL).

- [1] J. VanZwol, Power Electronics Technology, July 2006, pp. 4045, 2006.
- [2] F. K. Shaikh and S. Zeadally, Ren. Sust. Energy Rev., Vol. 55, pp. 1041–1054, 2016.
- [3] G. Sebald, D. Guyomar and A. Agbossou, Smart Mater. Struct., Vol. 18, 125006, 2009.
- [4] M. Gueltig, F. Wendler, H. Ossmer, M. Ohtsuka, H. Miki, T. Takagi and M. Kohl, Adv. Energy Mater., Vol. 7, 1601879, 2017.
- [5] J. Joseph, M. Ohtsuka, H. Miki and M. Kohl, Joule, Vol. 4, pp. 2718-2732, 2020.
- [6] M. Lallart, H. Miki, L. Yan, G. Diguët and M. Ohtsuka, J. Phys. D: Appl. Phys., Vol. 53, 345002, 2020.

Towards the *in situ* mechanical characterization of cerebral aneurysms: first steps of experimental and numerical designs.

ELyT Global
Biomechanics
Cerebral aneurysms



Affiliation

^aLaboratoire de Tribologie et Dynamique des Systèmes, UMR CNRS 5513, Ecole Centrale de Lyon, France

^bUniversity of Lyon, University Claude Bernard Lyon 1, IPSB-Faculty of Pharmacy, France

Abstract

Introduction

An intracranial aneurysm is a structural deformation of the cerebral arterial wall. The prevalence of this pathology is 5 % worldwide. The rate of rupture is between 0.8 % and 4 % and causes death in 50 % of cases [1].

This work deals with the mechanical characterisation of unruptured cerebral aneurysms. Unruptured aneurysms are generally found out accidentally during a routine imaging clinical examination and act as major public healthcare issue. [2]. Prognosis of aneurysmal rupture remains very difficult to predict notwithstanding continuous progress in its medical and surgical management. It is currently mainly based on morphological analysis of the aneurysms shape, combined with epidemiological patient criteria. Aneurysm wall biomechanics is not yet integral part of aneurysm rupture risk evaluation, even though the rupture is due to a mechanical deterioration of the vascular wall structure.

This study is a part of a larger project, the MECANEV project supported by Auvergne-Rhône-Alpes Region, whose aim is to quantify, *in vivo* and *in situ*, the mechanical behaviour of unruptured cerebral aneurysms. We present here the first steps of the experimental device design aimed at inducing a wall deformation on 3D printed aneurysm phantom. We also present the first numerical simulations of fluid structure interactions, aimed at sizing this experimental device.

Material and Methods

A pathological artery phantom was modeled using CATIA software, with the aneurysm located on the arterial bifurcation (Figure 1). The aneurysm's diameter is 12 mm, and the thickness of the arterial wall is 600 μm . This phantom was printed using stereolithography and led to an isotropic material with a Young modulus of 2.5 MPa (this modulus was identified using an indentation test for soft tissues).

This phantom was fixed in a tank and the complete fluidic circuit was being supplied by a pump at a flow rate of 500mL/min controlled by flowmeters at the inlet and outlet of the bifurcation (Figure 2). An entry point allowed the insertion of a deformation device into the aneurysm. This device was being supplied by a syringe pump pulsing a physiological fluid allowing to deform the aneurysm wall. These generated deformations were recovered by a stereo correlation system.

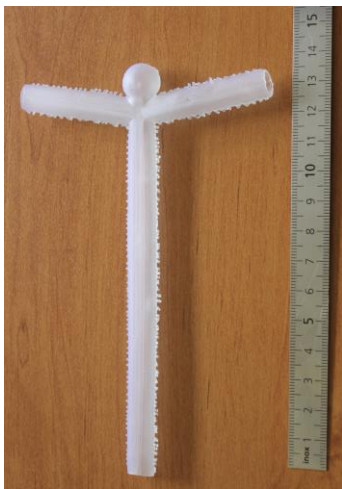


Figure 1: Phantom artery

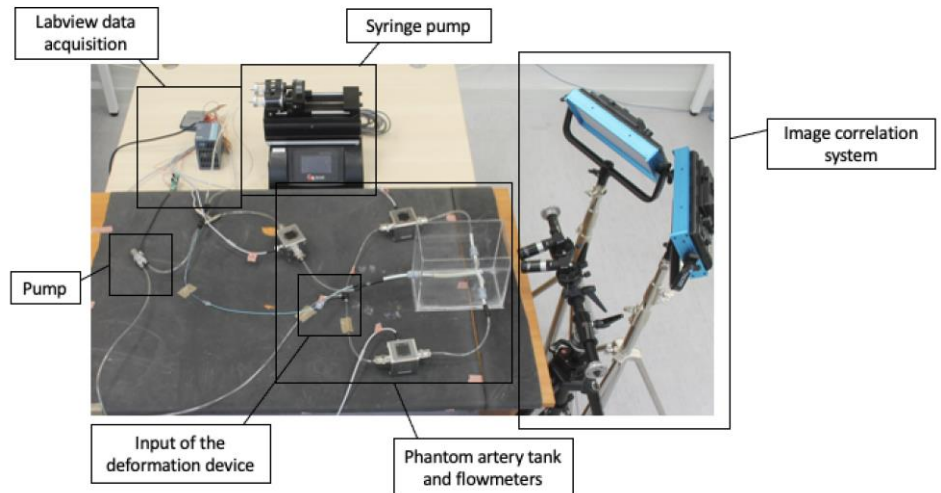


Figure 2: Experimental set-up

The previous arterial model designed on Catia was then applied on COMSOL Multiphysics Software in balance with the material and experimental. The artery's domain was modelled as an elastic linear isotropic material, the artery main flow was considered as a water laminar flow and the external domain was modelled as air. The flow pulsated by the deformation device was considered miscible with the artery main flow. As a consequence, the loading device was modelled with the Solid Mechanics module and a speed disruption was prescribed at the device exit that stood for the pulsated fluid. Fluid-solid interaction between the flows and the artery wall were considered using the dedicated fluid-structure interaction module. We worked with a 4 seconds flow simulation; the speed value increased from 0 to 1 second, reached and stayed at the willing value from 1 to 4 seconds.

For the fluid-structure interaction we considered a weak coupling: we computed all the flow in a time dependant step and then used the results in a stationary step. We were mainly interested in the resulting arterial wall displacements.

Results and discussion

Simulations were performed for an artificial artery with a 2.5 MPa Young Modulus, a 500 mL/min flow rate for the artery flow and a 150 mL/min flow rate for the pulsated flow.

Figure 3a shows the displacement profile at 1 second. Figure 3b shows the displacement of the inner artery wall.

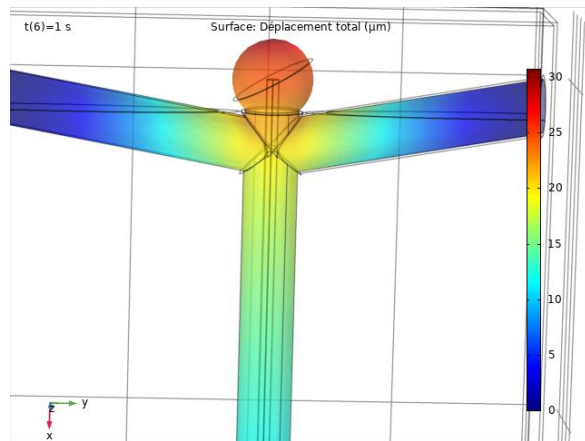


Figure 3a: Displacement profile at 1 second

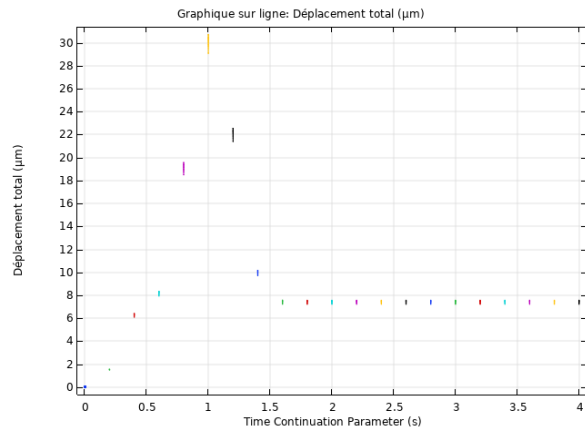


Figure 3b: Inner artery wall displacements

The maximum displacement observed is around 30 μm in the pulsated flow area. It can be noticed that the displacement decreases between 1 and 4 seconds to reach a peak value of 8 μm due to the flow behaviour.

Further improvements of the experimental and numerical models are planned: work on a more biofidelic phantom model, work on a hyperplastic anisotropic material for the artery in order to be closer from the real structure, use a non-Newtonian flow instead of water for the blood flow model and use a patient-specific model for the artery/aneurysm [3], [4].

Acknowledgment

The authors thank Chloé Dumot (Neurochirurgie, Hospices Civils de Lyon), Bertrand Houx (Ecole Centrale de Lyon), and Pascale Kulisa (Laboratoire de Mécanique des Fluides et d'Acoustique, UMR CNRS 5509, Ecole Centrale de Lyon, UCBLyon I, INSA 36 Avenue Guy de Collongue, 69134 Ecully Cedex, France) for their technical support and helpful discussions concerning the clinical aspects, the 3D printing process, and the fluid structure interaction simulations, respectively.

References

- [1] Sanchez, Mathieu, Identification du risque individuel de rupture des anévrismes cérébraux intra crâniens: une approche biomécanicienne, Laboratoire de mécanique et génie civil de Montpellier, 2012. 9
- [2] Vlak, M.H., Algra, A., Brandenburg, R., Rinkel, G.J., 2011. Prevalence of unruptured intracranial aneurysms, with emphasis on sex, age, comorbidity, country, and time period: a systematic review and meta-analysis. *The Lancet Neurology* 10, 626–636. [https://doi.org/10.1016/S1474-4422\(11\)70109-0](https://doi.org/10.1016/S1474-4422(11)70109-0)
- [3] Gerhard A. Holzapfel, Thomas C. Gasser, Ray W. Ogden. A New Constitutive Framework for Arterial Wall Mechanics and a Comparative Study of Material Models. *Journal of elasticity and the physical science of solids*, 2000, 61 (1), pp.1-48. hal-01297725
- [4] G. Mach^{1,5*}, C. Sherif^{2,5}, U. Windberger^{3,5}, R. Plasenzotti^{3,5}, A. Gruber^{4,5}. A Non Newtonian Model for Blood Flow behind a Flow Diverting Stent. 2016, Munich COMSOL Conference

Structured hexahedral meshing of a physiological model of vessel n-furcation for computational fluid dynamics

ELyT Global Engineering for health Simulation & Modeling

				
Méghane Decroocq ^{1,2,3}	Erwan Maury ¹	Prof. Guillaume Lavoué ²	Prof. Carole Frindel ^{1,3}	Prof. Makoto Ohta ³

¹ CREATIS, INSA Lyon, France

² LIRIS, INSA Lyon, France

³ ELyTMaX UMI 3757, CNRS – Université de Lyon – Tohoku University International joint Unit, Tohoku University, 980-8577, Sendai, Japan

Abstract

In the biomedical engineering field, computational fluid dynamics (CFD) simulation enables to study the relation between vessel geometry and blood flow. The method commonly used to produce a patient-specific boundary surface from medical images requires several steps [1] (e.g image filtering and segmentation, surface meshing, smoothing). As a result, the accuracy of the reconstructed surface is strongly impacted by the image resolution, noise and artifacts. More specifically, if the tubular and connected aspect of vessels can be used to help surface modeling, the parts where the mother vessel splits into 2 daughter vessels (bifurcations) or more (n-furcations) are the most challenging for the reconstruction [2].

Moreover, the resolution of fluid dynamics equations in three dimensions requires the fluid domain to be divided into cells to form a discretized computational mesh. Due to their ability to mesh automatically very complex shapes, unstructured meshes (with unorganized cells) are widely used for vascular networks with bifurcations, although they lead to higher computational cost and less accurate results [3]. The complex topology of vessel n-furcations is the main obstacle to the creation of more efficient meshes, such as structured hexahedral meshes [4].

Zakaria et al. [5] proposed a parametric model for non-planar bifurcations, illustrated in Fig. 1 a). Their model was validated in regard with both the anatomy and the blood velocity and pressure maps produced by numerical simulation and showed a good agreement with real cerebral bifurcations. It requires only a few physiological parameters (5 sections) and seems well suited for reconstruction of

bifurcations from incomplete or noisy data. In this work, we introduce an extension of the model of Zakaria et al. to planar n-furcations, and method to mesh it with structured hexahedral, flow oriented cells, as illustrated in Fig. 1 b).

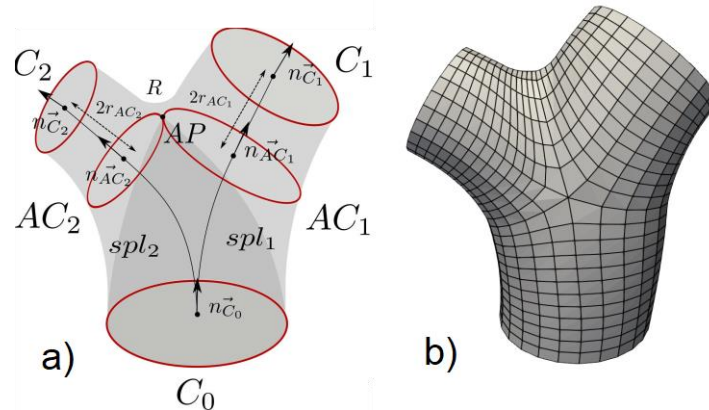


Fig 1. Bifurcation model and surface mesh produced with our method.

The proposed meshing relies on three successive steps; computation of the branch separation planes, initialization of the meshing grid and projection on the surface of the model. The mesh is then refined by node relaxation and local smoothing of the apical region. The cells of the produced mesh have a high geometrical quality, and requires less elements to reach mesh independency for numerical simulation. The n-furcation mesh can easily be extended with inlet and outlet vessels to model the whole vascular network.

Acknowledgement

This work has been supported by the Région Auvergne-Rhône-Alpes through the “Pack Ambition Internationale” action. The thesis of M. Decroocq is co-funded by INSA Lyon and ElyTMax.

References

- [1] Lesage, D., Angelini, E. D., Bloch, I., & Funka-Lea, G. (2009). A review of 3D vessel lumen segmentation techniques: Models, features and extraction schemes. *Medical image analysis*, 13(6), 819-845.
- [2] 6,690,816 : "Systems and methods for tubular object processing" Stephen R. Aylward, Elizabeth Bullitt, Daniel Fritsch, Stephen M. Pizer, February 2004
- [3] Vinchurkar, S., & Longest, P. W. (2008). Evaluation of hexahedral, prismatic and hybrid mesh styles for simulating respiratory aerosol dynamics. *Computers & Fluids*, 37(3), 317-331
- [4] Ghaffari, M., Hsu, C. Y., & Linninger, A. A. (2015). Automatic reconstruction and generation of structured hexahedral mesh for non-planar bifurcations in vascular networks. In *Computer Aided Chemical Engineering* (Vol. 37, pp. 635-640). Elsevier.
- [5] Hasballah Zakaria, Anne M Robertson, and Charles W Kerber. A parametric model for studies of flow in arterial bifurcations. *Annals of biomedical Engineering*, 36:1515, 2008

Endothelial cells distribution after the flow exposure experiment

ELyT Global Medical Application Engineering for Health

	Zi WANG ^{1,2}		Yukiko KOJIMA ^{1,3}		Narendra Kurnia PUTRA ⁴		Assistant Prof. Hitomi ANZAI ¹
	Prof. Jean- Paul RIEU ⁵		Hiroki TANIHO ⁶		Prof. Naofumi OHTSU ⁶		Prof. Makoto OHTA ¹

Affiliation

¹Institute of Fluid Science, Tohoku University, Japan

²Graduate School of Biomedical Engineering, Tohoku University, Japan

³Graduate School of Engineering, Tohoku University, Japan

⁴Instrumentation and Control Research Group, Faculty of Industrial Technology, Institut Teknologi Bandung, Bandung, Indonesia

⁵Institut Lumière Matière (Institute of Light and Matter, ILM, UMR 5306), Université Claude Bernard Lyon 1

⁶Faculty of Engineering, Kitami Institute of Technology, Japan

Abstract

Background:

Cardiovascular diseases (CVDs), such as aneurysms and stenosis, are one of the most life-threatening disease world widely [1]. Millions of deaths caused by the CVDs annually. Stent implantation has been one of the primary and the promising treatments for the stenosis and other CVDs as a low invasiveness and quick operation. This metal mesh structure of stent is usually deployed at the target position on the blood vessel re-open the narrowed the lumen as a scaffold. The stent expansion procedure during the operation may cause the endothelium lesion by the mechanical force. To repair the lesion, quick endothelialization process is necessary.

There are several ways for the quick endothelialization such as surface treatment and flow control. Ohtsu et. al., developed anodization method to improve the cells behavior on the stent surface [2]. However, the anodization method was examined under without flow condition.

Recently, we developed a chamber with placement of stent strut to find the EC response by the stent struts and the flow. An in-vitro parallel flow chamber could control the flow condition as a certain value according to the inlet flow drives the attention to investigate ECs response to WSS [3].

Objective:

To evaluate the anodization method on stent endothelialization enhancement after the flow exposure experiment, observations of ECs distribution on the surfaces of stent strut (with/without anodization) was performed.

Method:

To evaluate the ECs adhesion enhancement, bare metal stent struts (without surface treatment, as control) and anodized stent strut were prepared and placed on the ECs layer and perform flow exposure using the flow chamber. ECs were exposed for 24 hours under WSS condition of 2 Pa. Flow conditions inside the chamber were analyzed by using computational fluid dynamics (CFD) simulation. After fluoresce stain, ECs distributions were observed on the surfaces of stent struts.

Result:

The endothelialization rate, represented by ECs density, on the anodized side surfaces of the stent struts is higher than the without anodization stent strut side surfaces (Figure 1).

Conclusion:

The anodization method on stent struts surface treatment could enhance ECs adhesion then may accelerate endothelialization after stent implantation.

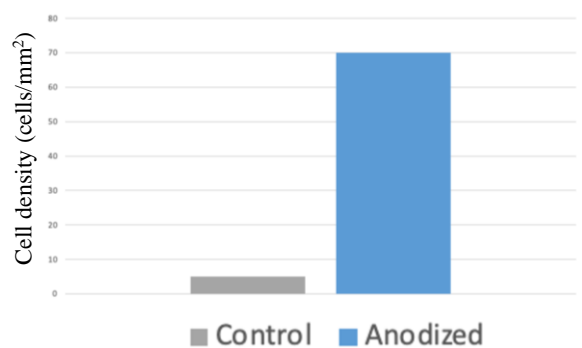


Figure 1, ECs density on the surface of stent strut, 24 hours flow exposure experiment, one stent strut, N=1

References:

- [1] J. A. Finegold, P. Asaria, and D. P. Francis, ‘Mortality from ischaemic heart disease by country, region, and age: statistics from World Health Organisation and United Nations’, *Int. J. Cardiol.*, vol. 168, no. 2, pp. 934–945, Sep. 2013, doi: 10.1016/j.ijcard.2012.10.046.
- [3] K. Yamasaki, M. Hirano, S. komai, H. Taniho, and N. Ohtsu, ‘Cell responses on Ni-free anodized layer of NiTi alloy with various surface morphologies’, *Appl. Surf. Sci.*, vol. 531, p. 147351, Nov. 2020, doi: 10.1016/j.apsusc.2020.147351.
- [2] H. Anzai *et al.*, ‘Endothelial cell distributions and migration under conditions of flow shear stress around a stent wire’, *Technol. Health Care Off. J. Eur. Soc. Eng. Med.*, vol. 28, no. 4, pp. 345–354, 2020, doi: 10.3233/THC-191911.

In situ characterization and modeling of the deformation and fracture of an aluminum foam

ELyT Global

Scientific topic: - Materials and structure design - Simulation and Modeling"

	S. Dancette *		Y. Amani *		J. Luksch **
	A. Jung **		E. Maire *		

Affiliation

* Univ Lyon, INSA Lyon, CNRS UMR5510, Laboratoire MATEIS, F-69621, Villeurbanne Cedex, France

** Saarland University, Lehrstuhl für Technische Mechanik, Campus A4.2, 66123 Saarbrücken, Germany

Abstract

The tensile deformation and fracture of an aluminum foam is investigated in this work. The mechanical behavior is studied at two scales:

(a) the struts constituting the foam are studied individually first [1] using a micro-tensile machine designed by Jung et al. [2] and Digital Image Correlation. The 3D structure of the studied struts was imaged first by X-ray tomography to reveal their actual 3D geometry as well as the local presence of intermetallic particles in the microstructure.

(b) The 3D deformation and damage of a whole block of foam is then investigated by X-ray tomography under tensile deformation [3]. This was carried out using both (i) high resolution stitching tomography of the initial state of the foam in order to capture its microstructural details and (ii) lower resolution tomography to image its deformation and damage in situ during tension.

A Finite Element (FE) model of the foam behavior is then build based on the actual 3D structure obtained by tomography. The image-based FE model allows quantitative consideration of the local presence of brittle intermetallic particles in the prediction of deformation and damage using a new microstructure-informed Gurson-Tvergaard-Needleman model. It allows a good discrimination of potential fracture zones in the foam.

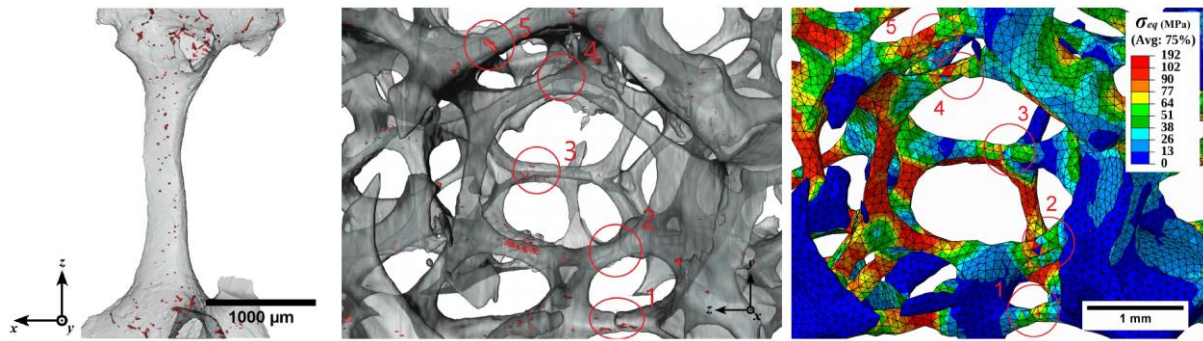


Figure: Intermetallic particles in a single strut (a) and in the foam (b) as observed by tomography. (c) FE element model.

References:

- [1] Y. Amani, S. Dancette, J. Luksch, A. Jung, E. Maire, "Micro-tensile behavior of struts extracted from an aluminum foam", *Mater. Charact.*, 110456 (2020).
- [2] A. Jung, M. Wocker, Z. Chen, H. Seibert, "Microtensile testing of open-cell metal foams - Experimental setup, micromechanical properties", *Mater. Des.*, 88, 1021-1030 (2015).
- [3] Y. Amani, S. Dancette, E. Maire, J. Adrien, J. Lachambre, "Two-Scale Tomography Based Finite Element Modeling of Plasticity and Damage in Aluminum Foams", *Materials*, 11, 1984 (2018).

Beating Thermal Coarsening in Nanoporous Materials via High-Entropy Design

ELyT Global
Themes: Materials and structure design
Scientific topic: Energy

	Associate Prof. Takeshi WADA¹		Assistant Prof. Soo-Hyun JOO^{1,2}		Prof. Hidemi KATO¹
---	---	---	---	---	--------------------------------------

Affiliation

¹ Institute for Materials Research, Tohoku University, Japan

² Department of Materials Science and Engineering, Dankook University, Korea

Abstract

Minimizing the ligament sizes of nanoporous metals is technically challenging because the coarsening follows a universal empirical correlation with homologous temperature. Ligament coarsening is a surface-diffusion-dominated process, and the relationship between the melting point and diffusion is apparent in the conventional metallic materials. Although nanoporous materials produced by dealloying have outstanding physical properties due to their unique bicontinuous structure, the undesirable coarsening leads to degradation of physical properties. To overcome this intrinsic thermal coarsening, we utilized high-entropy design into the dealloying process.

The high-entropy alloys (HEAs), which is characterized by the nearly equiatomic composition of more than five components, are attracting much attention in metallurgy. In such compositionally complex alloys, configuration entropy is maximized and the disordered solid-solution phase become thermodynamically stable rather than the ordered compound phase. The HEAs possess attractive mechanical properties such as high strength, ductility, superplasticity, etc. at an elevated temperature. The main reason of such unique characteristics is considered as the high thermal stability of fine microstructure. The grain growth in HEAs is exceptionally slow because of the sluggish diffusion, namely, the increase the activation energy due to the variety of atomic size in the constituents. As the ligament coarsening in nanoporous metals is analogous to the grain growth of polycrystalline materials, we expected the high-entropy design in nanoporous materials has a potential for achieving an exceptional fine porous structure and high stability against the coarsening.

To synthesize the nanoporous HEA, we utilized liquid metal dealloying (LMD), a unique technique to fabricate non-noble porous materials. The high-entropy design of LMD based on the enthalpy of mixing is depicted in Figure 1. The composition of the nanoporous HEA is carefully established among elements immiscible with the Mg melt, and then the selected TiVNbMoTa HEA is alloyed with 75 at%

miscible Ni. During LMD in the Mg melt, it is expected that Ni atoms selectively dissolves while the five immiscible elements rearrange their atomic configuration into a ligament. Following this new and practical strategy, many LMD systems can be designed to produce various nanoporous HEAs.

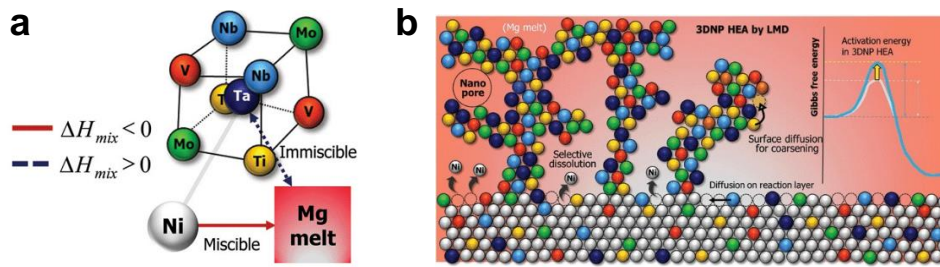


Figure 1 (a) Schematic of the high entropy design in the liquid metal dealloying using a (TiVNbMoTa)-Ni precursor alloy and Mg melt. The illustration of the expected nanoporous HEA formation mechanism via a rearrangement of atoms and ligament formation⁽¹⁾.

The precursor (TiVNbMoTa)₂₅Ni₇₅, mainly consists of two FCC solid-solution phases, was immersed in Mg melt for 10 min at 837 K. The average ligament size achieved in a unimodal porous structure is just 10 nm and the corresponding specific surface area reached as high as 55.7 m²/g. The diffraction pattern proves that the porous metal forms BCC lattice with its chemical composition of Ti_{13.29}V_{26.67}Nb_{19.91}Mo_{27.77}Ta_{12.16}Ni_{0.2} (at.%), falling into the HEA. This is the smallest ligament size ever reported in the dealloyed nanoporous metals.

Figure 2 shows ligament size versus inverse homologous temperature in conventional porous materials and the developed HEAs for the fixed dealloying time of 10, 20, or 60 min. Pure and binary porous metals evidently follow the general relationship of ligament size versus homologous temperature in a log-log scale. However, the linear relationship shifts down by one order of magnitude in smaller-size regime for the developed nanoporous HEAs. The activation energy for coarsening of nanoporous HEA was calculated to be 301.8 kJ/mol, being much higher than those reported for surface diffusion of each element. Thus, our new nanoporous HEA overcomes the universal effect of temperature on the coarsening of nanomaterials.

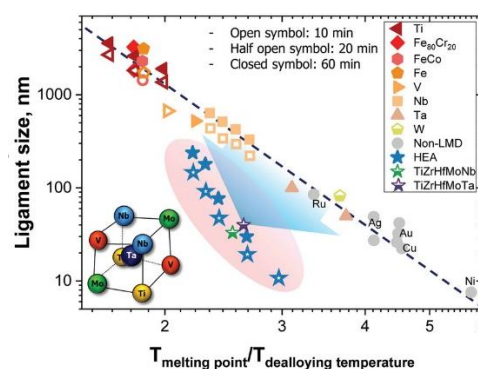


Figure 2 Ligament size versus homologous temperature in conventional nano- and microporous materials and the developed HEAs for the fixed dealloying time of 10, 20, or 60 min⁽¹⁾.

Reference

(1) S.-H. Joo, J. W. Bae, W.-Y. Park, Y. Shimada, T. Wada, H. S. Kim, A. Takeuchi, T. J. Konno, H. Kato, I. V. Okulov, Adv. Mater. 32 (2020) 1906160.

Tensile properties and microstructure of cellulose nanofiber reinforced silkworm silk fibers

Hiroki Kurita¹, Teruyoshi Kanno², Zhenjin Wang², Fumio Narita¹



Affiliation

¹ Graduate School of Environmental Studies, Tohoku University

² Graduate School of Engineering, Tohoku University

Abstract

Cellulose nanofiber (CNF) is a promising next-generation eco-friendly nanomaterial that could be used to synthesize low-cost, lightweight, high-strength, renewable and sustainable nanocomposites. However, CNF-based composites synthesized in previous studies have shown moderate mechanical properties, which may be due to the lack of nanofibril alignment. A flow-focusing method—which disperses the fibrils in liquid and orients them along the flow direction—has been reported to effectively increase the alignment of nanofibrils. A similar assembly procedure occurs in silkworms during the spinning process *in vivo*—which provided the inspiration for the research. This example demonstrates a novel eco-friendly method for drawing silk fiber strengthened with CNF, which could provide an alternative to post-functionalization approaches involving hazardous organic solvents.

In recent years, a novel technique which enabled to easily and directly obtain a silk fibroin solution without the use of organic solvents by applying a simple grinder for silk cocoons has been reported. The purpose of this study is to develop nanocellulose/silkworm silk composite fibers, focusing on direct feeding of silkworm with nanomaterials. CNF was added to the silkworm diet to improve the mechanical strength of the silk produced. Tensile testing was performed to understand the mechanical properties of the drawn silk fiber. We also studied the surface of the silk fiber to confirm the presence and orientation of the nanofibrils. Furthermore, Fourier transform infrared spectroscopy (FTIR) was used to confirm the possible changes in the conformation of the silk fiber due to the introduction of CNFs. In addition,

the finite element analysis was carried out to estimate the volume fraction of CNF aligned in the silk fiber.

The silkworm larvae were divided into three sample sets and reared on artificial diets with different CNF contents (0, 5 and 10 wt.%), as shown in Fig. 1(a). Silk was reeled from the harvested cocoon and denoted C-0, C-5, and C-10 based on the CNF content, respectively (Fig. 1(b)). Fig. 1(c) shows the setup of the tensile test conducted in this study. A 30 mm long bave was taken and 5 mm at both ends was fixed to a paper board using an adhesive as shown in Fig. 1(d). The adhered sections of the bave acted as the grip sections. The paper board was cut close to the grip section before the experiment was started by raising the jig. The tensile test was performed with a 20 N micro strain testing machine (MST-1, Shimadzu Co., Kyoto, Japan) at room temperature and relative humidity of 50–70 %. Stroke control mode was used with a crosshead speed of 20 mm/min.

Fig.2(a) shows the typical stress–strain curve for CNF/silk composite fibers. The fracture strength for the C-0 specimen is good agreement with previously published data. The cross-sectional areas of the silk fibers used to determine the tensile stress were estimated from the SEM images to be 393, 272 and 356 μm^2 for the C-0, C-5 and C-10 specimens, respectively. It was observed that the Young’s modulus and fracture strength of the C-5 specimen increased 1.8 and 1.6 times, respectively, compared with those of the C-0 specimen. However, the Young’s modulus and fracture strength of C-10 decreased compared with C-0 despite a higher concentration of CNFs being fed to the silkworms (Fig.2(b) and (c)).

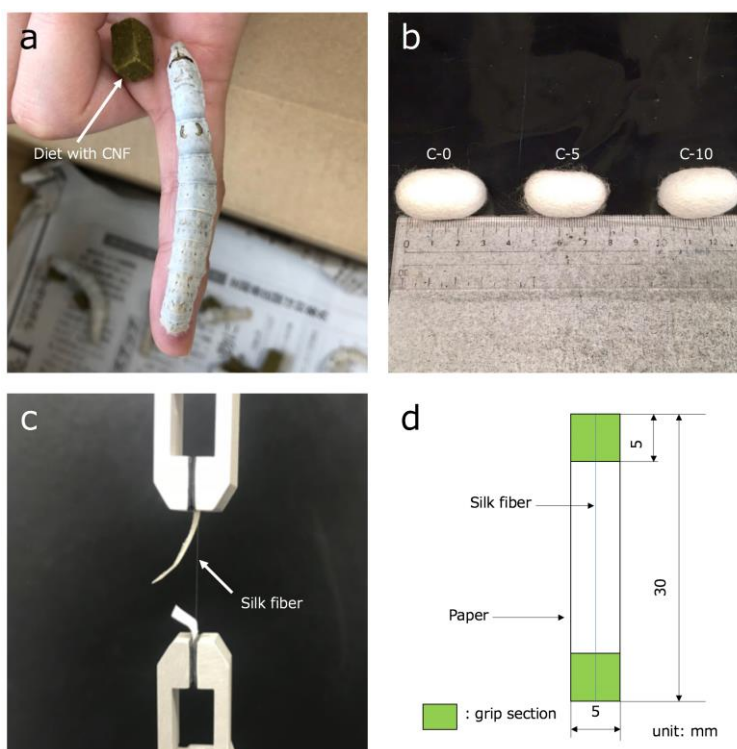


Fig. 1 Photographs of (a) a silkworm and the CNF containing feed, (b) cocoons with different CNF wt%, (c) a fiber specimen mounted on the tensile testing experimental setup; and (d) Schematic diagram of the tensile testing specimen.

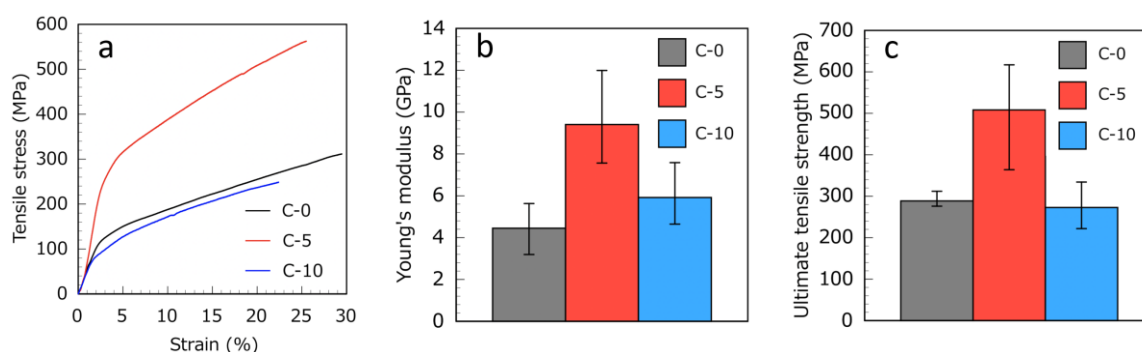


Fig. 2 (a) Typical stress–strain curve, (b) measured Young's modulus, and (c) measured ultimate tensile strength of CNF/silk composite fibers.

CarboEDiffSim : Simulation off Carbon electro-diffusion in iron with phase change

ELyT Global

Theme: Energy Scientific topic: Modelisation/Simulation

	Mr. Kairi Kita ^{1), 2)}		Assistant Prof. Takuya Mabuchi ^{2), 3)}
	Prof. Patrice Chantrenne ⁴⁾		Prof. Takashi Tokumasu ²⁾

Affiliation

- 1) Finemechanics, Graduate School of Engineering, Tohoku University
- 2) Institute of Fluid Science, Tohoku University
- 3) Frontier Research Institute for Interdisciplinary Sciences, Tohoku University
- 4) MATEIS, INSA de Lyon, Université de Lyon

Abstract

Since the structure of iron depends on the internal carbon concentration and temperature, carbon diffusion in iron has a great influence on the mechanical properties of iron. Generally speaking, the main driving force of carbon diffusion was considered to be only heat. In the Spark Plasma Sintering (SPS) method, carbon diffusion by an electric field as well as heat has attracted a great deal of attention. However, carbon diffusion by an electric field has not been sufficiently investigated. Carbon diffusion by an electric field may cause a change in the internal structure of iron. Therefore, it is possible to greatly contribute to the quality of material production using Spark Plasma Sintering or induction heating methods by investigating the carbon diffusion with an electric field. In this research, molecular dynamics is used to clarify the effect of electric field on the carbon diffusion in iron: the electric field dependence of carbon diffusion inside iron were investigated as the function of the temperature. In the simulation,

we investigated the transport characteristics of carbon in an iron from the average displacement and velocity at each temperature and each electric field strength.

In this study, the EAM (Embedded Atom Method) often used to reproduce atomic behavior of metals) potential was used as the intermolecular potential. To analyze the temperature dependence as a calculation condition, the electric field strength was kept constant to be 0.010 V/\AA and the temperature was changed from 1300 K to 1800K. In order to analyze the electric field dependence, the temperature was kept constant to be 1600 K and the electric field strength was changed from 0.006 V/\AA to 0.018 V/\AA . Here, the electric field was applied in the x-axis direction.

The initial structure of the simulation system is shown in Fig. 1. Here, red represents iron atoms and yellow represents carbon atoms. As shown in the figure, 4000 iron atoms in the body-centered cubic lattice are arranged, and one carbon atom is arranged in the structure. To simulate electromigration, an equivalent electronic charge is given to the Carbon atom which is then submitted to an electric force due to the electric field.

Regarding the electric field dependence as shown in Fig. 2, it was found that the displacement of carbon becomes linear when the electric field strength is constant. This indicates that the velocity of carbon is constant, and the kinetic energy of carbon does not change in iron. This phenomena suggests that all the energy received from the electric field is transferred to the crystal lattice of iron by collision. It is also found that the velocity increases linearly with increasing electric field strength.

We analyzed the temperature dependence in the same method of electric field dependence. It was found that the displacement increases as the temperature rises. This is because the energy of the carbon atom increases as the temperature rises, and it becomes easier to overcome the energy barrier of the potential from one site to the other one. It was also found that the velocity increases linearly as the temperature rises. By using this gradient, we can predict the velocity of carbon transferred by an electric field at a low temperature, which is close to the actual system.

In order to investigate the effect of carbon diffusion by electric field on the structure of iron, we are going to analyze the temperature and the concentration of carbon at which the phase transformation of iron occurs in the presence of carbon in detail by using the thermodynamic integration method.

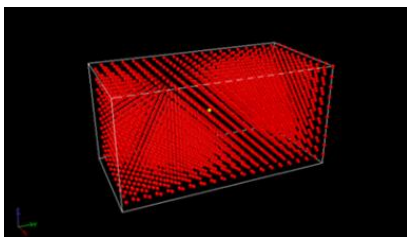


Fig.1 Initial structure

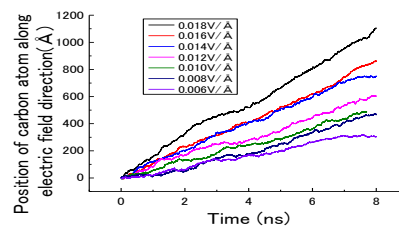


Fig.2 The position of carbon atom versus the time at different E

Research of 5d-4f fast emission in trivalent lanthanides-doped fluoro-oxide glasses as neutron scintillator materials

ELyT Global

Theme: Fast scintillators to detect neutrons.

Scientific topic: Materials and structure design

 <p>Pr BOULON Georges Dr GUYOT Yannick Pr DUJARDIN Christophe <i>Luminescence team, Institute Light- Matter (ILM) UMR 5306 CNRS- Claude Bernard/ Lyon 1 University . Campus Lyon Tech-La Doua 69622 Villeurbanne, FRANCE</i></p>  <p>Dr GUZIK Malgorzata <i>Faculty of Chemistry, University of Wroclaw,</i> u. Joliot-Curie 14, Wroclaw 50- 383, POLAND</p>	 <p>Pr YOSHIKAWA Akira Pr KAMADA Kei Pr KUROSAWA Shunsuke <i>Research Laboratory on Advanced Crystal Engineering, Institute for Materials Research (IMR), Tohoku University, 2-1-1 Katahira, Aoba-ku, Sendai, 980-8577, JAPAN</i></p>	 <p>Pr SARUKURA Nobuhiko Dr EMPIZO Melvin Dr YUKI Minami Dr CADATAL-RADUBAN Marilou Pr MURATA Takahiro Dr KAWANO Keisuke, Pr YAMANOI Kohei, Dr SHIMIZU Toshihiko <i>Institute of Laser Engineering, (ILE) Osaka University 2-6 Yamadaoka, Suita, Osaka 565-0871, JAPAN</i></p>
--	--	---

Abstract

Scintillators are luminescent materials that absorb the incident high-energy radiation and convert it into more accessible optical emissions. In particular, scintillators are the core sensing components that drive capabilities and impose limitations on radiation detectors [1]. Research efforts are then geared towards the design and development of potential scintillator materials. For example, bulk single crystals are investigated due to their good quantum efficiencies. However, large-area and high-quality crystals that are required for most radiation detection applications are difficult to produce

because of the restrictions by their crystal growth technologies including high production costs and slow growth processes. We have subsequently developed the complex fluorophosphate glass, $20\text{Al}(\text{PO}_3)_3\text{-}80\text{LiF}$ (APLF) as a host material for rare earth ions-doped neutron scintillators. Similar to other known fluorophosphates, APLF contains aluminum metaphosphate [$\text{Al}(\text{PO}_3)_3$] which is more stable to moisture than other metaphosphates. APLF glass also has a lithium (Li) content of $31.6 \text{ mmol cm}^{-3}$ which is comparable to that of a commercial cerium-activated Li aluminosilicate glass scintillator, KG2 ($36.0 \text{ mmol cm}^{-3}$). This high Li content is essential in enhancing the detector sensitivity to low-energy (270 keV) fast neutrons.

We have successfully doped APLF glasses with trivalent rare earth ions like praseodymium (Pr^{3+}) [2], cerium (Ce^{3+}) [3] and neodymium (Nd^{3+}) [4] to obtain decay times of $4f^{n-1}5d \rightarrow 4f^n$ VUV and UV emissions under optical, X-ray and radioactive excitations. We got values of 5.3 ns, 28.9 ns and 5 ns, respectively. Indeed we take advantage of the rare earth ions' electric-dipole allowed interconfigurational $4f^{n-1}5d \rightarrow 4f^n$ transitions which have fast emission decays, faster than the 39.8 ns decay of the commercial glass scintillator,

We will show mainly the spectroscopic properties of these new host materials which result in promising scintillators in time-of-flight (TOF) detectors for high-counting-rate fast neutron detection first in the Gekko XII LASER of the Osaka University used for high energy density physics and inertial confinement fusion (ICF) research.

[1]C. Dujardin, E. Auffray, E. Bourret-Courchesne, P. Dorenbos, P. Lecoq, M. Nikl, A.N. Vasil'ev, A. Yoshikawa, R.-Y. Zhu, Needs, trends, and advances in inorganic scintillators, IEEE Trans. Nucl. Sci. 65 (2018) 1977–1997.

[2]M.J.F. Empizo, M. Cadatal-Raduban, T. Murata, Y. Minami, K. Kawano, K. Yamanoi, T. Shimizu, N. Sarukura, M. Guzik, Y. Guyot, G. Boulon, Spectroscopic properties of Pr^{3+} -doped $20\text{Al}(\text{PO}_3)_3\text{-}80\text{LiF}$ glasses as potential scintillators for neutron detection, J. Lumin. 193 (2018) 13–21.

[3]Y. Minami, J.L. Gabayno, V.C. Agulto, Y. Lai, M.J.F. Empizo, T. Shimizu, K. Yamanoi, N. Sarukura, A. Yoshikawa, T. Murata, M. Guzik, Y. Guyot, G. Boulon, J.A. Harrison, M. Cadatal-Raduban, Spectroscopic investigation of praseodymium and cerium co-doped $20\text{Al}(\text{PO}_3)_3\text{-}80\text{LiF}$ glass for potential scintillator applications, J. Non.-Cryst. Solids. 521 (2019) 119495.

[4] M. J. F. Empizo, Y. Minami, K. Yamanoi, T. Shimizu, M. Yoshimura, N. Sarukura, T. Murata, A. Yamaji, A. Yoshikawa, M. Guzik, Y. Guyot, G. Boulon, Marilou Cadatal-Raduban, Investigations on the electric-dipole allowed $4f^25d \rightarrow 4f^3$ broadband emission of Nd^{3+} -doped $20\text{Al}(\text{PO}_3)_3\text{-}80\text{LiF}$ glass for potential VUV scintillator application, J. of Alloys and Compounds 856 (2020) 158096.

Characterization of gas-atomized powders and electron beam melted Co-Cr-Mo-C alloys

Theme: engineering for health Scientific topic: Materials and structure design



Affiliation

1. Deformation Processing Lab., IMR, Tohoku University
2. MATEIS, UMR5510, INSA Lyon

Abstract

[Introduction] Because of excellent wear resistance, corrosion resistance, and biocompatibility, Co-Cr-Mo (CCM) alloys have been applied to biomedical applications. Recently, electron beam melting (EBM), a powder-bed-fusion additive manufacturing, is getting attention as a promising manufacturing process for CCM alloys. In a previous study, we have developed high-carbon CCM alloys for industrial cutter by using EBM. The powder quality is an important factor for obtaining good mechanical performance in EBM built parts. In this study, we produced the gas-atomized Co-Cr-Mo powders with different carbon contents and examined the characteristics of raw powder and EBM built parts.

[Experimental procedures] Co-27Cr-6Mo-xC ($x = 0.04, 0.22, 1.5, 2.0$ and 2.5 mass%) powders were manufactured by Ar gas atomization. EBM fabrication was conducted using those powders under same building conditions. SEM observations and X-ray CT measurements were conducted for both raw powders and built parts. EPMA elemental mapping, EBSD analysis, and tensile tests were also conducted on the EBM built samples.

[Results and Discussion] X-ray CT successfully captured spherical gas pores, which were produced during gas atomization, in the powders. The amount of porosity in powders increased with increasing the carbon content. In contrast, porosity was hardly identified in the 0.04C and 0.22C EBM samples

with cellular structures. Further increase in the carbon content resulted in the higher volume fraction of pores in the EBM built parts and caused the cellular to dendritic transition. The highest porosity was obtained in the 2.0C EBM sample, while the 2.5C built sample with an eutectic structure had less porosity than the 2.0C sample. These results indicate that the porosity in the EBM samples depends on the solidification process during EBM. The precipitates observed in the EBM samples also varied from the σ -phase to $M_{23}C_6$ carbide, and a mixture of $M_{23}C_6$ and M_7C_3 carbides were observed in the high-carbon built parts.

Accordingly, adding carbon dramatically increases the hardness and the ultimate tensile strength. However, such carbide precipitations introduced cracks upon tensile loading, resulting in the reduced ductility. It should be noted that the formation of complex eutectic structure in the 2.5C built sample resulted in negligible mechanical anisotropy with respect to the building direction.

Role of Charge Carrier Transport in the mechanisms of Polyurethane Actuation

ELyT Global

**Project: Theory for Electrostriction of Polymeric Actuator.
TEmpuRA**

Theme: Materials and structure design



¹ LGEF, INSA Lyon, Université de Lyon, Villeurbanne, Rhône Alpes, 69621, France

² ElyTMaX UMI 3757, CNRS – Université de Lyon – Tohoku University, International Joint Unit, Tohoku University, Sendai, Japan & Lyon, France

³ Lyon Center, IFS -Tohoku U., Université de Lyon, INSAVALOR, Villeurbanne, 69621, France

⁴ MATEIS, INSA Lyon, CNRS, Université de Lyon, Villeurbanne, Rhône Alpes, 69621, France

⁵ IMP, INSA Lyon, CNRS, Université de Lyon, Villeurbanne, Rhône Alpes, 69621, France

⁶ IFS, Tohoku University, Sendai, Japan

Abstract

Electroactive polymers (EAP) are attractive for numerous large deformation actuator applications. However, the understanding of the mechanisms responsible for the deformation of polymer under an electric field remains challenging because of their complex structure and chemistry, and the presence of impurities.

Those materials are usually thin films covered with two electrodes. It is generally admitted that the main mechanisms of compressive actuation of dielectric elastomers are respectively: Maxwell stress and electrostriction. Maxwell stress is an extrinsic compressive stress coming from the mutual attraction of the two opposite charged electrodes. The electrostriction is an intrinsic contribution coming from the orientation of dipoles and the attraction of phases having different polarities in heterogeneous materials.¹⁻³ Our recent study on polyurethane showed that the mechanical and electrical time constants are different, and that the time scale of actuation kinetics better matches that of electricity.⁴ Moreover, those two mechanisms cannot explain properly the bending actuation under an electric field observed on film with a clamped and a free ends (Fig.1)⁵. This effect might be explained by the presence of charges near the surface, such as ions, holes or electrons.^{5,6} Energy density gradients inside the samples

would be at the origin of the expansion of the surface near the electrodes.^{6,7}

In order to understand our observations, we started to model such a behavior and to perform some numerical simulations. The main hypothesis is that the macroscopic deformation results from the diffusion of electric charges towards the electrodes. Assuming that the mobilities of the negative and positive charges are different, their migration towards the electrodes should have different kinetics. The gradient of charge density should induce body forces near the surfaces which, in turn, cause the sample to bend, assuming that there are no equivalent forces near the opposite electrode. For a period of time long enough to allow the migration of all electrical charges, it can be expected that the bending will (i) pass through a maximum and then (ii) tend to zero. The schematic scenario is shown in Fig.1, and the preliminary results of the simulation versus experimental data are presented on Fig.2.

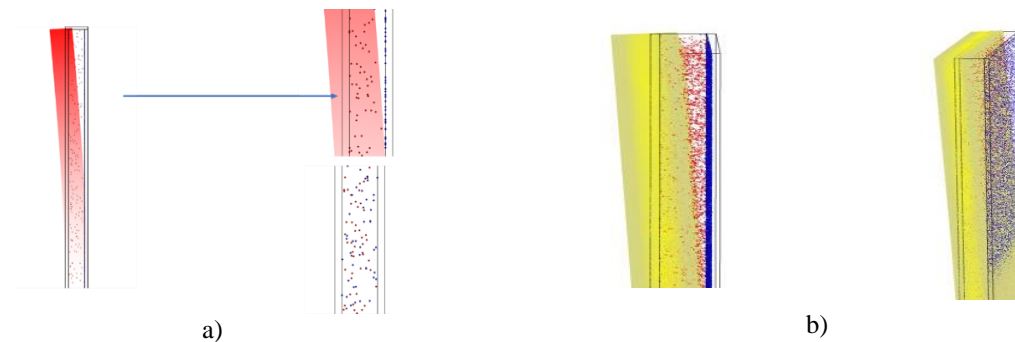


Fig.1: schematic scenario where blue particles move faster than red particles. Due to the energy gradient, the thin sample first bends towards the left: examples of a) 2D calculations and b) 3D calculations.

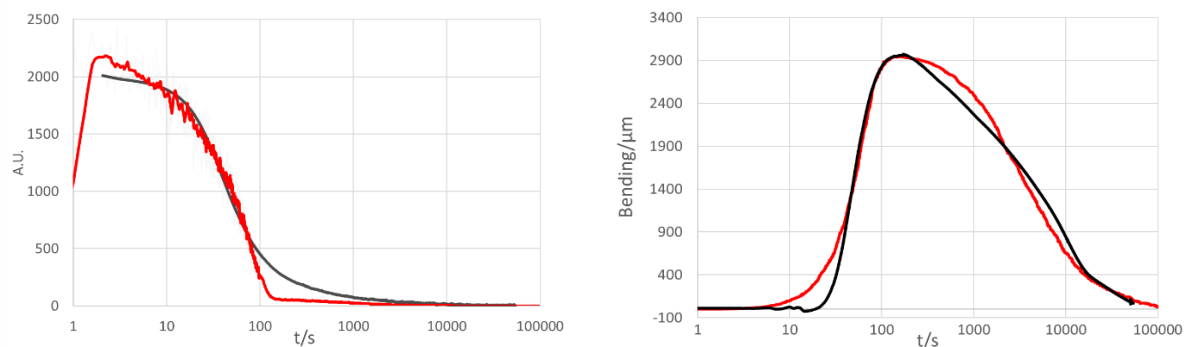


Fig.2: Preliminary results of simulation (red curves) versus experimental data (black curves). Left: electrical current density as a function of time, Right: idem but for the bending deflection

These promising results need to be confirmed on model materials, to avoid the uncertainty of the exact origins of electrical charges. This work is ongoing.

[1] B. Kim, Y.D. Park, K. Min, J.H. Lee, S.S. Hwang, S.M. Hong, B.H. Kim, S.O. Kim, and C.M. Koo, *Adv. Funct. Mater.* 21, (2011), 3242.

[2] Y. Zhang, V. Perrin, L. Seveyrat, and L. Lebrun, *Smart Mater. Struct.* 29, (2020), 055007.

[3] M.H. Jomaa, K. Masenelli-Varlot, G. Diguët, L. Seveyrat, L. Lebrun, K. Wongtimnoi, C. Vechambre, J.M. Chenal, and J.Y. Cavaillé, *Polymer (Guildf)*. 62, (2015), 139.

[4] M.H. Jomaa, L. Seveyrat, V. Perrin, L. Lebrun, K. Masenelli-Varlot, G. Diguët, and J.Y. Cavaillé, *Smart Mater. Struct.* 26, (2017), 035049.

[5] G. Diguët, J.Y. Cavaillé, G. Sebald, T. Takagi, H. Yabu, A. Suzuki, R. Miura, *Computational Materials Science* 190(2021) 110294

[6] M. Watanabe, N. Wakimoto, H. Shirai, and T. Hirai, *J. Appl. Phys.* 94, (2003), 2494.

[7] M. Watanabe, T. Kato, M. Suzuki, Y. Hirako, H. Shirai, and T. Hirai, *J. Polym. Sci. Part B Polym. Phys.* 39, (2001), 1061.

Influence of mechanical surface treatment on passive and oxide behavior of 304L Stainless Steel

(OPSCC project)

ELyT Global Energy Materials & Structure design Surfaces & Interfaces

	H. Abe ¹ T. Miyazaki ¹ Y. Watanabe ^{1,2}		B. Ter-Ovanesian ³ N. Mary ³ B. Normand ³ K. Jaffre ^{2,3}
---	---	--	--

Affiliation

¹ Graduate School of Engineering, Tohoku University, 6-6-01-2 Aoba, Aramaki, Aoba-Ku, Sendai, Japan

² ElyTMaX UMI 3757, CNRS–Université de Lyon–Tohoku University, International Joint Unit, Sendai, Japan

³ Université de Lyon, INSA-Lyon-UCBL-CNRS, UMR CNRS 5510 MATEIS, Villeurbanne Cedex, France

Abstract

1. Introduction

The 304L Stainless Steel (SS) is used in boiling water reactors (BWR) and pressurized water reactors (PWR) as reactor vessel internals primary circuit because of its good corrosion resistance and mechanical properties. After casting, forming, machining, or even repair of those SS structural components, post-treatments of mechanical surface finish are applied. Generally, these surface finishing operations such as grinding, wire brushing, machining, produce surface states that compromise the corrosion resistance of oxidative and passive materials [1]. These processes effectively affect the electrochemical and mechanical stabilities of the material at the microstructure scale and also the passive film properties [2]. Within this framework, the main objectives of this project are:(i) to establish the correlation between surface modifications (macroscopic defects, roughness, residual stresses, chemical, and microstructural alterations) and the properties of passive films (room temperature);(ii) to understand how these modifications affect the properties of these passive films; (iii) Then to apply the same methodology to understand how these modifications affect the properties of oxides at high-temperature water (BWR, PWR).

To highlight the influence of surface finishing process used in maintenance, the corrosion and oxidation behavior of grinded and mechanically polished samples (2400-SiC, diamond paste 1µm and colloidal silica polishing) of 304L SS have been studied.

2. Striking Results

Firstly, the features of microstructural modification at the subsurface have been characterized with SEM, FIB and TEM observations. The ground samples exhibit a larger subsurface recrystallization zone (in addition to a deformed layer and a hardened one) than the mechanically polished samples. The highest surface roughness and residual compressive stresses were also determined for this surface condition.

Then, relationship between the electrochemical results, the stability and the resistance of the passive film can be drawn regarding the microstructural modifications related to surface treatments [3]. If the overall passive behavior in borate buffer solution is similar for all the samples, the present study reveals that the number of doping species, the capacitance value, and the thickness of the passive film are influenced by the roughness, the defects on the surface, and also by the residual compressive stresses. Consequently, the passive film formed on the more disordered and reactive surface is the thinnest and the less stable. Then, dry grinding affects detrimentally the passive behavior and the corrosion resistance of 304 L SS. The study performed with chloride containing solution corroborates this conclusion by evidencing an enhanced reactivity when the sample is immersed in a chloride environment. The corrosion resistance is significantly affected by the surface finishing.

The influence of mechanical surface treatment on the oxidation behavior of 304L SS was then investigated in simulated BWR and PWR environments [4]. The surface state after mechanical surface treatment only impacts the oxidation kinetics due to the modifications of the surface. As a result, the density of the outer oxide-hydroxide precipitates is higher for the ground surface than for the polished surface down to 2400 SiC. Indeed, the ultrafine grain layer, acting as a diffusion short circuit, promotes the dissolution of metallic elements. Moreover, the capacitance of the inner oxide formed on the ground surface is higher than for the other two surfaces. This result is associated with a decrease in the donor density with the degree of surface treatment: the thicker the inner oxide, the lower the doping density. This part of the study also allowed to estimate the role of the environment on the oxidation process. For both test environments, the oxide formed has a duplex structure composed of an outer oxide-hydroxide precipitates rich in Fe and an inner oxide rich in Cr. Nevertheless, for simulated PWR environment, the outer oxide-hydroxide precipitates are larger, denser, than for the BWR one. Simulated PWR environment is more oxidizing than the BWR one. To conclude this part, the electrochemical reactivity of thermally oxide is more affected by the environment chemistry than by the mechanical surface treatment.

3. Prospects

In the present work, the different oxidation features were characterized and the stability of these oxides was evoked. Therefore, perform some SCC tests could be a straightforward perspective to (i) understand the effect of surface finish on SCC susceptibility of alloys, (ii) establish the relations between the surface modifications, the oxide properties and oxidation behavior and SCC susceptibility, (iii) and consequently propose an approach to optimize surface and subsurface.

References :

- [1] M. Moine, N. Mary, B. Normand, L. Peguet, A. Gaugain, H.N. Evin, Tribo electrochemical behavior of ferrite and ferrite–martensite stainless steels in chloride and sulfate media, *Wear*. 292–293 (2012) 41–48. doi:10.1016/j.wear.2012.06.001.
- [2] B. Ter-Ovanesian, N. Mary, B. Normand, Passivity Breakdown of Ni-Cr Alloys: From Anions Interactions to Stable Pits Growth, *J. Electrochem. Soc.* 163 (2016) C410–C419. doi:10.1149/2.0381608jes.
- [3] K. Jaffré, B. Ter-Ovanesian, H. Abe, N. Mary, B. Normand, Y. Watanabe, Effect of Mechanical Surface Treatments on the Surface State and Passive Behavior of 304L Stainless Steel, *Metals* 2021, 11(1), 135; doi:10.3390/met11010135
- [4] K. Jaffré, H. Abe, B. Ter-Ovanesian, N. Mary, B. Normand, Y. Watanabe, Influence of Mechanical Surface Treatments on Oxide Properties Formed on 304L Stainless Steel in Simulated BWR and PWR Primary Water, Submitted June 2021 @ *Journal of Nuclear Material*.

Modeling ferroelectric phase transitions for energy harvesting

ELyT Global

Theme: Energy

Scientific topic: - Materials and structure design
- Simulation and modeling



¹Univ. Lyon, INSA-Lyon, LGEF EA682, F-69621, France

²ELyTMax UMI 3757, CNRS – Université de Lyon – Tohoku University, International Joint Unit, Tohoku University, Sendai, Japan

³Centre for Nanoscience and Nanotechnology, University of Paris-Saclay - CNRS, Palaiseau, France

⁴FEMTO-ST Institute, University of Bourgogne Franche-Comté, CNRS (UMR 6174), ENSMM, 26 rue de l'Épitaphe, 25030 Besançon, France

⁵New Industry Creation Hatchery Center (NICHe), Tohoku University, 6-6-10 Aramaki-Aoba, Aoba-ku Sendai, Miyagi 980-8579, Japan

⁶Sendai Smart Machine Co., Ltd. (SSM), 6-6-40 Aza-Aoba, Aramaki, Aoba-ku, Sendai, Miyagi 980-8579, Japan

*mickael.lallart@insa-lyon.fr

Abstract

Ferroelectric materials are of great interest due to the panel of applications they feature such as wireless sensor, memories, transducers and so on. Their properties to convert mechanical excitation into an electrical signal or conversely is the most attractive feature of these materials. One of their remarkable properties is the ability to have successive phase transitions with temperature, applied stress or electric field. While very little studies proposed to take advantage of such transitions ([1, 2]), this study aims at proposing to use them for energy harvesting purpose. As a first step, the work reported here proposes a model for such phase transitions.

Energy harvesting from residual energy in the environment is a promising way to power wireless sensors or other devices in harsh or remote conditions. In fact, the advantages of this method are the low cost and the absence of maintenance and replacement of batteries. There are several types of energies in the environment that can be converted into electrical energy like vibration, solar radiation, wind... The harvesting of vibrational energy is a field of huge interest due to the large possibility of applications and ubiquity of the source. Finding the best piezoelectric material for energy harvesting with lead free composition to replace the currently widely used PZT compositions is an actual challenge in the field of energy harvesting. Some perovskites gained a lot of interest in the past decade due to their high dielectric constant and their different domain of applications such as energy harvesting.

A lot of perovskite structures such as BaTiO₃, KNO and KTN undergo three phase transitions from cubic to tetragonal, tetragonal to orthorhombic, orthorhombic to rhombohedral with temperature, pressure or electric field. The mechanism of phase transitions is very complex and there are few approaches to describe them. We can note the renormalization group which work very well but is very complex in his formalism. An easier way to describe them is based on the mean field approximation. However, close to the transitions, this approximation fails to describe properly experimental observations. Fortunately in ferroelectric materials the nature of transition allows describing them in the frame of Landau theory (mean field approximation) due to their long-range interactions [3]. For

ferroelectrics, Devonshire used in the 1950's the Landau theory to describe the phase transitions of these materials. This theory, known as Landau-Devonshire theory, consists of developing the free energy term in power of an order parameter which is the polarization for ferroelectrics. The free energy is given by:

$$F = \alpha_1(P_1^2 + P_2^2 + P_3^2) + \alpha_{11}(P_1^4 + P_1^4 + P_1^4) + \alpha_{12}(P_1^2 P_2^2 + P_1^2 P_3^2 + P_2^2 P_3^2) + \alpha_{123} P_1^2 P_2^2 P_3^2 + \alpha_{111}(P_1^6 + P_2^6 + P_3^6) + \alpha_{1112}(P_1^2(P_2^4 + P_3^4) + P_2^2(P_1^4 + P_3^4) + P_3^2(P_2^4 + P_1^4)) + \alpha_{11111}(P_1^8 + P_2^8 + P_3^8) + \alpha_{11122}(P_1^4 P_2^4 + P_1^4 P_3^4 + P_2^4 P_3^4) + \alpha_{11112}(P_1^6(P_2^2 + P_3^2) + P_2^6(P_1^2 + P_3^2) + P_3^6(P_1^2 + P_2^2)) + \alpha_{1123}(P_1^4 P_2^2 P_3^2 + P_1^2 P_2^4 P_3^2 + P_1^2 P_2^2 P_3^4) \quad (1)$$

Our work is based on the Landau-Devonshire approach to describe the phase transitions and the physical properties of ferroelectric perovskites with a classic ferroelectric behavior such as BaTiO₃ and KNO. This phenomenological model allows obtaining the phase diagram and a lot of physical properties such as polarization, dielectric permittivity, piezoelectric coefficients and so on as a function of the applied temperature, stress and electrical field [4]. In the light of the model, the idea is to predict the ideal P-E cycle which allows to harvest as much energy as possible. To include the stress and electric field dependence, we need to add an elastic and electrostatic contribution to the free energy and perform a Legendre transformation to get the free enthalpy which is expressed as (with respect to cubic symmetry):

$$\Delta G = F - \frac{1}{2} s_{11}(\sigma_1^2 + \sigma_2^2 + \sigma_3^2) - s_{12}(\sigma_1 \sigma_2 + \sigma_1 \sigma_3 + \sigma_2 \sigma_3) - \frac{1}{2} s_{44}(\sigma_4^2 + \sigma_5^2 + \sigma_6^2) - Q_{11}(\sigma_1 P_1^2 + \sigma_2 P_2^2 + \sigma_3 P_3^2) - Q_{12}(\sigma_1(P_2^2 + P_3^2) + \sigma_2(P_1^2 + P_3^2) + \sigma_3(P_1^2 + P_2^2)) - Q_{44}(\sigma_4 P_2 P_3 + \sigma_5 P_1 P_3 + \sigma_6 P_1 P_2) - E_1 P_1 - E_2 P_2 - E_3 P_3 \quad (2)$$

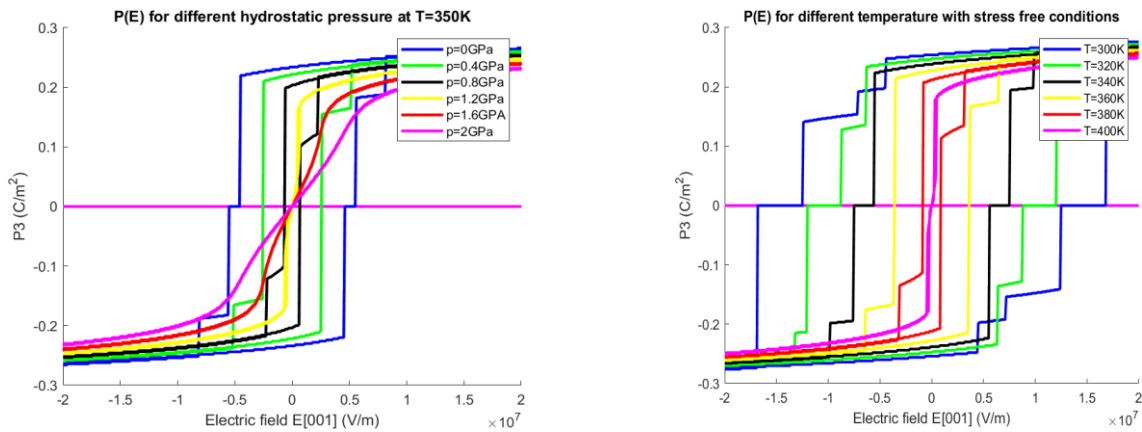


Figure 1. P-E cycles for several pressures of temperatures.

The next step of this work is to apply this phenomenological model to the ferroelectric relaxor KTN. This is a challenging objective due to the lack of publications in the literature. This lack of publications is due to the fact that ferroelectric relaxors have other contributions to the polarization than intrinsic one. The other contribution to the polarization is called the extrinsic one and cannot be describe in the frame of Landau theory [5]. This extrinsic polarization come from the presence of polar nanoregion near and above the Curie temperature. However, this contribution is negligible in ferroelectric phases and if an electric field is applied to obtain a single domain state [6].

Acknowledgement

This work was supported by Agence National de la Recherche, grant ANR-20-CE05-0026 (project FIESTA).

References

- [1] D. Guyomar, S. Pruvost and G. Sebald, *IEEE Trans. Ultrasonics, Ferroelec. Freq. Cont.*, 55(2), 279-285, 2008, doi: 10.1109/TUFFC.2008.646.
- [2] Dong, W. (2015). Characterization, Modeling, and Energy Harvesting of Phase Transformations in Ferroelectric
- [3] Karin M. Rabe, Karin M. Rabe, Charles H. Ahn, and Jean-Marc Triscone. 2007. *Physics of Ferroelectrics: A Modern Perspective* (1st. ed.). Springer Publishing Company, Incorporated.
- [4] Wang, J.J. & Wu, P. & Ma, Xingqiao & Chen, L.. (2010). *Journal of Applied Physics*. 108. 114105-114105. 10.1063/1.3504194
- [5] Li, Huan & Hao, Tian & Gong, Dewei & Meng, Qingxin. (2013). *Journal of Applied Physics*. 114. 10.1063/1.4817493.
- [6] Lu, Xiaoyan & Fan, Jinhui & Zhang, Hangbo & Wu, Huaping & Li, Hui & Cao, Wenwu. (2020) *Ceramics International*.

Magnetization mechanisms NDT

ELyT Global

Theme (to precise) Scientific topic (to precise)

	Shurui Zhang ^{1,2}		Sho Takeda ²
	Gael Sebald ³		Tetsuya Uchimoto ^{2,3}
	Benjamin Ducharne ^{3,4}		

Affiliation

1. Graduate School of Engineering, Tohoku University, Sendai, Japan
2. Tohoku University, Institute of fluid science IFS, Sendai, Japan.
3. ELyTMaX UMI 3757, CNRS – Université de Lyon – Tohoku University, International Joint Unit, Tohoku University, Sendai, Japan.
4. LGEF, INSA Lyon, Villeurbanne, France.

Abstract

Magnetism can take different aspects in contemporary non-destructive testing. For example, it can be used to transfer information without contact like in eddy current testing, to generate a

mechanical force like in magnetic particle inspection, or simply its distortion by potential defects like in metal magnetic memory inspection. In this project, we focus on the magnetization mechanisms of ferromagnetic steel. Ferromagnetic steels are used in the construction, transportation, and energy domain. In the steel industry, destructive and non-destructive controls are already omnipresent. Still, evaluations based on the magnetization mechanisms show many advantages (non-destructive, low-cost, no contamination, etc.), and steel producers and end-users are very attentive to any progress.

In the first hand, we have the mechanical properties to be observed:

- the residuals stresses and strains,
- the surface heterogeneities (macroscopic defects),
- the long-term degradation (creep, aging, structural health monitoring).

On the other hand, we have the magnetization mechanisms:

- the magnetic domain wall bulging (in the low amplitude range [1][2]),
- the domain wall irreversible motions (in the middle amplitude range),
- the magnetization rotation (in the high amplitude range),
- the domain wall frequency dependence, ripples, and avalanches phenomena [3],
- the macroscopic eddy currents (Skin effect [4]).

The objective is to generate links, connections, correlations, etc. The first part of the job consists of developing experimental situations where the magnetization mechanisms can be isolated. The observation of the magnetic Barkhausen noise is a good example [5]. It provides a signal limited to the domain wall irreversible motions contribution.

All the current use of industrial devices based on the magnetization mechanisms rely on rejection thresholds and time-consuming calibration procedures. The targeted properties have to be identified in a first-place using imaging, destructive tests, etc.

In the second part of this work, we are developing predictive simulation tools. It allows to understand, and it constitutes an elegant way to avoid the calibration procedures. Still, this approach is emerging, and progress has to be made before industrial used.

[1] B. Gupta, B. Ducharne, T. Uchimoto, G. Sebald, T. Miyazaki, T. Takagi, "Comparison of electromagnetic nondestructive testing of creep-degraded high-chromium ferritic steels", *NDT & E Int.*, vol. 118, 102399, 2021.

[2] S. Zhang, B. Ducharne, T. Uchimoto, A. Kita, "Simulation tool for the Eddy Current Magnetic Signature (EC-MS) non-destructive method, *J. of Mag. and Mag. Mat.*, vol. 513, 167221, 2020.

[3] S. Zhang, B. Ducharne, S. Takeda, G. Sebald, T. Uchimoto, "Low-frequency behavior of laminated electric steel sheet: investigation of ferromagnetic hysteresis loops and incremental permeability", *J. of Mag and Mag. Mat.*, under revision, 2021.

[4] B. Gupta, B. Ducharne, T. Uchimoto, G. Sebald, T. Miyazaki, T. Takagi, "Non-destructive testing on creep degraded 12% Cr-Mo-W-V Ferritic test samples using Barkhausen noise", *J. of Mag. and Mag. Mat*, Vol. 498, 166102, 2019.

[5] B. Gupta, B. Ducharne, G. Sebald, T. Uchimoto, "A space discretized ferromagnetic model for non-destructive eddy current evaluation", *IEEE Trans. on. Mag*, Vol. 54, Iss. 3, 2018.

Shape optimization with respect to mechanical stability criteria

ELyT Global

Project ELyT lab : R7 – Robust Multi Objective optimization design approaches

	<p>Koji SHIMOYAMA¹</p> <p>Pradeep MOHANASUNDARAM^{1,2} Double degree PhD student</p>	 	<p>Sébastien BESSET²</p> <p>Frédéric GILLOT²</p>
---	---	---	--

¹*Tohoku University, IFS*

²*Ecole Centrale de Lyon, LTDS DySCo Team*

Abstract : The main aim of the project is to optimize the structures involved in braking system for vibro-acoustic properties arising from friction induced vibration, commonly known as squeal noise. The complex nature of the problem demands an efficient optimization strategy considering the computation cost. This problem is addressed through defining the expensive evaluation of the Stability criteria (representing the magnitude of the squeal noise) with the meta-model and using the Efficient Global Optimisation (EGO) search algorithms. The multi-objective definition of the optimization results in pareto-optimal solutions obtained through genetic algorithm for the considered shape parameters.

1. Context

The brake squeal noise is considered to be a very challenging problem since there is no stand-alone mechanism to explain the behavior, though there are many mechanisms which explains in their own respective sense. This makes it hard to define a criteria for the squeal noise to be considered for optimization. But one of the methods which has proven to be efficient is complex eigenvalue analysis which gives a measure of instability. Combined with an isogeometric formulation of the system, an EGO scheme is set-up to generate pareto-optimal solutions in an effective yet realistic computational time. Such generation is made possible with a dedicated algorithm [1,2]

2. Achieved results

One pareto optimal set result is shown below, and enable generation of innovative designs close to topological applications with advantage of keeping the CAD numerical scheme intact.

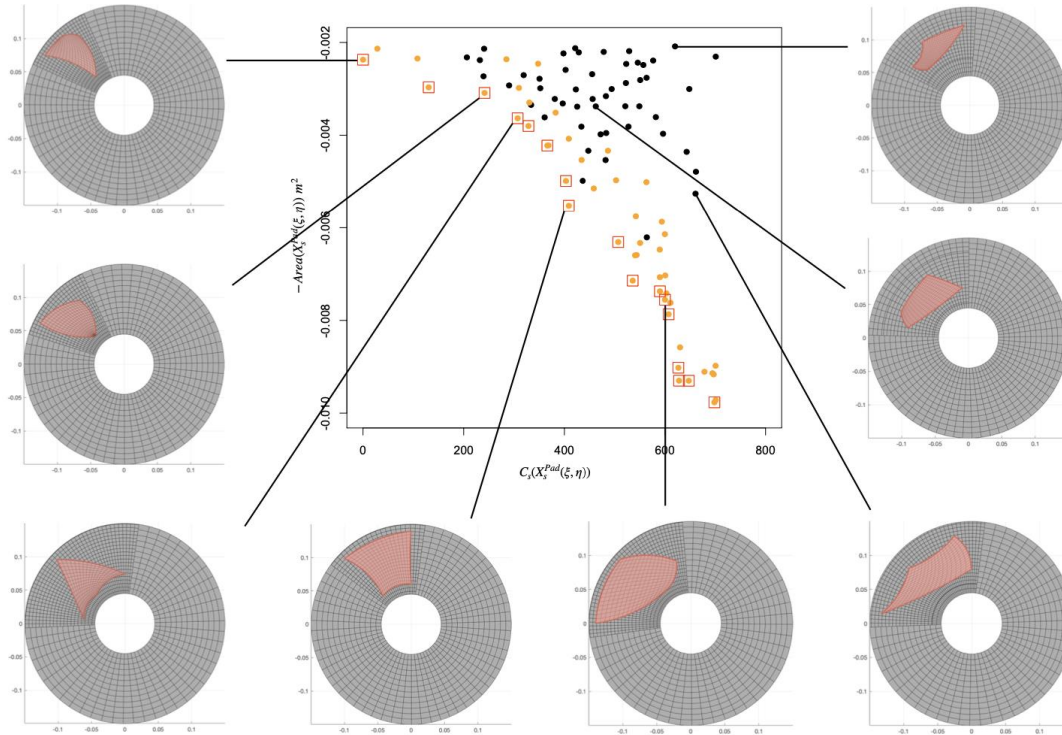


Figure 1 : Results showing some pareto-optimal solutions. Two objectives are f_1 stability criteria and f_2 pad area (-).

Next steps are to improve the exploration range with more parameters taken into account and uncertainties related to them. Robustness will also have to be considered.

References :

[1] Mohanasundaram, P., Gillot, F., Besset, S., Shimoyama, K., *Multi-references acquisition strategy for shape optimization of disc-pad-like mechanical systems*, Structural and Multidisciplinary Optimization, Accepted, May 2021, doi: 10.1007/s00158-021-02947-7
 [2] Mohanasundaram, P., Gillot, F., Shimoyama, K., Besset, S., *Shape optimization of a disc-pad system under squeal noise criteria*. *SN Appl. Sci.* **2**, 547 (2020). <https://doi.org/10.1007/s42452-020-2175-8>

Simulations and Experiments Exploring the Role of OH-Termination in the Lubricity and Stability of H-free DLC

Project ELyT Lab: T2 –**TRIBOCHEM**: Mechanisms of lubrication of ta-C by gas.

	<p>Momoji Kubo IMR Tohoku University 2-1-1 Katahira, Aoba-ku Sendai 980-8577, Japan</p>		<p>Yang Wang IMR Tohoku University 2-1-1 Katahira, Aoba-ku Sendai 980-8577, Japan</p>
	<p>Maria Isabel De Barros Bouchet LTDS Ecole Centrale de Lyon 69134, Ecully, France</p>		<p>Jean Michel Martin LTDS Ecole Centrale de Lyon 69134, Ecully, France</p>

Abstract

1. Introduction

Diamond-like carbon (DLC) is a promising protective coating to reduce the friction and wear of materials. Tribochemical reactions at DLC friction interface plays a significant role in the lubricity. As we previously reported, existence of hydrogen termination on DLC surfaces suppresses the formation of interfacial C-C bonds and hence leads to a low friction coefficient.[1] However, the low friction state of H-terminated DLC cannot be maintained for long-term, limiting its application.[2] Thus, we conduct a joint study using both computer simulation and experiment to explore the possibility of OH-terminated DLC as a new low friction material with high stability.

2. Computer simulations

We perform molecular dynamics simulations of ta-C with both H- and OH-terminations to investigate the effect of hydroxyl group on the friction behaviors, comparing with the DLC with only H-terminations. Our originally developed tight-binding quantum chemical molecular dynamics simulator, “Colors”, is used to handle the tribochemical reactions at the friction interface. Simulation of both models are performed for 20 ps, at a sliding velocity of 100 m/s and temperature of 300 K. Since no interfacial bonds are formed under such low load, the addition of OH-termination increases the atomic-level roughness and causes the hydrogen bond interaction across the interface, collaboratively resulting in a higher friction coefficient than the ta-C with only H-terminations. However, when the normal load increases to 7 GPa, friction coefficient of DLC with only H-terminations increases more and more during friction simulation because H-terminations cannot bear such high load and hence a large number of interfacial C-C bonds are formed [3]. Surprisingly, for the DLC with a portion of OH-terminations, friction coefficient keeps at a low value even under the high load of 7 GPa, because the addition of OH-terminations increases the distance between sliding substrates and hence suppresses the formation of interfacial bonds. However, friction increases due to rougher surfaces at the atomic scale.

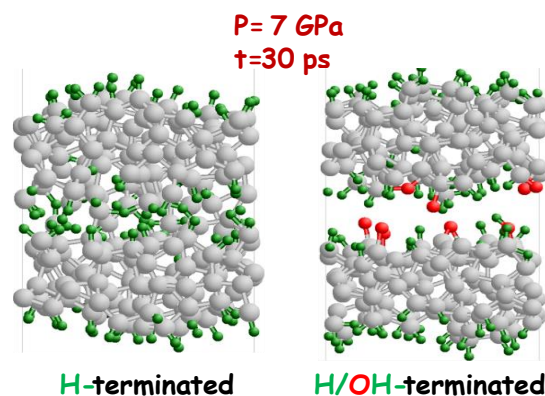


Figure 1: Snapshot of sliding interfaces @ 7 GPa with H (left) and H/OH termination (right).

3 Friction experiments and surface analysis

A set of friction experiments was carried out under deuterated glycerol gas (1 hPa) instead of 800 hPa hydrogen. In this case the friction decreases and is very stable with a friction coefficient of about 0.05 and this has been repeated several times [3]. Using SIMS analysis, we have evidenced that the sliding surface becomes enriched in H and OH terminations (Figure 2). However, it is worthy to notice that friction decrease with H/OH-terminated carbon surfaces is much less than with H-termination ones with hydrogen gas (showing superlubricity).

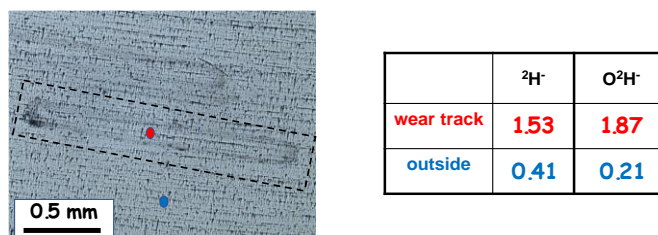


Figure 2: Friction of ta-C coatings under 1 hPa D-glycerol. SIMS analyses showing tribo-induced H/OH termination.

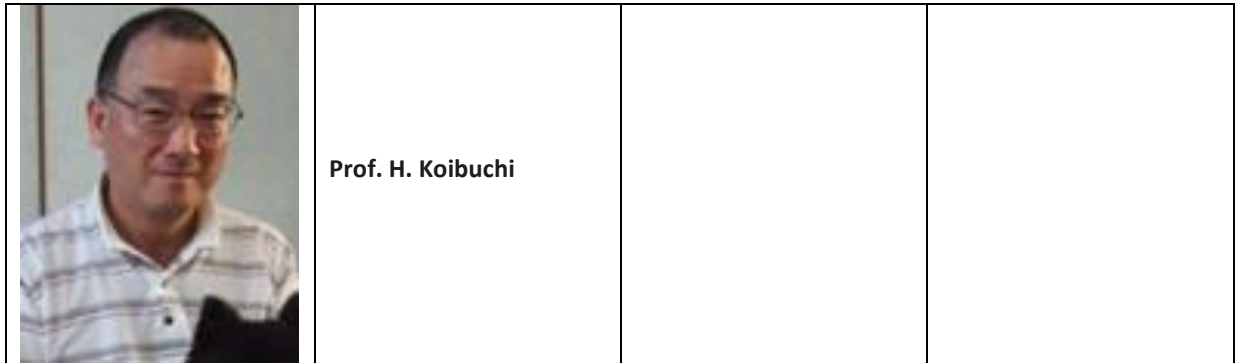
It is concluded that H_2 can lubricate ta-C coatings providing superlow friction (CoF below 0.01) but is not able to survive long friction duration without seizure at high contact pressure. Surprisingly, high partial pressure of H_2 is needed suggesting a possible role of molecular hydrogen in the contact. At the opposite, H/OH terminated carbon surfaces are not able to provide such superlow friction but no seizure is detected during friction at high contact pressure, in excellent agreement with computer simulations.

References

- [1] K. Hayashi, K. Tezuka, N. Ozawa, T. Shimazaki, K. Adachi, and M. Kubo, Tribochemical Reaction Dynamics Simulation of Hydrogen on a Diamond-like Carbon Surface Based on Tight-Binding Quantum Chemical Molecular Dynamics. *J. Phys. Chem. C* **115** (2011) 22981-22986.
- [2] J. Fontaine, M. Belin, T. Le Mogne, and A. Grill, How to restore superlow friction of DLC: the healing effect of hydrogen gas, *Tribol. Int.* **37** (2004) 869-877.
- [3] Y. Wang et al, Role of OH-termination in mitigating friction of DLC under high load: A joint simulation and experimental study. *Langmuir*, 37, (2021) 20, 6292-6300.

Langevin Navier-Stokes simulation of the protoplasmic streaming

ELyT Global Flow field in plant cells Brownian motion of fluid particles



Affiliation

H.Koibuchi*, Sendai Kosen, Natori, Japan

Abstract

We study protoplasmic streaming in plant cells such as chara brauni by simplifying the flow field to be two-dimensional Couette flow with Brownian random force inside parallel plates (Fig.1). Protoplasmic streaming is attracting many interests in many areas, including agriculture-technology and biotechnology[1,2]. The plant size depends on the velocity of streaming, and the driving force originated in molecular motors [3]. Therefore, it is interesting to study detailed information on the velocity. In a recent numerical study, experimentally observed peaks [4,5] in the velocity distribution are simulated by 2D Langevin Navier-Stokes (LNS) equation for vortex and flow function variables [6]. However, 3D flows, in general, follow the NS equation for velocity. This paper simulates the streaming by 2D LNS equation for velocity and pressure and check whether peaks of velocity distribution are observed or not. A dimensional analysis studies the dependence of numerical results on the strength D of Brownian random force and physical parameters such as kinematic viscosity and size of cells. We find from this analysis how the peak position moves depending on these parameters. In this presentation, numerical results will be reported, and the detailed information on the dimensional analyses will be reported elsewhere.

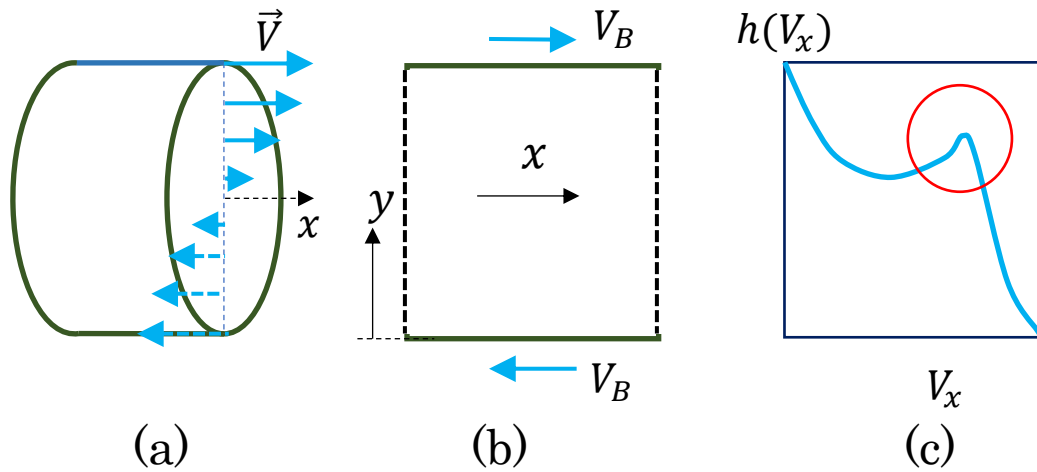


Fig.1 Illustrations of (a) protoplasmic streaming, (b) 2D computational domain, and (c) distribution of velocity. (a) Arrows denote velocity of flows, where circular flows on the cylindrical surface in real plant cells are assumed to be parallel to x-direction. (b) V_B denotes the fixed boundary velocity. (c) experimentally observed peaks in the histogram of velocity distribution $h(V_x)$ in Ref. [6].

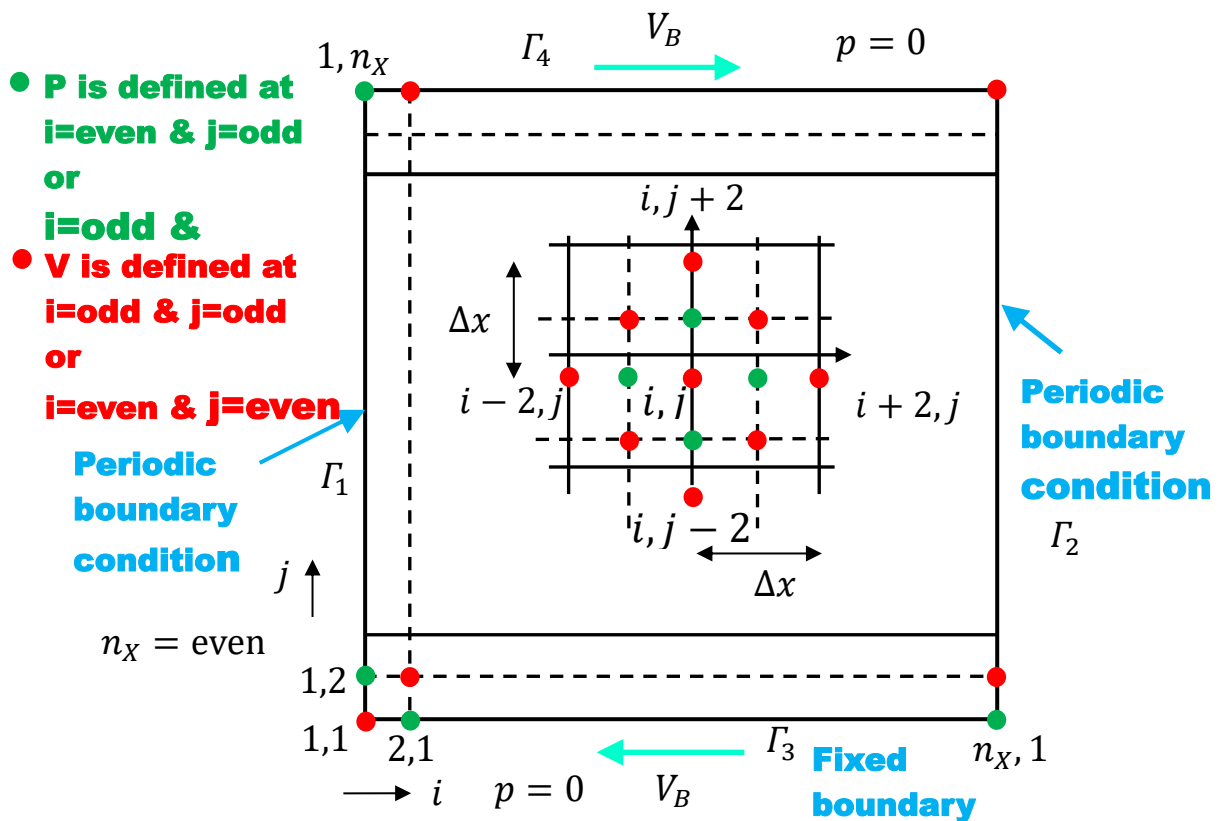


Fig.2 Staggered lattice (lattice 1) used in the simulations with Marker and cell (MAC) method.

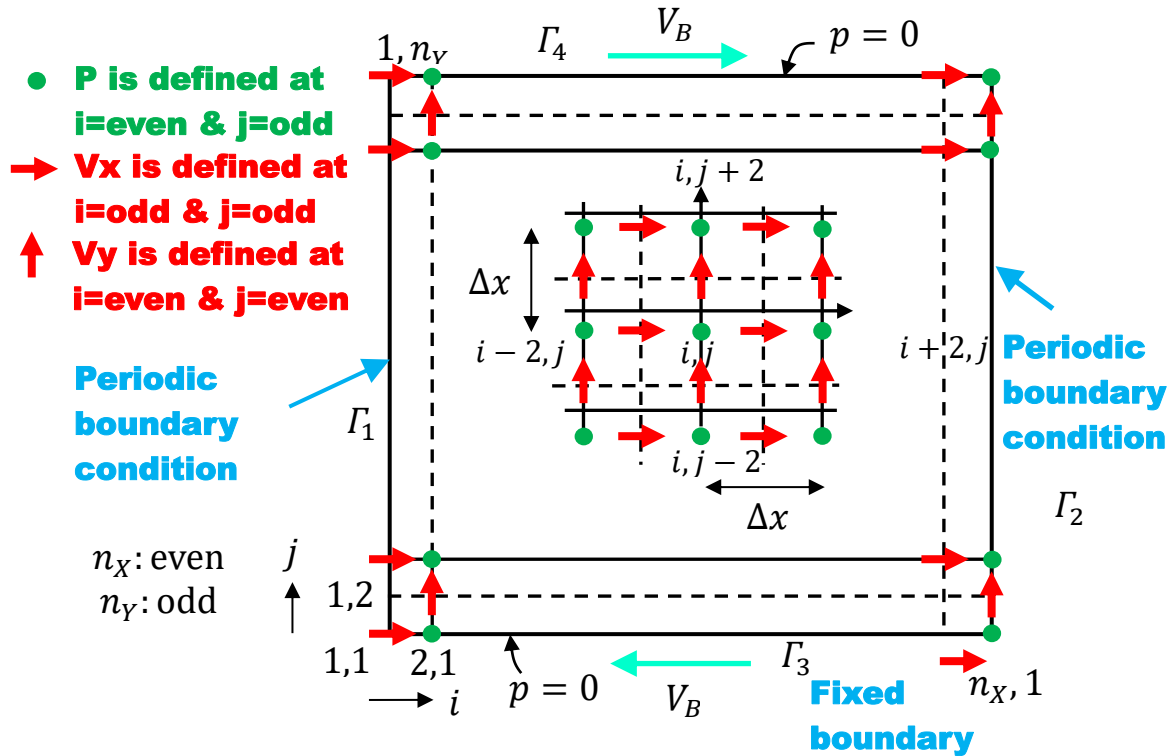


Fig.2 Staggered lattice (lattice 2) used in the simulations with Marker and cell (MAC) method.

Figures 1 and 2 show two different staggered lattices used in the simulations. Detailed information will be reported in the presentation.

Langevin Navier-Stokes equation is given by

$$\frac{\partial \vec{V}}{\partial t} = -(\vec{V} \cdot \nabla) \vec{V} - \rho^{-1} \nabla p + \nu \nabla^2 \vec{V} + \vec{\eta},$$

$$\nabla \cdot \vec{V} = 0,$$

where \vec{V} , p are velocity and pressure, $\vec{\eta}$ denotes Brownian random force, and ρ , ν are density and kinematic viscosity.

Simulations are relatively time-consuming, and tentative results of the velocity distribution obtained on lattices 1 and 2 are shown in Fig. 3.

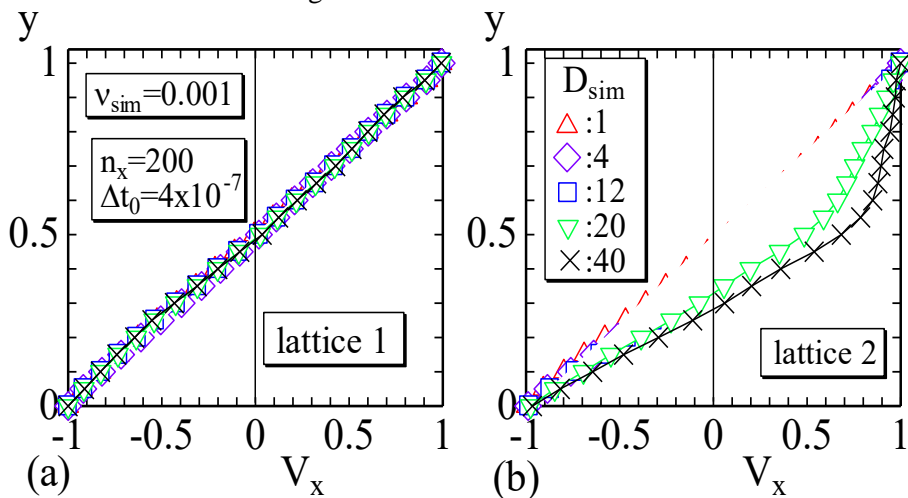


Fig.3 The dependence of velocity V_x on y . (Convergence seems not yet sufficient.)

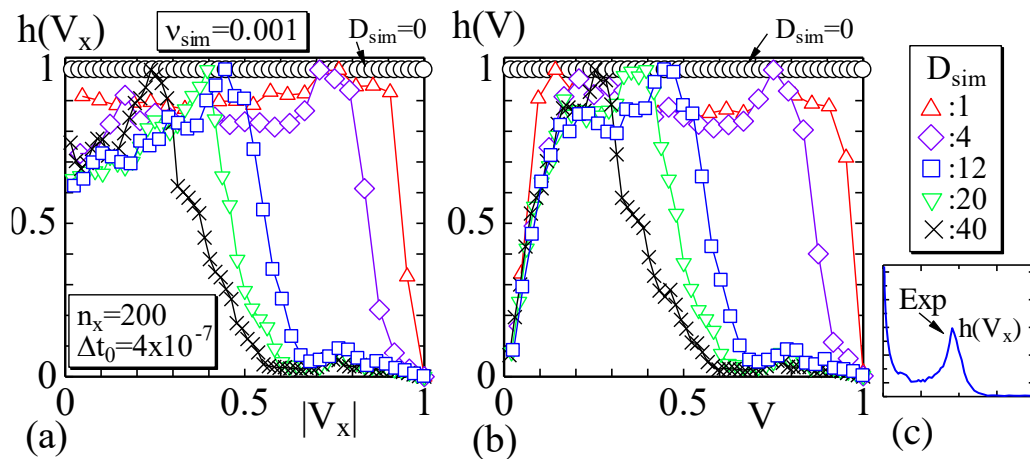


Fig.4 Velocity distribution obtained on staggered lattice 1. The peak position of $h(V_x)$ moves left with increasing D_{sim} .

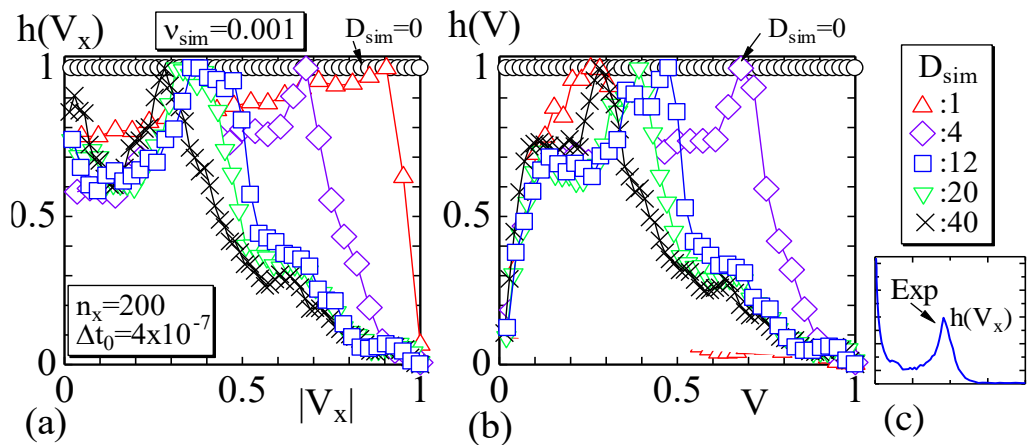


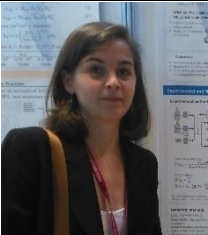
Fig.5 Velocity distribution obtained on staggered lattice 2. The peak position of $h(V_x)$ moves left with increasing D_{sim} .

References

[1] J.-W. Meent, I. Tuval, and R. E. Goldstein, "Nature's microfluidic transporter: Rotational cytoplasmic streaming at high Péclet numbers," *Phys. Rev. Lett.* 101, 178102 (2008).
 [2] M. Tominaga and K. Ito, "The molecular mechanism and physiological role of cytoplasmic streaming," *Curr. Opin. Plant Biol.* 27, 104–110 (2015).
 [3] M. Tominaga, A. Kimura, E. Yokota, T. Haraguchi, T. Shimmen, K. Yamamoto, A. Nakano, and K. Ito, "Cytoplasmic streaming velocity as a plant size determinant," *Dev. Cell* 27, 345–352 (2013).
 [4] R. V. Mustacich and B. R. Ware, "Observation of protoplasmic streaming by laser-light scattering," *Phys. Rev. Lett.* 33, 617–620 (1974).
 [5] R. V. Mustacich and B. R. Ware, "A study of protoplasmic streaming in *Nitella* by laser Doppler spectroscopy," *Biophys. J.* 16, 373–388 (1976)
 [6] V. Egorov, et.al, *Phys. Fluids* 32, 121902 (2020); <https://doi.org/10.1063/5.0019225>

Local stabilization dynamics of ammonia/methane non-premixed flames

ELyT Global Energy Science and technology for utilization of carbon-free energy carriers

	Sophie COLSON IFS, Tohoku University		Manuel KUHNI CETHIL, INSA de Lyon		Akihiro HAYAKAWA IFS, Tohoku University
	Hideaki KOBAYASHI IFS, Tohoku University		Cédric GALIZZI CETHIL, INSA de Lyon		Dany ESCUDIE CETHIL, INSA de Lyon

Abstract

1. Introduction

Ammonia is a promising carbon-free energy carrier [1,2]. Indeed, it can be transported and stored handily at a reasonable cost. In addition, ammonia can be used directly as a fuel in industrial applications and is thus attractive in the context of the decarbonization of the industry. Nonetheless, the use of ammonia as a fuel can be challenging due to its low laminar burning velocity [3], leading to poor stabilization, and its low flame temperature. NO_x can also be produced in the combustor if not carefully monitored [4]. To ease stabilization, blending ammonia with other fuels can be considered [5]. In this study, the use of ammonia and methane blends was considered as a solution for gradual CO₂ emissions reduction in existing facilities currently fueled by natural gas. This work aims to understand how ammonia addition will affect flame stabilization from a fundamental point of view, using a simple jet flame configuration. In previous work the stabilization domain of ammonia was investigated from a global perspective, looking at the aerodynamics of the jet, and the stabilization domain of attached and lifted flames was determined [6]. It could be observed that ammonia addition led to a drastic reduction of the stabilization domain, which could not be fully explained by the change in the laminar burning velocity of the mixtures.

In the present work, the local dynamics leading to liftoff were thus further investigated to understand the origin of the observed decrease. To do so, the position of the flame tip was monitored when gradually increasing the jet velocity for various ammonia-methane mixing ratios. The thermal interactions with the burner were also monitored through temperature measurements at the burner lip.

2. Experimental setup

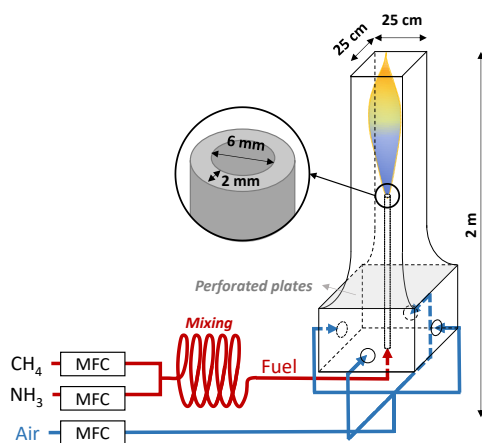


Figure 1. Experimental setup.

3. Results

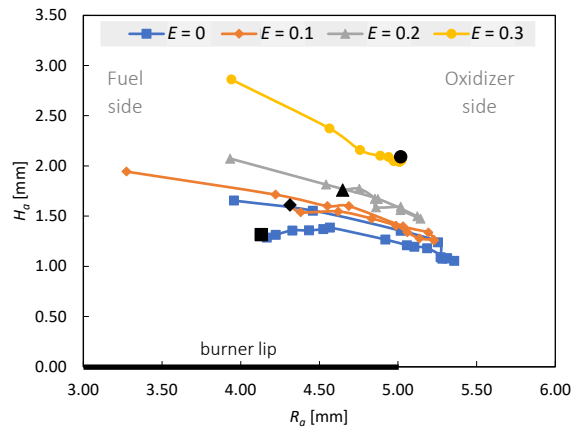


Figure 2. Flame tip position evolution with jet velocity up to liftoff.

Results on the flame position evolutions are introduced in Fig. 2. As observed from methane flame position evolution in blue and similar to previous works [7], the flame position changes with an increase in the jet velocity: first, going

The experimental setup used in this study is the non-premixed jet facility of the CETHIL in Lyon as represented in Fig. 1. Fuels are mixed and injected through a central pipe of length $L = 950$ mm, outer diameter $D_o = 10$ mm and inner diameter $D_i = 6$ mm. The fuel pipe is surrounded by an air coflow supplied from the bottom of the setup and going through perforated plates and a convergent to ensure a uniform velocity profile at the pipe outlet. The burner lip temperature was measured at the edge of the burner lip and 6 mm under to estimate the conduction heat flux through the burner. Flame tip position was obtained from CH^* chemiluminescence image of the flame using Abel deconvolution for increasing jet velocity up to liftoff.

toward the oxidizer side and lower positions following the jet broadening and the motion of fuel-oxidizer mixing contours; then, going back toward the jet axis, due to the air dragged in the wake of the burner lip for larger velocities finally reaching the liftoff position denoted in black. Similar observations could be done with ammonia/methane flames, but liftoff appeared earlier as ammonia is increase, and the flame eventually not going back toward the jet axis. Ammonia/methane flames stabilized gradually closer to the center axis with larger ammonia content, due to the larger stoichiometric mixture fractions, and higher above the burner lip, due to both the lower burning velocity and change in stoichiometric mixture fraction. Those combined effects led to a reduction of the region where both mixing and local velocity enable the flame stabilization, explaining the earlier liftoff with larger ammonia content observed in the global approach study [6].

References

- [1] H. Kobayashi, A. Hayakawa, K.D.K.A. Somarathne, E.C. Okafor, Proc. Combust. Inst. 37 (2019) 109–133.
- [2] A. Valera-Medina, H. Xiao, M. Owen-Jones, W.I.F. David, P.J. Bowen, Prog. Energy Combust. Sci. 69 (2018) 63–102.
- [3] A. Hayakawa, T. Goto, R. Mimoto, Y. Arakawa, T. Kudo, H. Kobayashi, Fuel 159 (2015) 98–106.
- [4] E.C. Okafor, K.D.K.A. Somarathne, N. Iki, T. Tsujimura, H. Furutani, H. Kobayashi, Combust. Flame 211 (2020) 406–416.
- [5] E.C. Okafor, Y. Naito, S. Colson, A. Ichikawa, T. Kudo, A. Hayakawa, H. Kobayashi, Combust. Flame 187 (2018) 185–198.
- [6] S. Colson, M. Kuhni, C. Galizzi, D. Escudié, H. Kobayashi, Combust. Sci. Technol. *In press.* (2020).
- [7] C. Galizzi, D. Escudié, K.M. Lyons, M. Kühni, F. André, S. Lamige, Exp. Therm. Fluid Sci. 56 (2013) 45–52.

Modal approach for extracting flow structure related to the subsonic jet noise generation

ELyT Global

Aeroacoustics Simulation and modal analysis

	<p><i>Shota MORITA</i></p> <p><i>D1 Student</i> <i>Aerospace Fluid Engineering</i> <i>Lab.</i></p> <p><i>IFS/Tohoku Univ. JAPAN</i></p>		<p><i>Aiko YAKENO, Ph. D.</i></p> <p><i>Assistant Professor</i> <i>Aerospace Fluid Engineering</i> <i>Lab.</i></p> <p><i>IFS/Tohoku Univ. JAPAN</i></p>
	<p><i>Christophe Bogey, Ph. D.</i></p> <p><i>Directeur de Recherche CNRS</i> <i>Laboratoire de Mécanique</i> <i>des Fluides et d'Acoustique</i></p> <p><i>Ecole Centrale de Lyon,</i> <i>France</i></p>		<p><i>Shigeru OBAYASHI, Ph. D.</i></p> <p><i>Professor</i> <i>Aerospace Fluid Engineering</i> <i>Lab.</i></p> <p><i>IFS/Tohoku Univ. JAPAN</i></p>

Abstract

1. Introduction

Subsonic jet noise, which is generated by jet engines, is called “the vortex sound[1]” because it is mainly caused by the nonlinear and unsteady motion of various scale vortices. Figure 1 shows for instance, the sound field and vortex structures caused by a subsonic jet at a Mach number of 0.9. Thanks to the recent development of the computation technologies in fluid dynamics, large-scale and highly accurate unsteady jet simulations have become possible. Therefore, detailed aeroacoustics analysis data for subsonic jets have been obtained so far. However, it is difficult to understand the huge and complex turbulence data without the appropriate analysis methods.

In recent years, a mode decomposition method called Dynamic Mode Decomposition (DMD) [3] has attracted attention as one of the linear analysis methods. This method aims to extract a periodic phenomenon as a feature structure which is called “DMD mode” from large and complex unsteady flow data. It seems to have good compatibility with linear acoustic phenomena and is expected to clarify the aerodynamic noise characteristics of subsonic jets.

In this study, we try to extract the flow structures related to the noise generation in a subsonic jet by applying DMD, based on the unsteady data of pressure fluctuation from the direct numerical simulation (DNS) obtained by our joint researcher, Dr. Bogey[2].

2. Method

We extract the flow structures related to the noise generation by applying DMD to time-series data of pressure fluctuation and selecting DMD mode (periodic feature structure) at a Strouhal number St_D corresponding to the frequency peaks identified by frequency analysis.

Regarding the data under study, we used the sectional pressure time-series data in the two-dimensional

(x, z) plane at azimuthal angle $\theta = 0$ which have been recently obtained for a round free jet of $M = 0.9$ and $Re = 3125$ by Direct Numerical Simulation [2]. Figure 2 shows a instantaneous pressure distribution of this data. The radial direction z and the streamwise direction x are made non-dimensionalized by the radius r_0 of the jet nozzle, and $z=0$ is the central axis of the jet.

In the DMD method, we define two datasets such as $\mathbf{X} = \{\mathbf{x}_1, \mathbf{x}_2, \dots, \mathbf{x}_m\}$ and $\mathbf{X}' = \{\mathbf{x}_1, \mathbf{x}_2, \dots, \mathbf{x}_{m-1}\}$, where the pressure fluctuation time-series data at $t = k\Delta t$ is obtained as $\mathbf{x}(t) = \mathbf{x}_k = \{p_{1k}, p_{2k}, \dots, p_{nk}\}$. We consider a state transition matrix \mathbf{A} such that $\mathbf{X} = \mathbf{A}\mathbf{X}'$. At this time, the DMD mode is obtained as a vector $\boldsymbol{\phi}$ in an eigenvalue problem in Eq. (1).

$$\mathbf{A}\boldsymbol{\phi} = \lambda\boldsymbol{\phi} \quad (1)$$

Here, the amplification factor σ of the DMD mode $\boldsymbol{\phi}$ and the frequency St_D are obtained from the eigenvalue λ at this time as in Eq. (2).

$$\sigma = \frac{\ln(|\lambda|)}{\Delta t}, St_D = \frac{Arg(\lambda)}{2\pi\Delta t} \quad (2)$$

3. Results and Discussion

DMD was applied to the potential core of the subsonic jet (where the flow is laminar), the extracted feature structures (DMD modes) are shown in Figures 3 and 4. Here, $St_D \sim 0.47$ and 1.15 are the dominant frequency peaks near the jet exit. In particular, $St_D \sim 0.47$ is known as the Kelvin-Helmholtz (K-H) instability frequency. In Figs. 3 and 4, the eddies caused by the K-H instabilities in the shear layer extracted by DMD can be observed. This may lead to vortex collapse in the wake and the generation of turbulence. In addition to the K-H instability, a pressure wave-like structure coming from the wake is found on the jet axis. This upstream wave is currently under investigation.

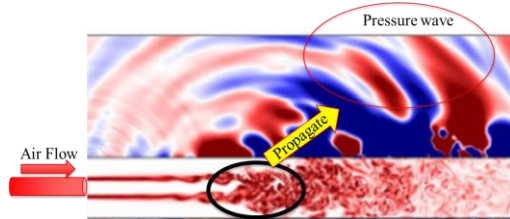


Fig.1 Subsonic jet simulation results.(Bogey,2019 [2])

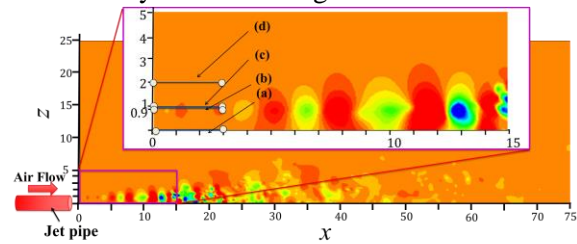


Fig.2 Instantaneous field of pressure as used in DMD.

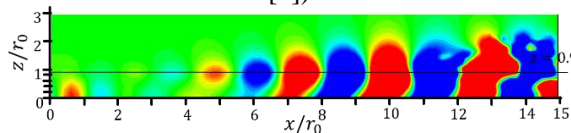


Fig.3 visualization results of the DMD mode of $St \sim 0.47$

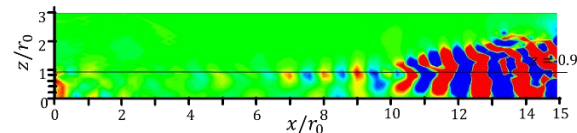


Fig.4 visualization results of the DMD mode of $St \sim 1.15$.

References

- [1] Powell, Alan. "Theory of vortex sound." *The journal of the acoustical society of America* 36.1(177-195), 1964.
- [2] C. Bogey, "Two-dimensional features of correlations in the flow and near pressure fields of Mach number 0.9 jets", AIAA SciTech Forum (2019-0806), 2019.
- [3] P. Schmid, "Dynamic mode decomposition of numerical and experimental data", *Journal of Fluid Mechanics*, 656(5-28), 2010.

JSPS Core to core 1st symposium: Construction of an international research exchange center for ammonia combustion and materials toward the realization of a low-carbon society

June 22nd

15:30 - 15:45 : Introduction of “Core to core program”

Prof. Kaoru Maruta and Prof. Takashi Tokumasu

15:45 – 16:15 : Role of ammonia combustion and Japan’s perspectives

Prof. Hideakii Kobayashi (invited)

16:15 – 16:55 : Panel Discussion “Materials System for Ammonia Combustion”

Moderator : Prof. Nicolas Mary

Keynote Talks

- a) “How about degradation of oxide ceramic thermal barrier coatings under reducing environment?”

Prof. Kazuhiro Ogawa

- b) “Wastage of austenitic heater tubes in a melamine production plant: mechanistic insight and implication to ammonia combustor materials”

Prof. Yutaka Watanabe

- c) “Introduction to the corrosion loop”

Prof. Nicolas Mary / Prof. Francois Ropital

- d) “Dynamics and kinetics of ammonia flames”

Prof. Fabien Halter

Lab poster list

Laboratory name	Institution
ELyTMaX	CNRS - Tohoku University – Univ. Lyon
Integrated Simulation Biomedical Engineering Lab. (Institute of Fluid Science)	Tohoku University
LGEF ¹	INSA Lyon
Lyon Center, Institute of Fluid Sciences	Tohoku University – ECL - INSA Lyon
MATEIS ²	INSA Lyon – CNRS – Univ. Lyon 1
Mechanical Systems Evaluation Laboratory (Institute of Fluid Science, Lyon Center)	Tohoku University
PRISME ³	INSA-Centre Val de Loire

¹ Laboratoire de Génie Electrique et Ferroélectricité (“Laboratory of Electrical Engineering and Ferroelectricity”)

² MATERiaux: Ingénierie et Science (“Materials: Engineering and Science”)

³ Laboratoire Pluridisciplinaire de Recherche en Ingénierie des Systèmes, Mécanique et Energétique (“Multidisciplinary Research Laboratory in Systems Engineering, Mechanics and Energy”)

Participant list

A

ABE Hiroshi (GSE Tohoku University)

ANZAI Hitomi (IFS Tohoku University)

B

BAIETTO Marie-Christine (LAMCOS INSA Lyon)

BERNARD Chrystelle (FRIS Tohoku University)

BESSET Sebastien (LTDS ECL)

BOULON Georges (ILM Univ. Lyon 1)

C

CARRERE Adrien (ILM Univ. Lyon 1)

CAVILLE Jean-Yves (ELyTMaX INSA Lyon/CNRS/Tohoku University)

CHANTRENNE Patrice (MATEIS INSA Lyon)

CHIBA Akihiko (IMR Tohoku University)

CLEMENTE Patrice (LIFO INSA CVL)

COATIVY Gildas (LGEF INSA Lyon)

COLSON Sophie (IFS Tohoku University)

CORRE Christophe (LMFA ECL)

COURBON Joël (MATEIS INSA Lyon)

D

DAISUKE Goanno (IFS Tohoku University)

DANCETTE Sylvain (MATEIS INSA Lyon)

DE BARROS-BOUCHET Maria Isabel (LTDS ECL)

DECROOCQ Méghane (CREATIS INSA Lyon / IFS Tohoku University)

DIATEZO Léopold (LGEF INSA Lyon)

DIGUET Gildas (AIMR Tohoku University)

DUCHARNE Benjamin (ELyTMaX INSA Lyon/CNRS/Tohoku University)

F

FABREGUE Damien (MATEIS INSA Lyon)

FAVE Alain (INL INSA Lyon)

FONTAINE Julien (CNRS / LTDS ECL)

FRIDRICI Vincent (LTDS ECL)

FRINDEL Carole (CREATIS INSA Lyon)

FUNAMOTO Kenichi (IFS Tohoku University)

G

GALIZZI Cedric (CETHIL INSA Lyon)

GESLIN Pierre-Antoine (MATEIS INSA Lyon)

GHERMAN Raphaël (LGEF INSA Lyon)

GILLOT Frédéric (LTDS ECL)

H

HAICHENG Song (IFS Tohoku University)

HALTER Fabien (ICARE Univ. Orléans)

HARTMANN Daniel (MATEIS Univ. Lyon 1)

HASEGAWA Masahiro (IFS Tohoku University)

HASHURO Muhammad Shiddiq Sayyid (IFS Tohoku University)

HENRY Daniel (LMFA ECL)

HESNARD Julie (ILM Univ. Lyon 1)

HLADKY Anne-Christine (CNRS)

Participant list

I

ITO Haruki (IFS Tohoku University)

J

JAY Jacques (CETHIL INSA Lyon)

JOLY-POTTUZ Lucile (MATEIS INSA Lyon)

K

KANDA Yuki (IFS Tohoku University)

KANEKO Yuya (GSE Tohoku University)

KAPSA Philippe (LTDS ECL)

KITA Kairi (IFS Tohoku University)

KITANO Ayumi (YUKI Précision SAS)

KOBAYASHI Hideaki (IFS Tohoku University)

KOBAYASHI Naohiro (IFS Tohoku University)

KOHATA Yutaro (IFS Tohoku University)

KOIBUCHI Hiroshi (Sendai Kosen)

KOJIMA Yukiko (IFS Tohoku University)

KOMIYA Atsuki (IFS Tohoku University)

KOSUKEGAWA Hiroyuki (IFS Tohoku University)

KOTARO Daibo (IFS Tohoku University)

KUBO Momoji (IMR Tohoku University)

KUHNI Manuel (CETHIL INSA Lyon)

KURITA Hiroki (GSES Tohoku University)

L

LALLART Mickaël (LGEF INSA Lyon)

LEFEUVRE Elie (C2N Paris-Saclay)

LIU Yuanyuan (LGEF INSA Lyon / Space Structure Lab / ELyTMaX)

LOMBARDI Giulia (ELyTMaX INSA Lyon/CNRS/Tohoku University)

M

MABUCHI Takuya (FRIS Tohoku University)

MAGOARIEC Hélène (LTDS ECL)

MAIRE Eric (MATEIS INSA Lyon)

MALEVAL Jacques (CNRS)

MARTIN Jean-Michel (LTDS ECL)

MARUTA Kaoru (IFS Tohoku University)

MARY Nicolas (MATEIS INSA Lyon / ELyTMaX)

MASUDA Hisanori (IFS Tohoku University)

MATSUMOTO Ikuyo (Embassy of France in Japan)

MAURY Lilian (ELyTMaX INSA Lyon/CNRS/Tohoku University)

MIKI Hiroyuki (IFS Tohoku University)

MORITA Shota (DAE Tohoku University)

N

NAGAYAMA Kouichi (TFC Tohoku University)

O

OBAYASHI Shigeru (IFS Tohoku University)

OGABI Raphael (PRISME INSA CVL)

OGAWA Kazuhiro (IFS Tohoku University)

OHTA Makoto (IFS Tohoku University)

OLLIVIER Lucas (IFS Tohoku University)

P

PAN Fangjia (IFS Tohoku University)

Participant list

PARMO Parmo (INSA CVL)

PERRIN Véronique (LGEF INSA Lyon)

PLET Guillaume (LTDS ECL)

POULIN-VITTRANT Guylaine (GREMAN INSA CVL)

R

RAVIOL Jolan (LTDS ECL)

RIEU Jean-Paul (ILM Univ. Lyon 1)

ROPITAL François (MATEIS INSA Lyon)

S

SAITO Hiroki (GSE Tohoku University)

SAMET Oscar (INSA Lyon)

SATO Yutaka (GSE Tohoku University)

SEBALD Gael (ELyTMaX INSA Lyon/CNRS/Tohoku University)

SEVEYRAT Laurence (LGEF INSA Lyon)

SHIMOYAMA Koji (IFS Tohoku University)

SHINDO Yugo (IFS Tohoku University)

SHIRAISHI Keiichiro (IFS Tohoku University)

SHOJI Tetsuo (NICHe Tohoku University)

SOMA Tomoya (Medicinal Hub NEC & Tohoku Univ.)

T

TAKAGI Toshiyuki (TFC Tohoku University)

TAKANA Hidemasa (IFS Tohoku University)

TAKEDA Kazuki (IFS Tohoku University)

TAKEDA Sho (IFS Tohoku University)

TAXIL Gaspard (LGEF INSA Lyon)

TERMENTZIDIS Konstantinos (CETHIL INSA Lyon)

TER-OVANESSIAN Benoît (MATEIS INSA Lyon)

TOKUMASU Takashi (IFS Tohoku University)

TONGLAI Song (IFS Tohoku University)

U

UCHIMOTO Tetsuya (IFS Tohoku University)

UNOURA Sayaka (IAC Tohoku University)

W

WADA Karen (IFS Tohoku University)

WADA Takeshi (IMR Tohoku University)

WANG Zi (GSBE Tohoku University)

WANG Zihao (NICHe Tohoku University)

WATANABE Mikihiro (IAC Tohoku University)

WATANABE Yutaka (GSE Tohoku University)

X

XUEN Way Sze (GSE Tohoku University)

Y

YAKENO Aiko (IFS Tohoku University)

YAMANAKA Kenta (IMR Tohoku University)

YAN Linjuan (LGEF INSA Lyon)

YUSE Kaori (LGEF INSA Lyon / IFS LyC)

Z

ZHANG Shurui (IFS Tohoku University)

ZHOU Xinwu (IFS Tohoku University)

